Target-cell-specific synaptic properties in neocortical microcircuits

Arne Vladimir Blackman

Department of Neuroscience, Physiology and Pharmacology

University College London

2015

Thesis submitted to University College London for the degree of Doctor of Philosophy. The work presented is my own; where information has been derived from other sources it has been indicated.

Abstract

A major focus of modern neuroscience is to establish the links between structure, physiology and function in neural cells and circuits. One key strand of this effort is in establishing the number and properties of cardinal cell types; increasing evidence suggests that many physiological and functional properties of neural circuits may be cell- and synapse-specific. Cortical interneurons are one group of cells which may be comprised of a large number of distinct classes with differing genetic, physiological and functional properties. Studies suggest that axonal morphology may be one of the most useful and simple indicators of these interneuronal types. The results presented in this thesis contribute to knowledge of both anatomical cell-type classification and the function of presynaptic NMDA receptors in visual cortex. Firstly, the utility of two-photon microscopy to create neural reconstructions suitable for cell-type classification is validated. However, reconstructions created from two-photon imaging suffer from errors when used in computer modelling due to overestimation of neurite diameters when compared to biocytin reconstructions of the same cells. Cell-type classification from two-photon imaging is then utilised in elucidating the target-cell-specific expression and function of presynaptic NMDA receptors (preNMDARs) in layer 5 of visual cortex; controversy regarding the existence of these receptors may be explained by their selective expression at synapses from pyramidal cells onto particular postsynaptic cell types. The target-specific expression of preNMDARs, along with synapse-specific differences in short-term plasticity, contributes to the spatiotemporal remapping of inhibition across the somatodendritic axis of pyramidal cells during high-frequency firing, mediated by somatostatin and parvalbumin-expressing interneurons. Finally, the reconstructions, cell types and results from this work are used to develop and validate a time-saving approach based on Sholl analysis to classify cells from bitmap images without the need for laborious manual reconstructions – something which should facilitate high-throughput future studies of neural anatomy and morphology.

Acknowledgements

Thank you to Jesper Sjöström, who has been an excellent supervisor. Thank you also to Tom Mrsic-Flogel for co-supervision in the final part of this PhD.

Thanks also to Alanna Watt, Julia Oyrer, Mark Farrant, Robert Legenstein and all members of the Sjöström, Mrsic-Flogel, Watt and Farrant labs for help and support.

Special thanks to Stefan Grabuschnig, Kate Buchanan and Tiago Ferreira, who provided critical input to chapters 3, 4 and 5. Many thanks to Scientifica and Dale Elgar for supporting this project by lending equipment vital for its completion.

Most trivially but perhaps most importantly, thank you to Aaron Towlson and associates for providing coffee throughout.

Authorship Statement

Some work presented in this thesis was necessarily collaborative. Where this is the case, contributions and authorship for particular experiments and data are explicitly stated, at the beginning of each chapter.

Some of this thesis is adapted from previously published work of which I authored / contributed to, listed here: elements of the introduction and discussion are based on (Blackman, Abrahamsson et al. 2013), Chapter 3 is adapted from (Blackman, Grabuschnig et al. 2014), Chapter 4 is based on results presented in (Buchanan, Blackman et al. 2012), and Chapter 5 is based on results presented in (Ferreira, Blackman et al. 2014).

Table of Contents

List of tables

List of figures

List of abbreviations

2PLSM	Two-photon laser-scanning microscopy
5-HT	5-hydroxytryptamine
aCSF	Artificial cerebrospinal fluid
AMPA	α -Amino-3-hydroxy-5-methyl-4-isoxazolepropionic acid
APV	(2R)-amino-5-phosphonovaleric acid
bAP	Backpropagating action potential
BC	Basket cell
BH	Biocytin histology
CV	Coefficient of variation
EM	Electron microscopy
EPSC	Excitatory post-synaptic current
EPSP	Excitatory post-synaptic potential
FDDI	Frequency-dependent disynaptic inhibition
FI	Fluorescence imaging
FIDI	Frequency-independent disynaptic inhibition
FS	Fast spiking
GABA	γ-Aminobutyric acid
GAD	Glutamate decarboxylase
GFP	Green fluorescent protein
IN	Interneuron
IPSC	Inhibitory post-synaptic current
IPSP	Inhibitory post-synaptic potential
L1	Cortical layer 1
L2/3	Cortical layer 2/3
L4	Cortical layer 4
L5	Cortical layer 5
L6	Cortical layer 6
LGN	Lateral geniculate nucleus
LTD	Long-term depression
LTP	Long-term potentiation
LTS	Low-threshold spiking
MC	Martinotti cell
MK801	Dizocilpine

NMDA	N-methyl-D-aspartate
NMDAR	N-methyl-D-aspartate receptor
OLM	Oriens lacunosum-moleculare
PBS	Phosphate buffered saline
PC	Pyramidal cell
PCA	Principal component analysis
PFA	Paraformaldehyde
PPR	Paired-pulse ratio
preNMDAR	Presynaptic N-methyl-D-aspartate receptor
PV	Parvalbumin
SOM	Somatostatin
STD	Short-term depression
STDP	Spike-timing-dependent plasticity
STF	Short-term facilitation
STP	Short-term plasticity
V_m	Resting membrane potential
τ_m	Membrane time constant

1. Introduction

Understanding the relationship between anatomy, physiology and function in cortical circuits is a major goal for modern neuroscience. A key idea is that the exact patterns of synaptic connectivity between groups of neurons underlie their involvement in a particular function. Whilst much progress has been made in unravelling these relationships, the variety and number of cell types in neocortex, along with short- and long-term modifications to connectivity and synaptic strength, have proved challenging obstacles in linking circuits and behaviour. This chapter begins with an overview of basic concepts pertinent to cortical circuits, followed by a more detailed discussion of issues relevant to the aims of this thesis, in particular cell-type-specific differences in short-term synaptic dynamics and transmitter release.

1.1. The neocortex

The mammalian neocortex is the phylogenetically most recent part of the cerebral cortex, and is involved in a number of sensory, motor, and higher functions (Douglas, Markram et al. 2004). Despite large differences in, for example, size between species, the neocortex appears to retain a largely conserved structure, perhaps illustrated best in its lamination, which is typically described as comprising six distinct cell layers (Campbell 1905, Douglas and Martin 2004). Similarly, the cell types represented across cortical regions and species appear appreciably alike (Ramón y Cajal 1911). In contrast to these anatomical similarities, different cortical areas are involved in widely differing activities, from the cognitive functions of prefrontal cortex (Miller and Cohen 2001) to the representation of visual space in primary visual cortex (Hubel and Wiesel 1959). A large portion of research in neuroscience over the last century has been dedicated to understanding the links between cortical structure and function, raising questions such as the degree to which cortical structure represents a ‘canonical’ or modular circuit adapted to different functions, or is shaped by experience- and modality-

dependent differences in development (Douglas and Martin 2004, Kalisman, Silberberg et al. 2005, Harris and Mrsic-Flogel 2013).

1.2. Cortical circuitry

1.2.1. The laminar structure of cortex

Descriptions of differences in the number, arrangement and density of cells in cortex have been key in distinguishing between different cortical areas throughout the history of neuroscience. Mammalian neocortex is conventionally divided into six layers, although subdivisions and differences are evident; for example compare the subdivisions of layer 4 in macaque striate visual cortex with the lack of a granular layer 4 in primary motor cortex. In the early 20th century, the work of Brodmann described around 50 distinct cortical areas based on comparison of such cytoarchitechtonic differences (Brodmann 1909). The primary visual cortex can be divided into 6 layers, as is conventional for neocortex, with layers 1-6 spanning the space between the pia and white matter. Here, layer 4 lies in the middle of the column, contains spiny stellate cells and receives the majority of input from other regions of the brain (see below). Above layer 4 are the superficial layers, from the sparsely populated layer 1 to the pyramidal cell containing layers 2 and 3. Below layer 4 are the deep layers, 5 and 6, containing larger pyramidal cells (Lund 1973, Lund 1988). In mouse, visual area 17 exhibits a much broader layer 4 and smaller layers 3 and 5 than adjacent area 18, however L4 is less clearly subdivisable than for macaque (Caviness 1975).

1.2.2. Inputs and outputs

In addition to providing a tool for comparison between cortical areas, the different cellular layers exhibit differences in their inputs and outputs from and to other cortical and non-cortical areas. In macaque visual cortex, inputs from the lateral geniculate nucleus (LGN) mostly (but not entirely) arrive in layer 4 of primary visual cortex. Here, axons from the magnocellular (M), parvocellular (P) and koniocellular (K) pathways remain separate, and target layer 4Cα, 4A / 4Cβ, and L2/3 respectively (Hubel and Wiesel 1972, Lund

1973, Lund 1988). Whilst layer 1 has a very sparse distribution of cell bodies, it receives input from K pathway axons (Fitzpatrick, Itoh et al. 1983, Lachica and Casagrande 1992). In addition to input from the LGN, it must be noted that direct feedback projections to V1 from higher cortical areas are also present (Ungerleider and Desimone 1986, Shipp and Zeki 1989, Barone, Batardiere et al. 2000).

Similarly to inputs, layer-specific differences also exist in the outputs of V1. Broadly, such outputs are initiated by pyramidal cells; in macaque, these occur in layers 2, 3, 4B, 5 and 6. Pyramidal cells in layers 2 and 3 project to higher cortical areas such as V2, 3, etc. The larger pyramidal cells in layers 5 and 6 project to subcortical areas, for example L5 projecting to superior colliculus and L6 back to LGN (Lund 1973, Lund 1988). However, whilst it may be taken as a "rule of thumb" that corticocortical connections arise mainly from the superficial layers and subcortical projections arise from the deep layers, there are exceptions to this, for example in neocortical area 4 where projections to spinal cord and cerebellum originate from both layer 5 and 3 cells (Douglas, Markram et al. 2004).

1.3. Basic cortical circuits

Despite the recognition of the ordered and laminar structure of cortex, attempts to understand the functional properties of cells with reference to cortical circuit organisation remain challenging to this day (Gilbert 1983, Douglas and Martin 2004, Harris and Mrsic-Flogel 2013). Perhaps the most studied area of neocortex (and the area of study of this thesis) is primary visual cortex (Brodmann area 17 or V1) (Gilbert 1983). Some of the earliest and most well known attempts to construct a hypothetical visual cortical circuit come from the studies of Hubel and Wiesel, who proposed that so called 'simple' cells in cortex exhibit their elongated receptive fields due to converging input from multiple on- or off-centre cells in the lateral geniculate nucleus (LGN; see Figure 1-1), and similarly cells with 'complex' receptive fields inherit these properties from multiple simple cell inputs (Hubel and Wiesel 1962).

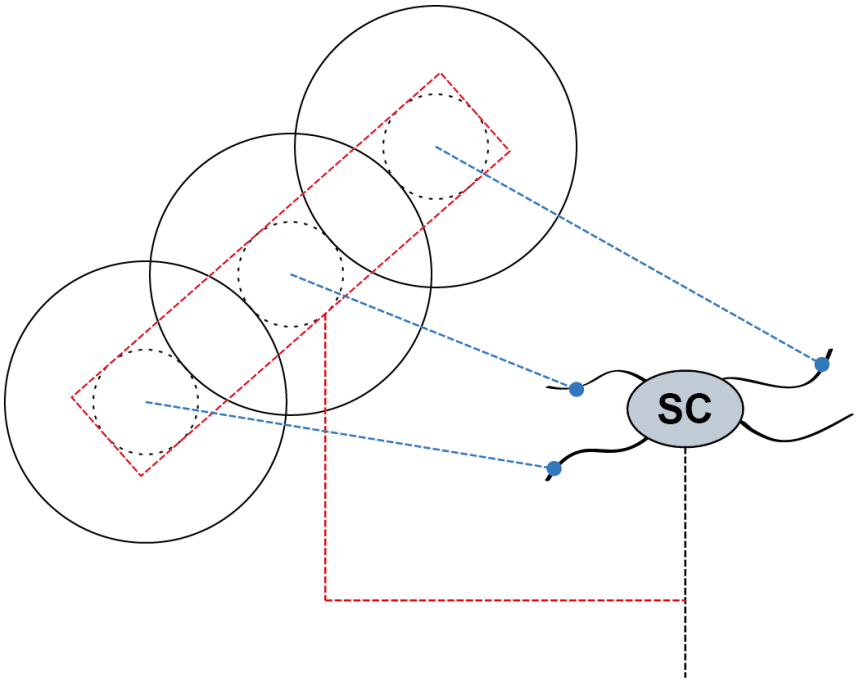

Figure 1-1: Hypothetical simple cell feedforward microcircuit

Based on observations of receptive field properties, Hubel and Wiesel (Hubel and Wiesel 1962) hypothesised the elongated receptive field of cortical simple cells may be derived from multiple LGN cells with centre-surround receptive fields. Here, 3 LGN ON-centre receptive fields are indicated to the left (circles / annuli); an oriented bar spanning these (red dotted line) would therefore excite all 3 cells and thus the simple cell (SC; right) receiving convergent input. SC output (black dotted line) is thus triggered by the oriented bar (red dotted line).

Whilst the feedforward circuits proposed by Hubel and Wiesel (Hubel and Wiesel 1962) were consistent with physiological recordings, it was not until the use of more advanced tracing techniques that the first defined anatomical visual cortical circuits were suggested (Gilbert 1983, Douglas and Martin 2004). Despite increasing evidence of more subtle properties such as functional subnetworks (Song, Sjostrom et al. 2005, Ko, Hofer et al. 2011, Harris and Mrsic-Flogel 2013) and the variety of inhibitory properties and connectivity (Brown and Hestrin 2009a, Fino and Yuste 2011, Hofer, Ko et al. 2011, Packer and Yuste 2011), the basic principles of the excitatory circuit and its laminar organisation suggested by Gilbert and Wiesel remain instructive (Gilbert 1983). In this model, the majority of thalamic input arrives in layer 4, where spiny stellate cells connect to pyramidal cells in the supragranular layers, which in turn project to layer 5. Layer 5 pyramidal cells (PCs) project both a connection back to the superficial layers and to layer 6,

where PCs close the loop by connecting to layer 4 (Gilbert 1983, Douglas and Martin 2004). Inhibitory smooth cells may be added to this to account for lateral inhibition (Hubel and Wiesel 1977, Douglas, Markram et al. 2004). Outputs are seen mainly from PCs in layers 5 (corticocortical and corticotectal) and 6 (corticothalamic). In contrast to the hypothetical model of (Hubel and Wiesel 1962), these anatomical models feature a large number of presumably recurrent loops (see Figure 1-2); this, along with the observation that only around 30% of asymmetric inputs to layer 4 cells are from the LGN (LeVay and Gilbert 1976), suggests that cortical circuits may compute (and modulate) a more complex representation of e.g. visual space than a simple hierarchical feedforward combination of retinal and thalamic receptive fields (Douglas and Martin 2004). Such connections, along with feedback and horizontal cortico-cortical processing, may enable the computation of visual features requiring parallel temporal and/or spatial comparison of activity, for example as in colour constancy under differing illumination, which would require the spatial comparison of changes in wavelength or photoreceptor activation over time (Douglas, Markram et al. 2004).

Although much insight can be gained from the combination of laminar connectivity maps and electrophysiological recordings of cells, fully understanding how functional properties of circuits emerge may require additional detail. On one level, in contrast to Peters' rule, which suggests synaptic connectivity may be explainable by the degree of axo-dendritic overlap between cells (Peters 1979) and may explain some selective features of cortical connectivity (Packer, McConnell et al. 2013), a great deal more cellular and subcellular specificity in connectivity has been described both among different classes of inhibitory cells (Markram, Toledo-Rodriguez et al. 2004, Ascoli, Alonso-Nanclares et al. 2008) and even very similar pyramidal cells differing in postsynaptic target (Brown and Hestrin 2009a, Brown and Hestrin 2009b). Furthermore, even if the connectivity between different cells was known with complete accuracy, this may not be enough to explain circuit function. For instance, synaptic connections are dynamic, changing in strength over both the short (Zucker and Regehr 2002) and long-term (Bliss and Collingridge 1993), and are furthermore subject to

modulatory control (Douglas, Markram et al. 2004); all these properties can affect the activity of a network. As an example, the nematode *C. Elegans* is a rare example of an organism for which the complete anatomical map of neuronal connections is known; yet, ambiguity in circuit function remains – a certain group of cells known as ADL neurons may drive opposite responses to a pheromone (avoidance or aggregation), an effect that is dependent on neuromodulation and as such is not predicted by the connectome (Bargmann and Marder 2013). Significant computations may also occur at the subcellular level (London and Hausser 2005), which are affected by morphology (Vetter, Roth et al. 2001). Unravelling the properties and function of cortical circuits, and neural circuits in general, may then require an integration of functional, anatomical and synaptic data. Whilst such multidisciplinary approaches have been challenging in the past, studies combining methods such as multiple whole-cell recordings, functional imaging, optogenetics and transgenics are beginning to enable the elucidation of relationships between connectivity, function and cell-type identity – cf. (Hofer, Ko et al. 2011, Ko, Hofer et al. 2011, Wilson, Runyan et al. 2012, Harris and Mrsic-Flogel 2013, Ko, Cossell et al. 2013, Bortone, Olsen et al. 2014).

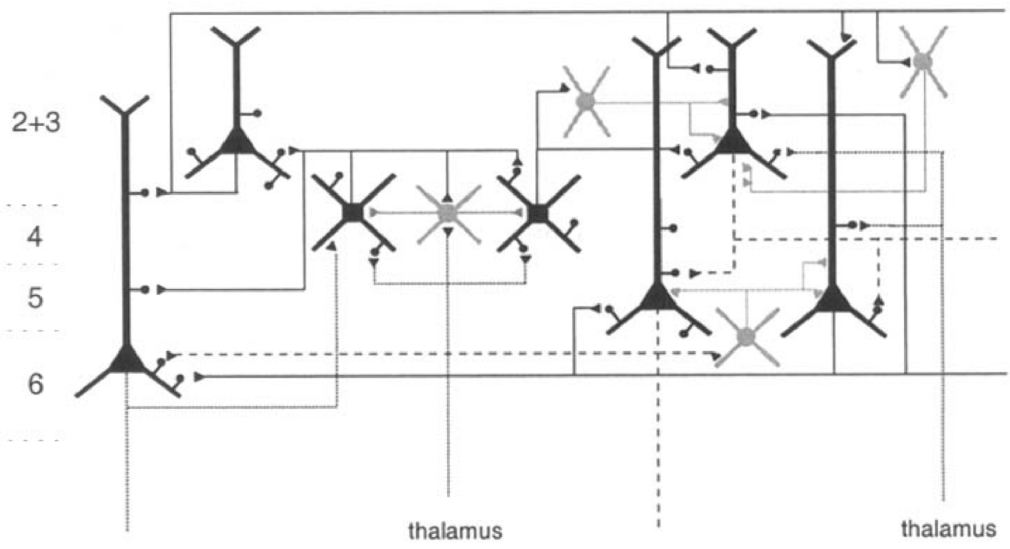

Figure 1-2: Basic visual cortical circuit

A simplified view of laminar and circuit organisation in visual cortex. Note the number of recurrent loops, and that whilst output mainly stems from layer 5 and 6 PCs, these may also receive input from thalamic or cortical connections. Layers are as indicated at left. Black cells = excitatory, grey cells = inhibitory. Adapted from (Douglas, Markram et al. 2004).

1.4. Cortical cell types

One of the factors complicating the understanding of cortical circuitry is the sheer number, density and complexity of cell types evident. Whilst most attempts to describe basic circuits simplify these to e.g. excitatory and inhibitory cells (Douglas and Martin 2004), further subtypes may display important functional differences that contribute to information processing (Brown and Hestrin 2009a). Efforts to classify and understand the plethora of neocortical cell types have been an active part of neuroscience since Ramón y Cajal (Ramón y Cajal 1911), and continue to this day, particularly with regard to inhibitory interneurons (Markram, Toledo-Rodriguez et al. 2004, Ascoli, Alonso-Nanclares et al. 2008, DeFelipe, Lopez-Cruz et al. 2013). Despite this complexity, the cortex appears to contain two basic classes of neuron, as described by Ramón y Cajal using the Golgi impregnation technique – neurons which exhibit dendritic spines (“spiny neurons”), and those which do not (“smooth neurons”). However, this is far from the only important distinction to be made; discrete cell types within these classes exhibit large differences in morphology, intrinsic physiology and genetic properties that likely exert specific functional effects within the neocortical

circuit. As such, classification of cell-type in studies exploring circuit properties is an important and illuminating step (Brown and Hestrin 2009a).

1.4.1. Spiny neurons

Spiny neurons are those that exhibit dendritic spines, protrusions onto which asymmetric type-1 synapses are formed (Gray 1959). Spiny neurons are excitatory (glutamatergic), and are composed of two major subgroups, defined by their morphology: pyramidal cells, which exhibit a striking apical dendrite, and spiny stellate cells, which do not.

Pyramidal cells

Pyramidal cells are the major class of excitatory cells in cortex, comprising around 70% of all neurons (Sloper, Hiorns et al. 1979). PCs are found throughout all cortical layers with the exception of layer 1. The defining feature of PCs is the prominent apical dendrite (Figure 1-3) extending from the soma and ascending through cortical layers. The PCs found in different layers and cortical areas may however differ drastically in size and arborisation; contrast, for example, the very large Betz cells found in layer 5 of motor cortex with the far smaller L2/3 PCs in visual cortex (Douglas, Markram et al. 2004). Classically, PCs exhibit regular (adapting response with afterhyperpolarisation) or bursting spiking properties (McCormick, Connors et al. 1985). PCs are the major output neurons of the cortex, but also provide a large amount of intra-area recurrent connections (see 1.3).

Whilst PCs are generally thought of as unambiguously identifiable (as compared to interneuron classes), it has been suggested that different classes of PC exist with different properties. For instance, in layer 5 of visual cortex (the area studied in this thesis), at least two types of pyramidal cell have been identified: thick tufted cells with an apical dendrite branching in layer 1, and slender tufted cells with a non-branching apical dendrite terminating in layer 2 (Larkman and Mason 1990). These types may differ in their projection targets with thick-tufted cells projecting to pons, and slender-tufted cells to striatum (Groh, Meyer et al. 2010). Similarly, connection

frequency between L5 PCs appears cell-type-specific, with corticostriatal cells forming reciprocal connections more often than other PCs, and connections between corticocortical and corticotectal PCs appearing with a high frequency (Brown and Hestrin 2009b).

Spiny stellate cells

Another group of excitatory cells is represented by the spiny stellate neurons, which are found in layer 4 and receive the majority (although see 1.3 and Figure 1-2) of thalamic input (Douglas, Markram et al. 2004). The defining feature of these cells is the lack of an apical dendrite, and the presence of spines on basal dendrites, although at a lower density than PCs (Ramón y Cajal 1911, Douglas, Markram et al. 2004).

1.4.2. Smooth neurons

Smooth neurons are inhibitory (GABAergic) cells lacking spines, and whilst they represent the minority of neocortical cells (around 20%) in terms of number (Douglas, Markram et al. 2004, Markram, Toledo-Rodriguez et al. 2004, Sahara, Yanagawa et al. 2012), they exhibit a huge variety of morphological, physiological, genetic and functional properties – so much so that the classification of these cells into distinct classes has identified over 15 types and remains a challenge in neuroscience to this day (Ascoli, Alonso-Nanclares et al. 2008, DeFelipe, Lopez-Cruz et al. 2013). Indeed, simply agreeing on a common language to describe these interneurons has required much effort (Ascoli, Alonso-Nanclares et al. 2008). These cells are usually described with reference to a combination of anatomical, physiological and genetic properties, however, axonal morphology is increasingly seen as a key indicator of type (Markram, Toledo-Rodriguez et al. 2004, Toledo-Rodriguez, Goodman et al. 2005, Ascoli, Alonso-Nanclares et al. 2008, DeFelipe, Lopez-Cruz et al. 2013). A feature of neocortical interneurons is the propensity of different IN classes to target particular subcellular regions of postsynaptic cells (e.g. perisomatic region, apical dendrites or axon initial segment) (Douglas, Markram et al. 2004, Markram, Toledo-Rodriguez et al. 2004). Along with the spiny stellate cells, smooth

inhibitory INs can be thought of as local circuit neurons, with few, if any, processes extending outside the neocortex (Ramón y Cajal 1911, Douglas, Markram et al. 2004). An overview of the properties of some of the best-defined INs is found below.

Basket cells

Perhaps the most prominent class of neocortical inhibitory interneurons are the basket cells (BCs), comprising up to 50% of all INs, and so called because of their basket-like axonal arborisation (Figure 1-3) around PC somata (Markram, Toledo-Rodriguez et al. 2004). A key feature of basket cells is their preference to form synapses on the perisomatic area of target cells, which may enable inhibitory control over the entire integrated synaptic input (Douglas, Markram et al. 2004, Markram, Toledo-Rodriguez et al. 2004). Typically, BCs exhibit fast-spiking electrophysiological properties, with smaller spike half-width than PCs (Wang, Gupta et al. 2002).

It has been suggested that BCs are comprised of further distinct subclasses, separated by differences in morphology; these are the large, small and nest basket cells (Wang, Gupta et al. 2002). These classes are thought to differ in morphology, with large basket cells exhibiting far wider arbours than the other classes (Wang, Gupta et al. 2002, Markram, Toledo-Rodriguez et al. 2004). Similarly, whilst most large and nest basket cells express the calcium-binding protein parvalbumin (PV), small basket cells differ with wide expression of vasoactive intestinal peptide (VIP) (Toledo-Rodriguez, Goodman et al. 2005).

Martinotti cells

Martinotti cells (MCs), named by Ramón y Cajal after Carlo Martinotti (Martinotti 1889), are most clearly defined by their typical morphology appearing similar to an ‘inverted’ PC (Figure 1-3), with downwards curving dendrites and an axon ascending to, and branching heavily in layer 1 (Wang, Toledo-Rodriguez et al. 2004). MCs are genetically defined most consistently by expression of the neuropeptide somatostatin (SOM), and typically exhibit

accommodating and occasionally bursting spiking properties, often with a low threshold for spike initiation (Wang, Toledo-Rodriguez et al. 2004, Toledo-Rodriguez, Goodman et al. 2005). MCs target the apical and oblique dendrites of neighbouring PCs, which may allow them to uncouple Ca^{2+} spikes and backpropagating somatic action potentials in PCs during frequency-dependent disynaptic inhibition between PCs (FDDI; see 1.9 and 4.5.4) (Silberberg and Markram 2007, Gidon and Segev 2012).

Chandelier cells

Chandelier cells are distinctive in that they form axo-axonic synapses (Somogyi 1977) and as such may be able to alter the output of target cells (Zhu, Stornetta et al. 2004). Anatomically, chandelier cells exhibit rows of vertical axonal boutons that are the origin of the 'chandelier' name (Markram, Toledo-Rodriguez et al. 2004). Chandelier cells often express PV (DeFelipe, Hendry et al. 1989). Interestingly, it has been suggested that chandelier cells may actually have a depolarising effect on nearby PCs (Woodruff, Xu et al. 2009). Defects in chandelier cell function have been implicated in schizophrenia (Lewis, Hashimoto et al. 2005).

Bitufted, bipolar and double bouquet cells

The group of INs comprised by bitufted (BTC), bipolar (BPC) and double bouquet (DBC) cells are similar in that they tend to exhibit bitufted or bipolar dendrites extending from either pole of the ovoid somata, and have dendrite-targeting axons (Markram, Toledo-Rodriguez et al. 2004). Whilst BPCs and DBCs have a tendency to express VIP, the expression patterns of different neuropeptides and calcium binding proteins in these cells are more ambiguous than MCs or BCs (Toledo-Rodriguez, Goodman et al. 2005). Although these cells have similar dendritic morphology, differences occur in axonal morphology; BPCs contact relatively few cells with a vertically oriented axon, BTCs exhibit more horizontal projections, and DBCs have a tight cluster of axonal collaterals (Douglas, Markram et al. 2004, Markram, Toledo-Rodriguez et al. 2004).

Cajal-Retzius and neurogliaform cells

These interneurons are perhaps less well studied, and both can be found in layer 1 (although neurogliaform cells may be found elsewhere) (Hestrin and Armstrong 1996, Markram, Toledo-Rodriguez et al. 2004). Cajal-Retzius cells are seen mostly during development; they exhibit a horizontal axonal projection within layer 1, and may be involved in neuronal migration (Hestrin and Armstrong 1996, Gil-Sanz, Franco et al. 2013). Neurogliaform cells have a dense local axonal arbour, and may provide volume transmission of GABA from boutons not associated with traditional synapses; however, this does not preclude their involvement in specific circuit functions such as the attenuation of thalamic-initiated feed-forward inhibition in barrel cortex (Chittajallu, Pelkey et al. 2013).

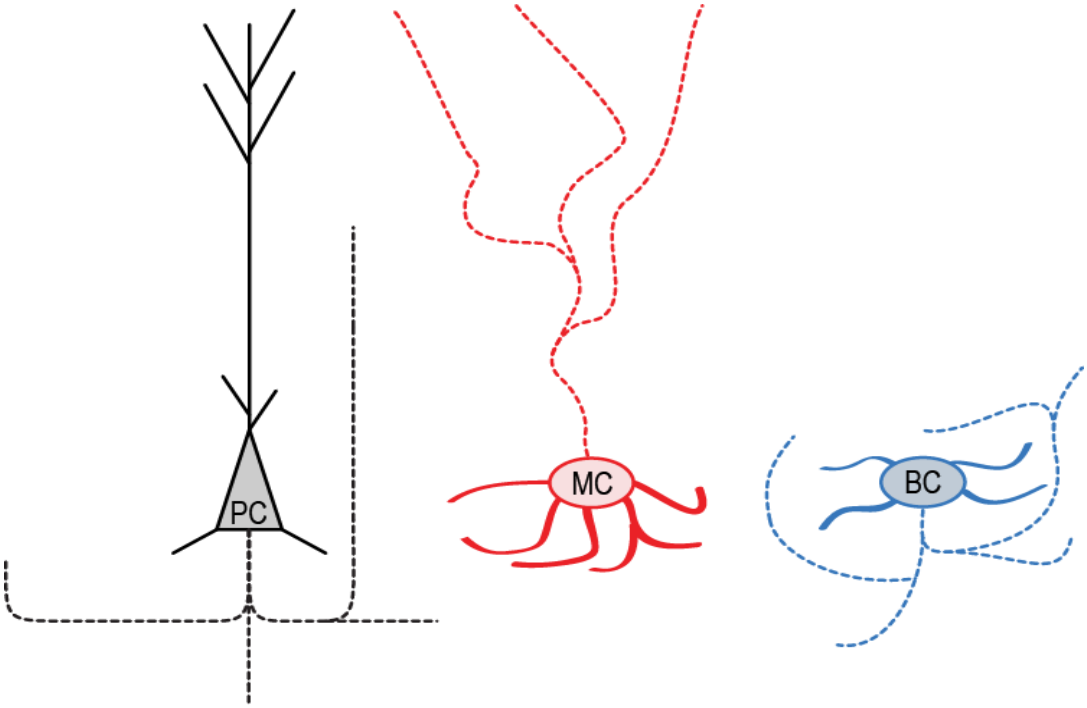

Figure 1-3: Examples of cortical cell types

Simplified representations of three common neocortical layer 5 cell types, indicating differences in morphology. PC = pyramidal cell, MC = Martinotti cell, BC = basket cell. Thick lines = dendrite, dotted lines = axon. Note that PC axon may project outside of neocortex. MCs exhibit an 'inverted' morphology compared to PCs, targeting apical and basal dendrites of postsynaptic cells. BCs form local perisomatic synapses on target cells, although further subtypes of BCs may exist, including large BCs with more pronounced horizontal collaterals (see text).

1.4.3. Why is identifying cell-type important?

Many different metrics are used to define particular cell classes, from the relative simplicity of an excitatory or inhibitory effect, to the complex combination of anatomical, electrophysiological, genetic and functional properties (see 1.4 and 1.11); such classification efforts are a major strand of neuroscience in themselves (Ascoli, Alonso-Nanclares et al. 2008, DeFelipe, Lopez-Cruz et al. 2013). Understanding what constitutes a particular cell type may in many cases allow fuller comprehension of functional network properties, for instance the temporal properties of FDDI mediated by Martinotti cells (Silberberg and Markram 2007). Similarly, distinct cell types may be involved specifically in disease, such as the observed PV IN hypofunction in schizophrenia (Nakazawa, Zsiros et al. 2012). The identification of cell types and their particular functional roles and deficiencies in disease may allow the development of targeted manipulations to specific cell groups to control and correct activity (Famm, Litt et al. 2013).

Understanding the stereotyped synaptic, genetic and network properties of particular cell groups (see 1.7, 1.8 and 1.9) may allow a greater understanding of the brain as a whole without the need for e.g. full-scale connectomics. As such, it is the belief of the author that there is an undeniable need and importance for cell-type classification – the challenge is in determining the correct parameters for this (see 1.11).

1.5. Further methods of identifying cortical interneurons

Whilst the cell types described in 1.4 are often classified by morphology and anatomy as summarised above, an increasing body of work attempts to classify such cells by electrophysiological properties, ion channel expression, chemical properties and connectivity (amongst others), alongside morphology (DeFelipe 1997, Gonchar and Burkhalter 1997, Kawaguchi, Karube et al. 2006). Although the classification of some key cortical interneuron types by anatomical methods and expression of molecular markers is summarised in section 1.4, alternative and complementary methods to identify and classify interneurons are also used. An overview of some of these is given below.

1.5.1. Developmental origins

One method to aid classification of cell types is to investigate their developmental origin; clear distinctions here may help indicate where cell types consist of classes as opposed to a continuum. For cortical interneurons, much work has focussed on IN subgroups defined by molecular or genetic markers (PV, SOM, etc.). Here, distinct regions in the telencephalon (Anderson, Eisenstat et al. 1997) have been implicated as origins for specific chemically defined cell classes. Whilst the primary sources of cortical INs are the medial and caudal ganglionic eminences, studies have also implicated the preoptic area (Gelman, Martini et al. 2009, Gelman, Griveau et al. 2011). In primates, some studies have also suggested a cortical origin of cortical INs (Jakovcevski, Mayer et al. 2011, Yu and Zecevic 2011).

The medial ganglionic eminence (MGE) has been identified as a major source of GABAergic cells in the cortex (Lavdas, Grigoriou et al. 1999, Wichterle, Garcia-Verdugo et al. 1999). Here, transplant experiments have identified MGE-derived interneurons as expressing PV or SOM – the two chemical markers expressed by usually distinct groups of INs that perhaps represent the majority of interneurons (as discussed above), including the major BC and MC classes (Butt, Fuccillo et al. 2005, Toledo-Rodriguez, Goodman et al. 2005). More recent studies have implicated the dorsal MGE in producing SOM cells, and the ventral and dorsal MGE in producing PV cells. Furthermore, chandelier cells appear to originate from the ventral MGE (Flames, Pla et al. 2007, Wonders, Taylor et al. 2008, Inan, Welagen et al. 2012).

An additional area identified as a major source of cortical interneurons in the caudal ganglionic eminence (CGE). Here, the dorsal (d) and ventral (v) areas of CGE express distinct transcription factors and have been suggested to be the origin of distinct interneuron populations; like MGE, vCGE expresses the homeobox[1] transcription factor *Nkx2.1.,* whilst the dCGE expresses the transcription factors *Gsh2* and *ER81* (Anderson, Eisenstat et al. 1997, Sussel, Marin et al. 1999, Nery, Fishell et al. 2002, Corbin, Rutlin et al. 2003, Nery, Corbin et al. 2003). Perhaps accordingly, the dCGE has been suggested to give rise to calretinin (CR) expressing interneurons, whilst the vCGE may be a source of SOM and PV INs. Interestingly, some Martinotti cells have been observed to co-express CR and SOM, raising the question of whether the MGE produces some CR INs, or if these cells may originate in the dCGE along with other CR+ INs (Wang, Toledo-Rodriguez et al. 2004, Toledo-Rodriguez, Goodman et al. 2005). In addition to CR, SOM and PV, the CGE has been identified as a source of INs expressing diverse molecular markers including NPY and VIP (Miyoshi, Hjerling-Leffler et al. 2010).

A further developmental factor to consider is temporal origin and birth date of INs. INs originating in the MGE generally follow an “inside-out” relationship to

[1] A ~180 base pair sequence encoding a DNA-binding protein domain

cortical layers, with later-born INs migrating past earlier-born INs to the superficial layers (Xu, Cobos et al. 2004, Butt, Fuccillo et al. 2005). In the CGE, this relationship is not so clear; for example, it has been observed that CR-expressing INs may follow an opposite pattern of migration (Butt, Fuccillo et al. 2005, Rymar and Sadikot 2007, Miyoshi, Hjerling-Leffler et al. 2010).

1.5.2. Transcription factors and fate determination

As mentioned above, fate determination of cortical interneurons may require differential expression of transcription factors. For example, MGE INs require *Nkx2.1*, and many also require *Lhx6* downstream of this (Lavdas, Grigoriou et al. 1999, Sussel, Marin et al. 1999, Xu, Cobos et al. 2004). Less is known, however, about how subclasses of IN (as defined by expression of molecular markers) are generated. It has been suggested that differential levels of sonic hedgehog signalling may have a role to play, with high levels specifying SOM INs and lower levels PV INs (Xu, Guo et al. 2010). SOX6 has been reported to be an important factor in postnatal IN subtype development (Azim, Jabaudon et al. 2009). Interestingly, it has been suggested that *Lhx6* may interact with either the transcription factor DLX1 to promote SOM IN fate determination, or DLX5/6 to promote a PV IN fate (Yang, Woodhall et al. 2006, Wang, Dye et al. 2010).

In the CGE the picture is perhaps less clear. Here, the transcription factor GSX2 (also known as GSH2) lies at the top of the hierarchy and acts to promote downstream gene expression of for example DLX2 and ASCL1 (Wang, Long et al. 2013). GSX2 is also involved in promoting CR IN identity (Xu, Guo et al. 2010). Additional transcription factors associated with CGE-derived IN fate determination include NR2F1, NR2F2, SP8 and PROX1 (Lodato, Tomassy et al. 2011, Ma, Zhang et al. 2012, Cai, Zhang et al. 2013, Rubin and Kessaris 2013).

Overall, the spatial and temporal origins of cortical interneurons, along with the transcriptional regulation of their fate, provides much insight into how different IN classes develop. However, there remains much work to be done

to fully elucidate how the plethora of IN types with different molecular markers and anatomical properties are generated. One potential challenge in doing this is in determining which are key indicators of cell type, as for example whilst the markers PV and SOM are often used as key indicators of IN classes, different cell types may exist within these populations (Toledo-Rodriguez, Goodman et al. 2005).

1.6. Synaptic transmission

Information processing in the brain is reflected by the interactions between, and activity patterns of groups of neurons. Neurons communicate via synapses, which are chemical or electrical junctions at which information may be passed between cells – typically formed at the close apposition between the axon of one (presynaptic) cell and the dendrite of another. The majority of synapses in the brain are chemical, and as such operate by the action potential induced release of neurotransmitter from pre- to postsynaptic cell (Eccles 1964).

Action potentials are forward propagating[2] regenerative waves of depolarisation that are induced when neurons are depolarised over a specific threshold (typically between -40 to -50 mV; cf. Table 4-1, Table 4-2), caused chiefly by the activation of voltage-gated ion channels and subsequent interplay between mainly inward, inactivating Na^+, and outward K^+ currents (Eccles 1964). When an action potential arrives at a presynaptic terminal, depolarisation may activate voltage-gated Ca^{2+} channels, leading to an influx of calcium triggering the release of neurotransmitter-containing synaptic vesicles into the synaptic cleft, where it may diffuse across and bind to neurotransmitter receptors on the postsynaptic cell membrane. In the case of ionotropic receptors, such neurotransmitter binding can cause the opening of ion channels and subsequent ion influx and depolarisation or hyperpolarisation of the postsynaptic cell, in effect communicating an electrical signal between the pre- and postsynaptic partners (Eccles 1964).

[2] Canonically – but backpropagating action potentials may also occur, cf. Chapter 3.

Neurotransmitter is thought to be released in discrete quanta (Fatt and Katz 1952, Del Castillo and Katz 1954).

As such, groups of connected neurons may be conceived of as forming a circuit analogous to an electrical circuit. However, whilst it is a common assumption that a train of action potentials is represented equally at the presynaptic terminal as at the axon initial segment (Douglas, Markram et al. 2004), this is not necessarily the case between pre- and postsynaptic partners; modifications to relayed information may take place at the synapse and / or in the postsynaptic cell – phenomena that both complicate and increase the power of neural computation.

As a simple example, synaptic transmission is principally one of two types, with opposing effects on the postsynaptic cell; excitatory transmission occurs mainly with the release of the neurotransmitter glutamate, whilst inhibitory transmission is chiefly carried out by the neurotransmitters γ-Aminobutyric acid (GABA) and glycine. As activation of ionotropic glutamate receptors such as AMPA (α -Amino-3-hydroxy-5-methyl-4-isoxazolepropionic acid) or NMDA (N-methyl-D-aspartate) receptors typically results in a net influx of positive ions, whilst activation of GABA receptors such as the ionotropic $GABA_A$ receptor results in e.g. an influx of negatively charged chloride ions, excitatory and inhibitory neurotransmission thus converts similar presynaptic activity into depolarising or hyperpolarising postsynaptic responses respectively (Eccles 1964, Douglas, Markram et al. 2004).

Synaptic connections are not limited to point-to-point excitatory or inhibitory transmission via glutamate and GABA. Whilst the action of those two neurotransmitters are usually thought of as fast (<1 ms) and short in duration (~ tens of ms) when acting though ionotropic receptors, these and other transmitters may have more tonic actions through e.g. metabotropic receptors acting though second messengers (McCormick 2004). Furthermore, the nature of synaptic transmission may be affected by neuromodulators such as 5-hydroxytryptamine (5HT) or dopamine, which

can be released as volume transmitters affecting many cells; whilst neuromodulation is not discussed in detail in this thesis, it is important to be aware of this as a further system affecting circuit function, with the possibility of quite specific effects on particular circuits (see 1.3 and (Bargmann and Marder 2013)).

1.7. Synaptic dynamics

In addition to circuit properties emerging from the presence of differing cell types, circuit features may be affected by differences at the level of the synapse. Far from being a simple point of excitatory or inhibitory transmission, synapses are known to undergo dynamic changes in strength, both in the short-term (during trains of activity) and long-term (over minutes, hours and years). As the output of neurons must be determined in part by the strength of their synaptic inputs, the constant flux of these input strengths is likely to have an important and integral role in circuit function. Below is a brief overview of the function and mechanisms of such synaptic plasticity on both the long (minutes to weeks and longer) and short (tens of ms to minutes) term scales; the scope of this thesis is mainly concerned with the phenomenology and functional implications of cell-type-specific differences in short-term synaptic plasticity and transmission.

1.7.1. Long-term synaptic plasticity

One of the most studied forms of dynamic changes in synaptic strength is that on the time scale of hours to days (perhaps longer); such changes are referred to as long-term synaptic plasticity, and are widely thought to underlie, for example, learning and memory (Bliss and Collingridge 1993, Nabavi, Fox et al. 2014). Although others before may have suggested similar ideas (Markram, Gerstner et al. 2011), the most well-known suggestion of such a process comes from (Hebb 1949):

> *"When an axon of cell A is near enough to excite cell B and repeatedly or persistently takes part in firing it, some growth process or metabolic*

change takes place in one or both cells such that A's efficiency, as one of the cells firing B, is increased."

The first physiological evidence for such a phenomenon was found some years later (Bliss and Lomo 1970, Bliss and Lomo 1973, Lomo 2003). That such long-term potentiation (LTP), where high-frequency electrical stimulation resulted in increased EPSP (excitatory postsynaptic potential) amplitude, was observed in hippocampus (an area involved in memory) provided support for the link between Hebb's postulate and learning and memory – subsequently inspiring a huge amount of experimental work (Bliss and Collingridge 1993, Malenka and Nicoll 1999). An opposite effect where failure of a presynaptic cell to cause its postsynaptic partner to fire, leading to depression of that input's strength, is also evident and termed long-term depression (LTD) (Linden and Connor 1995). Canonically, long-term synaptic plasticity is thought to depend on differing amounts of Ca^{2+} entry via postsynaptic NMDA receptors, with large amounts causing LTP and smaller amounts causing LTD, although see (Nicoll and Malenka 1995).

Long-term plasticity has been found to involve many more phenomena than canonical Hebbian potentiation, for example spike-timing-dependent plasticity has been described (Abbott and Nelson 2000, Markram, Gerstner et al. 2011) where plasticity is induced by the precise timing of action potentials in pre- and postsynaptic cell pairs, and may follow Hebbian, anti- or non-Hebbian rules (for example LTP when a postsynaptic spike precedes a presynaptic spike). Cortical plasticity may depend on a combination of such mechanisms involving rate, timing and cooperativity of inputs (Sjostrom, Turrigiano et al. 2001). Similarly, multiple mechanisms for long-term plasticity are evident across brain areas and synapse and cell-types; for example, timing-dependent LTD (tLTD) may depend on pre- or postsynaptic NMDA receptors at different connections in cortex (Duguid and Sjostrom 2006, Larsen, Smith et al. 2014).

Whilst some of the results presented in this thesis have implications for long-term plasticity (see for example Chapter 4), it is not the primary focus of this

thesis, and as such is not discussed in detail here – for reviews see e.g. (Linden and Connor 1995, Abbott and Nelson 2000, Feldman 2009, Markram, Gerstner et al. 2011).

1.7.2. Short-term synaptic plasticity

In addition to the long-term synaptic plasticity summarised above, short-term changes in synaptic dynamics are also evident over much smaller time scales, from milliseconds to seconds (Zucker and Regehr 2002, Regehr 2012). Such short-term plasticity (STP) can result in both facilitation and depression of postsynaptic responses (or a mixture), and is chiefly thought to result from presynaptic mechanisms, although some postsynaptic effects such as receptor desensitisation are also important (Zucker and Regehr 2002, Regehr 2012). STP is usually measured with reference to the paired-pulse ratio (PPR; sometimes extended to multiple pulses in a train), where $PPR = \frac{A_2}{A_1}$, with A = amplitude of postsynaptic response; as such, STP has PPR with depression < 1 < facilitation (Regehr 2012). Measures describing facilitation have also been used (Atluri and Regehr 1996). Short-term plasticity can also describe changes in strength on longer time scales (tens of seconds to minutes) such as augmentation or long-lived depression, however these are not discussed in detail here (Regehr 2012).

Short-term facilitation

Short-term facilitation (STF) is the phenomenon where, for example, postsynaptic EPSPs increase in amplitude during stimulation from a presynaptic action potential train. Most proposed mechanisms underlying STF involve presynaptic Ca^{2+} changes during a train (Zucker and Regehr 2002, Regehr 2012), including simple increases in residual calcium affecting synaptotagmin-mediated release (Katz and Miledi 1968, Fernandez-Chacon, Konigstorfer et al. 2001), calcium acting via a distinct calcium sensor with slower kinetics (Bertram, Sherman et al. 1996), saturation of calcium buffers (Rozov, Burnashev et al. 2001) or modulation of voltage-gated calcium channels (Ishikawa, Kaneko et al. 2005). Presynaptic calcium-permeable

ionotropic receptors such as kainate receptors may also contribute (Sun and Dobrunz 2006).

Short-term depression

Short-term depression (STD) is seen as the inverse of STF – a decrease in amplitude of postsynaptic responses during a train. Whilst STD is similarly thought to result from mainly presynaptic mechanisms (Zucker and Regehr 2002, Regehr 2012), these may be somewhat different to those in STF, and as such have a contrasting effect. One popular theory to explain synaptic depression is that it is caused by depletion of the readily releasable pool of synaptic vesicles; that is, release probability is sufficiently high enough, and replenishment sufficiently slow enough that pulses subsequent to the first in a train will lead to less vesicle release and depressed postsynaptic responses (Zucker and Regehr 2002, Regehr 2012). However, this model may not be comprehensive as, for example, at some synapses the magnitude of depression is not dependent on the size of the first stimulus in a train (Thomson and Bannister 1999). Other suggested mechanisms include impaired vesicle fusion following previous fusion and release, or use-dependent changes / reductions in presynaptic calcium entry (Regehr 2012).

Functional implications of short-term plasticity

Such differences in short-term dynamics at synapses may have specific functional consequences for information processing in neural circuits. A simple example of this would be filtering properties; conceptually, it is easy to imagine how a facilitating synapse acts as a high-pass filter by preferentially transmitting information during high-frequency activity, and a depressing synapse acts as a low-pass filter by accentuating the first (and not subsequent) spikes in a presynaptic train. Such properties could be combined to produce functionally relevant circuits; for example, a simple three-cell circuit with one postsynaptic neuron innervated by two separate presynaptic cells with opposite plasticity could result in direction or temporal sensitivity (Figure 1-4), as if the facilitating synapse is activated before the

depressing synapse this should result in a larger postsynaptic response than vice-versa (Regehr 2012).

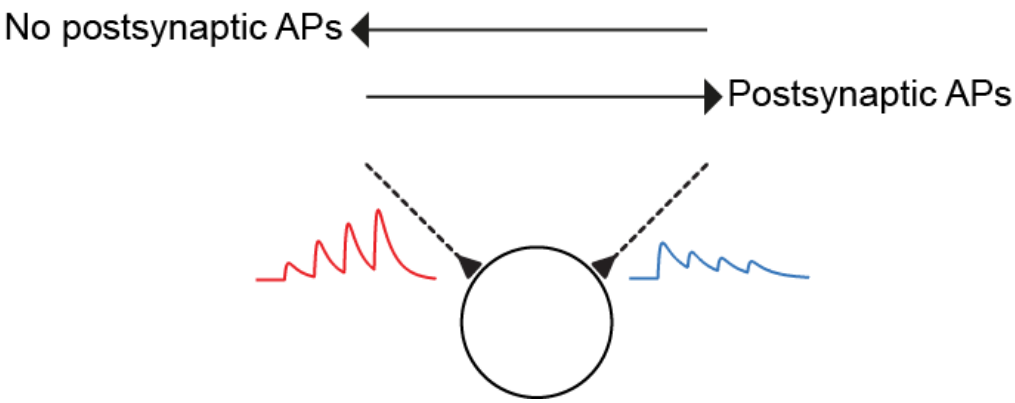

Figure 1-4: Direction selectivity as a consequence of STP

As discussed in the text and reviewed in (Zucker and Regehr 2002, Regehr 2012, Blackman, Abrahamsson et al. 2013), STP may have specific functional consequences. Above is a simple illustration of this in a three-cell circuit, where one postsynaptic cell is contacted by a facilitating synapse (left) and a depressing synapse (right). If the facilitating synapse is activated before the depressing synapse, the postsynaptic cell should receive a larger input that the converse, as higher amplitude depolarisations from each synapse should coincide. In other words, if the stimulus moves from left to right, this should result in a larger postsynaptic depolarisation than if the stimulus moves from right to left.

Similarly, depressing synapses may be involved in sensory adaptation and gain control (Abbott, Varela et al. 1997), whilst facilitating synapses could detect bursts of activity (Matveev and Wang 2000). The possibility of such differences warrants investigation of whether differing forms of STP are displayed at particular synapses and pathways or at different stages of development; such observations may imply and provide evidence for STP controlling the specific transfer of particular parts of information to e.g. different cell types or functional subnetworks – cf. (Zucker and Regehr 2002, Regehr 2012, Blackman, Abrahamsson et al. 2013). As discussed below and in later chapters, specific differences in STP may affect the spatiotemporal remapping of inhibition (Silberberg and Markram 2007, Berger, Silberberg et al. 2010).

1.8. Cell-type-specific circuit properties

As discussed above, the multiple intrinsic and integrative properties of differing neural cell types, along with the dynamic and plastic nature of synaptic transmission, significantly complicate the task of understanding how the functional properties of cells and circuits emerge from the underlying anatomy and physiology. Just as connections between neocortical pyramidal cells appear to be non-random (Song, Sjostrom et al. 2005) with functionally related cells forming sub-networks (Ko, Hofer et al. 2011), connections between distinct cell types appear to have different and specific synaptic and connective properties (Brown and Hestrin 2009a). For example, in contrast to connections between excitatory cells, PV and SOM expressing inhibitory neurons appear to form unspecific connections to many pyramidal cells (Fino and Yuste 2011, Packer and Yuste 2011). Fully understanding cortical circuit function may thus require both robust identification of cell types and the rules that govern connectivity and synaptic dynamics between them. Whilst cell-type specificity is evident across properties such as long-term plasticity (Nissen, Szabo et al. 2010) and connectivity (Lee and Reid 2011) amongst others, one area where an increasing body of research suggests specific and functionally relevant differences is in cell-type-specificity in short-term plasticity (Blackman, Abrahamsson et al. 2013).

1.9. Cell-type-specific short-term plasticity in neocortex

It may be a useful feature of cortical processing for cells to convey different elements of their input to functionally distinct outputs, such as different cell types; for example, short-term facilitating synapses may emphasise high frequency spike trains, whilst short-term depressing synapses may prioritise temporal coherence of inputs over rate coding. Interestingly, increasing evidence in many brain areas suggests that even a single presynaptic cell may exhibit stereotyped short-term plasticity dependent on both pre- and postsynaptic cell type, implying both that different cell types may

preferentially transmit and receive different information, and that postsynaptic cell type may influence the molecular and functional properties of the presynapse (Blackman, Abrahamsson et al. 2013).

Some of the earliest evidence for such cell-type-specific STP was described in crustacean motor synapses, where a particular motor axon may exhibit either facilitation or depression dependent on postsynaptic muscle fibre identity (Atwood 1967, Atwood and Bittner 1971). Advances in techniques such as multiple cell patch-clamp recordings have allowed the more recent investigation of such properties in neocortex (along with other areas; see Chapter 6 for discussion and Figure 1-5). In developing rat somatosensory cortex, L5 PCs were found to connect to other PCs with depressing synapses and bipolar INs with facilitating synapses, even when the synapses were formed from the same presynaptic axon (Markram, Wang et al. 1998).

Further differentiation of target-cell-specific STP in neocortex has been possible with the combination of multi-cell electrophysiology and anatomical and genetic characterisation of cell types. In L2/3, connections from PCs to bitufted, SOM-expressing INs exhibited facilitation, whilst connections to multipolar, PV-expressing INs exhibited depressing synapses (Reyes, Lujan et al. 1998). In agreement, bouton calcium levels are reported to depend on the target cell, with L2/3 PC connections to multipolar INs exhibiting three times larger Ca^{2+} signals than connections to bitufted INs (Koester and Johnston 2005). Similarly, inhibitory connections from bitufted cells could be facilitating when contacting other bitufted cells, whilst connections to multipolar INs were depressing (Reyes, Lujan et al. 1998). Indeed, it has been reported that many different types of neocortical IN may form synapses with target-specific dynamics onto different IN types and PCs; importantly, these dynamics are also affected by presynaptic cell type – distinct anatomically and electrophysiologically defined IN types formed stereotyped synapses onto PCs (Gupta, Wang et al. 2000).

Whilst it is perhaps easier to study cell-type-specific differences in STP at connections from excitatory cells to either excitatory cells or inhibitory cells

due to the clearer distinction between cell types, this does not preclude differences in STP between excitatory cell types (Markram, Wang et al. 1998). However, comparison of reported STP between studies of excitatory-excitatory connections suggest smaller differences; neocortical L4 stellate cells connect with depressing synapses (Egger, Feldmeyer et al. 1999), as do L4-L2/3 connections (Brasier and Feldman 2008) and L5 PC-PC connections (Markram, Wang et al. 1998).

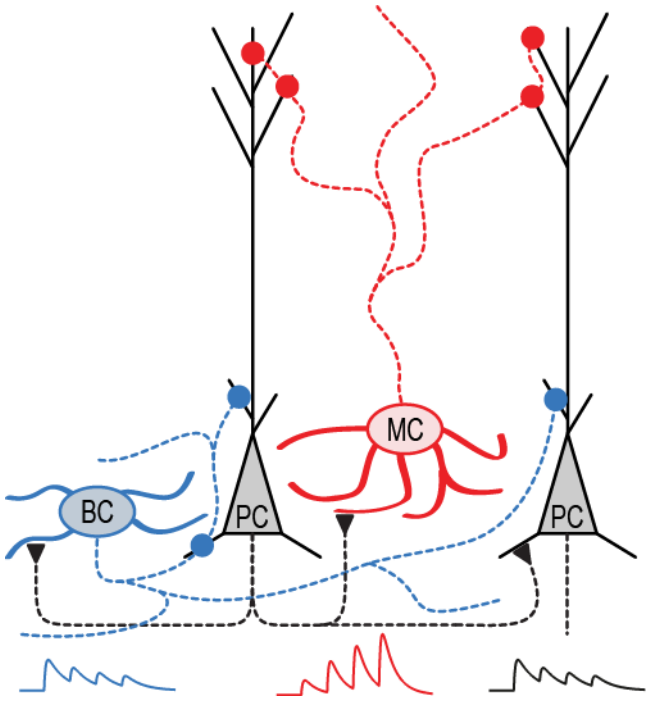

Figure 1-5: Cell-type-specific STP in neocortical layer 5

In developing neocortical L5, PCs connect to both PCs (black) and BCs (blue) with depressing synapses, whilst PC-MC (red) connections are facilitating (Markram, Wang et al. 1998, Silberberg and Markram 2007). Because of this, MCs are activated later during high-frequency firing, leading to temporally separated perisomatic and (apical) dendritic inhibition mediated by BCs and MCs respectively (due to the location of IN-PC synapses) (Silberberg and Markram 2007, Buchanan, Blackman et al. 2012). Dotted lines = axon, thick lines = dendrite. All synaptic traces (bottom of figure) are purely illustrative and are simulated based on data in (Buchanan, Blackman et al. 2012). Figure adapted from (Blackman, Abrahamsson et al. 2013).

1.9.1. Functional implications of cell-type-specific STP

Cell-type-specific differences in STP may underlie particular functional effects in the neocortical microcircuit. For example, L5 PCs connect to BCs with depressing synapses, whilst connections to MCs are facilitating; this allows two temporally distinct inhibitory microcircuits between PCs to be

activated by the same (or different) stimuli – a frequency-independent BC-mediated disynaptic inhibition, and a frequency-dependent disynaptic inhibition (FDDI) mediated by MCs, requiring high-frequency presynaptic AP trains (Silberberg and Markram 2007). As MCs typically target PC apical dendrites whilst BCs target the perisomatic region, differences in STP may thus result in sequential somatic and dendritic inhibition in PCs during high-frequency firing (Markram, Toledo-Rodriguez et al. 2004, Silberberg and Markram 2007, Buchanan, Blackman et al. 2012). MC-mediated FDDI may be particularly suited to self-limit and synchronise activity during high-frequency firing (Berger, Silberberg et al. 2010). Similarly, as L5 PC plasticity is affected by the degree of dendritic depolarisation (Sjostrom and Hausser 2006), MC inhibition may modulate this.

Cell-type-specific changes in STP have been observed in response to sensorineural hearing loss; whilst thalamic drive onto fast-spiking INs was reduced after cochlear ablation, thalamic inputs to low threshold-spiking INs remained strong but shifted from facilitation to depression (Takesian, Kotak et al. 2013). As both these apparently differing effects acted to reduce inhibitory output onto L2/3 PCs, it may be the case that contrasting changes in cell-type-specific STP act in concert to for example compensate for diminished activity after sensory deprivation.

1.9.2. Developmental changes in STP

A further complicating facet of short-term plasticity that perhaps implies specific developmental roles for particular forms of STP is its tendency to change with age; in several brain regions and synapse types, STP appears to switch from depression to more facilitating dynamics (i.e. from high to lower probability of release) – cf. (Reyes and Sakmann 1999, Zhang 2004, Oswald and Reyes 2008, Cheetham and Fox 2010). It has been suggested that such a switch may relate to the development of inhibition, as mature inhibition may allow synapses to display a wider range of STP without risking runaway excitation (Cheetham and Fox 2010). Such changes may be the result of developmental alterations in transmitter release mechanisms and

calcium signalling; for example, at the calyx of Held[3], a reduction in depression between P7 and P14 (Iwasaki and Takahashi 2001) is accompanied by a shift from expression of N-type to P/Q-type Ca^{2+} channels (Iwasaki and Takahashi 1998), although such Ca^{2+} channel changes are not seen in visual cortex (Iwasaki, Momiyama et al. 2000).

Such developmental switches in STP may occur at different times; for example the switch occurs later in visual cortex than barrel cortex (Cheetham and Fox 2010). Whilst this may imply that particular sensory experience is required for the change in STP to occur, as visual cortex develops more slowly (Cheetham and Fox 2010), experiments in auditory cortex organotypic slice culture, and hippocampus with activity reduced via tetanus toxin injection still observed the STP switch (Wasling, Hanse et al. 2004, Chen and Buonomano 2012). As such, it may be the case that developmental STP changes may rely on different mechanisms in different areas. Similarly, it may be the case that differential STP development allows the STP of certain synapses to become either more similar or dissimilar with age; for example, thalamic connections onto fast-spiking INs in auditory cortex develop to be more depressing whilst those onto low-threshold-spiking INs become more facilitating (Takesian, Kotak et al. 2013). Whilst neither of these ideas has been explored extensively to the knowledge of the author, the fact that STP can change with age adds another element and complicates the interpretation of studies performed at particular developmental stages (for instance Chapter 4).

1.10. Cell-type-specific mechanisms controlling transmitter release

1.10.1. Signalling cell-type identity

The existence of cell-type-specific forms of STP suggests that synapse-specific mechanisms for stereotyped control of neurotransmitter release exist, perhaps in contrast to, for example, STP being altered by active

[3] A very large synapse in the auditory brainstem.

learning rules (Markram and Tsodyks 1996), although these may still be present. Indeed, it may be the case that presynaptic terminal properties may even be determined in part by the identity of their postsynaptic partners (Sylwestrak and Ghosh 2012, Blackman, Abrahamsson et al. 2013); for example, expression of a transsynaptic regulator gene, Elfn1, may signal the identity of SOM-positive *oriens lacunosum-moleculare* (OLM) INs to their presynaptic partners in hippocampal CA1, and in turn promote facilitation (Sylwestrak and Ghosh 2012). This may be controlled by synapse-specific expression of presynaptic GluR6-containing kainate receptors (Sylwestrak and Ghosh 2012). Signalling of identity between pre- and postsynaptic cells through such mechanisms may be a step in the establishment of stereotyped cell-type-specific synaptic properties; it has been speculated that such processes may take place through the interaction of particular synaptic adhesion molecules such as cadherins or neuroligins (Dalva, McClelland et al. 2007, Blackman, Abrahamsson et al. 2013).

1.10.2. Presynaptic ionotropic receptors

Whilst e.g. synaptic adhesion molecules may be involved in signalling cell identity, the subsequent regulation of neurotransmitter release and synaptic properties could be achieved by a wide variety of potential mechanisms; for example through RIM proteins controlling vesicle priming (Deng, Kaeser et al. 2011, Han, Kaeser et al. 2011) or expression of differing Munc13 isoforms (Rosenmund, Sigler et al. 2002) – also cf. (Zucker and Regehr 2002, Thomson 2003).

In addition to the above and other factors – including postsynaptic synapse-specific receptor expression (Toth and McBain 2000) – increasing evidence suggests a role for presynaptic ionotropic receptors in control of neurotransmitter release (Engelman and MacDermott 2004). Such processes could be ideally placed to regulate short-term plasticity and cell-type-specificity in synaptic properties with e.g. synapse-specific expression of certain presynaptic receptors modulating release probability.

As an example, presynaptic kainate receptors (a form of ionotropic glutamate receptor) are present at many synapses and may regulate neurotransmitter release (Chittajallu, Vignes et al. 1996, Engelman and MacDermott 2004). Interestingly, these receptors have been reported to underlie differential target-cell-specific effects, being involved in synaptic depression at cerebellar parallel fiber – stellate cell synapses and facilitation at parallel fiber – Purkinje cell synapses during high-frequency stimulation (Delaney and Jahr 2002). In hippocampus, activation of presynaptic kainate receptors may promote facilitation at Schaffer collateral synapses onto SOM-expressing, but not other INs (Sun and Dobrunz 2006), suggesting that differential expression of presynaptic receptors at particular synapses may in part control STP and thus elements of information transfer.

Presynaptic ionotropic control of neurotransmitter release is not limited to that mediated by kainate receptors; also implicated are presynaptic $GABA_A$ receptors, AMPA receptors and NMDA receptors, amongst others (Engelman and MacDermott 2004). As an illustration, cerebellar molecular layer interneurons express presynaptic Ca^{2+} permeable AMPA receptors at connections to other molecular layer interneurons, but not at basket cell – Purkinje cell synapses, suggesting that different subtypes of receptor may be selectively expressed at particular connections and in turn have differential effects on transmitter release (Rossi, Maton et al. 2008).

At certain synapses, transmitter release may be modulated by presynaptic NMDA receptors (preNMDARs; see Chapter 4). PreNMDARs have been described at many CNS synapses, where in many cases they facilitate transmitter release – cf. (Corlew, Brasier et al. 2008, Duguid and Smart 2009, Larsen, Corlew et al. 2011, Rodriguez-Moreno, Kohl et al. 2011, Buchanan, Blackman et al. 2012, Blackman, Abrahamsson et al. 2013, Duguid 2013, Kunz, Roberts et al. 2013). In neocortex, evidence suggests that preNMDAR expression may be synapse-specific, with L4-L2/3 synapses expressing preNMDARs and L4-L4 synapses lacking preNMDARs (Brasier and Feldman 2008). As such, preNMDARs may be an attractive candidate in controlling synaptic efficacy and dynamics in a cell-type-specific as well as

pathway-specific manner – cf. (Brasier and Feldman 2008, Buchanan, Blackman et al. 2012, Blackman, Abrahamsson et al. 2013, Larsen, Smith et al. 2014).

1.11. What defines a cell type?

The combination of short- and long-term changes in synaptic strength, integrative properties of cells, specific innervation domains, receptor expression and modulatory processes, amongst others, significantly complicate and lend power to cortical circuit function. Untangling and elucidating the function and specific expression of such circuit properties is thus a daunting task. However, much evidence, including that described in earlier sections, suggests that such properties are often stereotyped in a cell-type specific manner (Brown and Hestrin 2009a, Blackman, Abrahamsson et al. 2013). As such, determining and identifying what constitutes a particular cell type is perhaps an important and useful first step in understanding more complex circuit functions. However, this is no trivial task in itself; neurons exhibit a wide variety of physiological, genetic, functional and anatomical features that may be used to group them into classes, and determining what constitutes distinct classes versus within-class variation is a complex problem (Ascoli, Alonso-Nanclares et al. 2008). Furthermore, different labs and research groups use different criteria and language to describe cell types, additionally complicating cross-group data comparisons (DeFelipe, Lopez-Cruz et al. 2013).

Despite these issues, there seems to be broad agreement that neurons, and cortical interneurons in particular, are comprised of distinct or cardinal cell classes (Gupta, Wang et al. 2000, Markram, Toledo-Rodriguez et al. 2004, Ascoli, Alonso-Nanclares et al. 2008, DeFelipe, Lopez-Cruz et al. 2013, Kepecs and Fishell 2014). What defines a particular cardinal type is perhaps a point of more contention – studies have focused on genetic markers, electrophysiological properties, developmental origin, channel expression and functional properties, amongst others – for reviews see (Markram, Toledo-Rodriguez et al. 2004, Kepecs and Fishell 2014). This said, many

studies have elaborated on traditional descriptive anatomical classes (Ramón y Cajal 1911), focussing on the quantification of axonal morphology as an indicator of type (Ascoli 2006, Ascoli, Donohue et al. 2007, Ascoli, Alonso-Nanclares et al. 2008, Halavi, Hamilton et al. 2012, DeFelipe, Lopez-Cruz et al. 2013). Such anatomically defined classes may correlate well with the expression patterns of multiple genetic markers (Toledo-Rodriguez, Goodman et al. 2005), providing support for this method of classification.

It has been suggested that interneuron types may be ultimately defined by function (Kepecs and Fishell 2014), including computational functions such as subtraction and division (Wilson, Runyan et al. 2012) or circuit roles such as disinhibitory control (Kuhlman, Olivas et al. 2013, Pi, Hangya et al. 2013). However, in order to fully understand function it may be necessary to separate cell types using a combination of the previously described methods, as for example *in vivo* experiments focussing on genetically defined cell types using a single marker may not select homogenous populations with homogenous properties (Toledo-Rodriguez, Goodman et al. 2005, Kepecs and Fishell 2014). As such, anatomical characterisation, particularly when used in combination with genetic and physiological techniques, may provide an invaluable and complementary approach to elucidate distinct cell types which can then be related to functional properties both *in vitro* and *in vivo* – cf. (Gupta, Wang et al. 2000, Oliva, Jiang et al. 2000, Wang, Gupta et al. 2002, Chattopadhyaya, Di Cristo et al. 2004, Markram, Toledo-Rodriguez et al. 2004, Wang, Toledo-Rodriguez et al. 2004, Ascoli, Alonso-Nanclares et al. 2008, McGarry, Packer et al. 2010, Fino and Yuste 2011, Hofer, Ko et al. 2011, Katzel, Zemelman et al. 2011, Packer and Yuste 2011, Buchanan, Blackman et al. 2012, DeFelipe, Lopez-Cruz et al. 2013, Harris and Mrsic-Flogel 2013, Kepecs and Fishell 2014).

1.12. Aims of this study

This thesis aims to increase understanding of target-cell-specific properties of neocortical circuits by both the development and assessment of methods to identify cell types, and the application of these to a particular biological

question: the expression pattern and function of presynaptic NMDA receptors in developing mouse visual cortex. In **Chapter 3**, the utility of 2-photon imaging as a timesaving method from which to create 3D reconstructions of neurons and classify cells (but not to carry out multicompartmental simulations) is explored and verified in a way that should influence the design of future experiments. Using this method, the target-cell-specific expression pattern of presynaptic NMDA receptors in neocortical L5 (from PCs to other PCs and INs) is elucidated in **Chapter 4**. In **Chapter 5**, the results and cell types identified in previous chapters are used in the development and verification of a method to extract morphometrics directly from image stacks (bypassing reconstruction), which can be used to classify cortical INs; this may offer an even faster method to explore cell-type-specific properties in future high-throughput studies.

2. Materials and Methods

2.1. Slice preparation

All procedures were performed in accordance with the *UK Animals (Scientific Procedures) Act 1986* and the *Canadian Council on Animal Care* guidelines, with licences as appropriate. 300-µm-thick acute near-coronal slices containing primary visual cortex were obtained from P12 – P20 mice, unless otherwise stated. All "wild-type" experiments were performed using the C57BL/6 strain (Jackson Labs #664).

Slices were prepared as previously described for rat (Sjostrom, Turrigiano et al. 2001): mice were anaesthetised with isoflurane and decapitated. The brain was then quickly dissected in ice-cold artificial cerebrospinal fluid (aCSF), bubbled with 95% O_2 / 5% CO_2. A cut was made along the midline of the scalp to remove skin and fur, followed by careful removal of the skull with small forceps after cutting along the midline and making two small incisions at the base in the transverse plane. The brain was then directly removed to a dish with a 5% Sylgard base containing ice-cold aCSF (containing, in mM; NaCl 125, KCl 2.5, $MgCl_2$ 1, NaH_2PO_4 1.25, $CaCl_2$ 2, $NaHCO_3$ 26, Dextrose 25). Here, it was bisected along the midline and the cerebellum was removed. A section containing visual cortex was obtained from each hemisphere with a cut around 20˚ posterior to the coronal plane. These sections were then placed, on the cut surface, in the ice-cold aCSF filled slicing chamber of a Leica VT1200S vibratome, where 300-µm-thick sections were cut. Slices were then transferred to a chamber containing carbogenated aCSF where they were incubated at 37°C for up to one hour, followed by cooling to room temperature and storage for up to 5 hours. Slices used for experiments were typically the 3rd to 6th slices cut.

2.2. Basic electrophysiology

All electrophysiological experiments were carried out at 32-34°C, controlled by a Scientifica Ltd inline heater, and recorded and monitored offline in Igor Pro 6 (WaveMetrics Inc., Lake Oswego, OR) running in-house custom software (Sjostrom, Turrigiano et al. 2001).

For recording, slices were placed in the recording chamber of a SliceScope (Scientifica Ltd.) system. Slices were secured with a u-shaped platinum harp with fine nylon fibres. Slices were perfused with carbogenated aCSF using a Dymax 5 pump (Charles Austen); perfusion was set manually to ~5 ml/min.

2.2.1. Visualisation of slices and target cells

Slices were targeted using a SliceScope (Scientifica Ltd) and infrared video Dodt contrast (custom-built with a 1X telescope using Thorlabs LA1401 plano-convex lenses, a DG20-1500-MD diffuser and a hand-cut spatial filter made of blackout foil; mounted with QRC2A cage plates in a 60 mm cage). Neurons were patched at 400X or 600X magnification, using Olympus objectives (40X, 0.8 NA and 60X, 1.0 NA).

Medial primary visual cortex was targeted based on the presence of a granular layer 4. Cortical layer 5 was targeted below this layer and verified by the presence of the large ovoid somata (~10-20 μm in diameter) of L5 pyramidal cells, along with their thick apical dendrite. Interneurons were targeted by smaller, round somata (~8-10 μm), and where recorded cells are referred to as “INs” it indicates these ‘blind’ patched cells (i.e. targeted without transgenic fluorescent protein expression). Further confirmation of targeting specificity was gained by morphological analysis, investigation of firing properties and use of transgenic animals (see below). All recordings were made in L5; on the rare occasion that post-hoc inspection of Dodt contrast stacks revealed a L4 or L6 location, these recordings were discarded.

2.2.2. Data acquisition

All whole-cell electrophysiology recordings were made in current clamp (unless otherwise stated) using a MultiClamp 700B (Molecular Devices, Sunnyvale, CA) amplifier. Current clamp recordings were acquired at 10 kHz and filtered at 5-6 kHz to remove high frequency noise using PCI-6229 boards (National Instruments, Austin, TX) and custom software (Sjostrom, Turrigiano et al. 2001) running in Igor Pro.

2.2.3. Whole-cell patch-clamp recordings

Patch pipettes were pulled using a P-1000 electrode puller from Sutter Instruments, using medium-wall borosilicate capillaries. Pipettes were filled with internal solution containing (in mM; Na-Phosphocreatine 10, NaGTP 0.3, MgATP 4, K-HEPES 10, K-Gluconate 115, KCl 5). Internal solution was adjusted to 310 mOsm with sucrose to match mouse physiological osmolality (Bourque 2008), and aCSF to 338 mOsm, as this qualitatively increased the reliability and quality of recordings.

Pipettes were held and controlled by PatchStar micromanipulators (Scientifica Ltd). Positive pressure was applied before immersion in the bath solution to keep the pipette tip clear. Pipette offset was adjusted using the MultiClamp software in current clamp, thus setting voltage to 0 mV. Pipette resistance (R_{pip}) was ascertained by measuring the average steady state voltage response to the last 5 ms of 32 8-ms-long current steps of 1 nA at 50 Hz, as $V_{pip} = I_{pip} \cdot R_{pip}$; values of R_{pip} were 4-6 MΩ.

Pipettes were moved towards cells so that a dimple appeared on the cell surface. In voltage clamp with 0 mV holding voltage, positive pressure was released – and slight negative pressure applied if needed – to form a GΩ seal (<10 pA current in response to 10 mV test pulse). Holding voltage was switched to -70 mV (at which point holding current usually dropped to ~10 pA), and the membrane was perforated with negative pressure. Recordings were then made in current clamp, preferably with 0 pA holding current

(however some initially depolarised cells required a hyperpolarising holding current of ~10-50 pA to recover before recording).

During recordings, custom software measured series resistance, perfusion temperature, input resistance, resting membrane potential and EPSP amplitude. Series resistance and junction potential were not compensated. Recordings with >30% change in input resistance (measured with a 250 ms, 25 pA hyperpolarising current step) were discarded, as were those with more than 8 mV change in resting membrane potential. Series resistance was measured in current clamp by fitting a double exponential (Igor built-in) to the voltage drop in response to the hyperpolarising current step at the start of each trace; the amplitude of the faster drop was used with Ohm's law to calculate R_S.

2.2.4. Paired recordings

Connections between cells in neocortical L5 are sparse – particularly for PCs where the rate is ~10-15 % (Song, Sjostrom et al. 2005) – although connection rates from inhibitory cells to PCs may be higher (Packer and Yuste 2011). For this reason, quadruple simultaneous whole-cell recordings were used when recordings from paired cells were required, as the number of potential connections scales with electrode number as n • (n-1). With this method, GΩ seals were formed on four cells and broken through in quick succession, as this should result in more equal dialysis of cells.

To assess connectivity, five spikes were generated in each cell every 18 seconds at 30 Hz in all neurons during experiments (using 0.7-1.4 nA current injections). Spike trains were offset by 700 ms or more in each cell to prevent induction of long-term plasticity (Sjostrom, Turrigiano et al. 2001). Averages of 10-40 traces were used to determine connections.

2.2.5. Extracellular stimulation

In some experiments, extracellular stimulation was employed to elicit responses in a single patched cell in place of presynaptic spikes (as in paired

recordings). Here, aCSF filled stimulating electrodes with 2-10 µm tips were used. Electrodes were monopolar (medium wall patch pipette capillaries) or bipolar (theta-glass electrodes) with no apparent differences. Stimulating electrodes were placed around 20-100 µm from the recorded cell, within L5. After this, the position of the electrode and stimulation strength was altered until a stable and uncontaminated EPSP was achieved in the recorded cell. This required short-latency depolarising responses with a single peak, and the lack of variable-latency inhibitory down-strokes. Stimulated EPSPs did not change in amplitude during the baseline period (stability assessed with a *t*-test of Pearson's r). Once the above requirements were fulfilled, electrode position and stimulation strength remained constant throughout experiments. Stimulation was biphasic 100-200 µs long pulses delivered in constant voltage mode using an ISO-STIM 01D (NPI Electronic GmbH, Tamm, Germany) electrical stimulus isolator. Stimulation amplitude varied for different target cells but was around 15-40V.

2.2.6. Pharmacology

To block NMDA receptor activation extracellularly, D/L-APV (Sigma) was used at a concentration of 200 µM in aCSF, either bath applied or puffed with a micropipette. To enable cell-specific internal blockade of NMDA receptors, MK801 (Sigma) was applied at 2 mM in internal solution. When MK801 was used, positive pressure was minimised when patching cells in order to prevent unwanted blockade of NMDARs in other cells. In quadruple recordings, only one of the four cells was patched with MK801, and this was always the first cell patched.

2.2.7. Analysis of electrophysiology experiments

Evoked responses

EPSPs evoked by presynaptic spikes (paired recordings) or extracellular stimulation in recorded cells were averaged during baseline (5-10 mins long) and experimental (drug application) conditions. Experiments with unstable baseline were discarded, as determined by *t*-test of Pearson's r. To assess

drug effect, suppression of neurotransmission (preNMDAR mediated) was investigated. This was assessed by the ratio of the amplitude of the first EPSP in a train during drug application to that during baseline.

Short-term plasticity was assessed to investigate locus of effect. As in (Atluri and Regehr 1996) paired-pulse facilitation was measured as the difference between the first and second EPSP amplitudes in a train normalised to the amplitude of the first EPSP, defined as

$$PPF = \frac{EPSP_2 - EPSP_1}{EPSP_1}$$

with $EPSP_i$ as the i^{th} EPSP in a train. Although 30 Hz trains of 5 spikes were always used as stimulation, including responses $EPSP_3$ and beyond did not change results (Sjostrom, Turrigiano et al. 2007), so only PPF is reported. Changes in PPF after drug application were defined as

$$\Delta PPF = PPF_{drug} - PPF_{baseline}$$

As short-term plasticity depends mostly on presynaptic mechanisms (Zucker and Regehr 2002), changes in PPF should indicate a presynaptic effect.

Quantal analysis is a technique originally developed based on the view, at the neuromuscular junction, that the observed amplitude of evoked responses seems to vary in a step-wise manner where responses are multiples of a unit size corresponding to that of a spontaneous potential (Del Castillo and Katz 1954). Whilst for very low release probabilities such quantal release may be described by Poisson statistics, for higher release probabilities a binomial model may be more appropriate. Here, a simple binomial model is often used, with constant P and n for certain release conditions (as described below) (McLachlan 1978). Further complicating factors may be evident, particularly at central synapses. For instance, the amplitude of responses may be affected by dendritic filtering, nonlinear summation of quantal responses may occur due to changes in driving force, and spontaneous potentials may be difficult to distinguish from background noise (for review see Korn and Faber 1991).

Analysis of the coefficient of variation was used in this thesis to provide some indication of pre or postsynaptic locus of effect on EPSP amplitude in electrophysiology experiments, as described previously (Malinow and Tsien 1990, Larkman, Hannay et al. 1992, Sjostrom, Turrigiano et al. 2007), although other methods are used to confirm location of preNMDARs (Buchanan, Blackman et al. 2012). The coefficient of variation, CV, is defined as the standard deviation over the mean,

$$CV = \frac{\sigma}{M}$$

If a simple binomial model of responses is assumed, then

$$M = nPq$$

where n = number of release sites, P = probability of release and q = quantal size. Similarly, variance is described by

$$\sigma^2 = nP(1-P)q^2$$

As such, if quantal parameters are invariant,

$$CV = \sqrt{\frac{(1-P)}{nP}}$$

Therefore, if q is altered, CV is unaffected. Conversely, changes in P affect CV and M at least equally. Changes in q are usually taken as indicators of a postsynaptic effect, whilst changes in e.g. P indicate presynaptic modifications. Thus, for a reduction in mean amplitude (i.e. synaptic depression), when $\frac{1}{CV^2}$ is plotted against M and responses are normalised to baseline, points below the diagonal indicate a chiefly presynaptic locus of effect, whilst points on the horizontal or above the diagonal indicate a postsynaptic locus (Faber and Korn 1991). It should finally be noted that this method depends on assumptions such as that a single input elicits EPSPs, and that some parameters are invariant (Faber and Korn 1991).

Intrinsic electrophysiological properties of cells

Electrophysiological properties of recorded cells, such as spiking properties, were assessed using custom software running in Igor Pro by quantifying input-output relationships to various hyper- or depolarising current steps. Properties of action potentials were measured, such as spike threshold

(threshold membrane voltage required to elicit a spike), spike height (amplitude in mV from threshold to peak of spike), spike half-width (width of spike at half amplitude), spike afterhyperpolarisation (measured from spike threshold to post-spike minimum) and rheobase (minimal current in nA required to elicit a spike). Properties of spike trains were also measured, including frequency and accommodation (final inter-spike interval / first inter-spike interval for a rheobase train).

2.3. Transgenic mice

In order to gain specificity when targeting cortical interneuron subtypes, two transgenic mouse lines were utilised. For targeting of parvalbumin-expressing INs, a line expressing green fluorescent protein (GFP) in PV+ but not SOM or CCK+ INs was used (Chattopadhyaya, Di Cristo et al. 2004); for targeting somatostatin-expressing INs, a line expressing enhanced GFP (offering higher-intensity emission) in these cells was used (Oliva, Jiang et al. 2000). Both these lines expressed GFP under the control of the *GAD67* promoter. GFP-expressing cells from either line were targeted for recording by acquiring a two-photon laser-scanning microscopy (2PLSM) image containing the cell of interest and surrounding cells, and re-identifying during patching by comparison of this with the live image. Correct cell targeting was verified by co-localisation of Alexa 594 (included in internal solution, see below) and GFP signals. Where cells are referred to as “PV” or “SOM”, it indicates INs targeted for recording with GFP expression in the above animals.

2.4. Imaging systems

2.4.1. 2-photon laser-scanning microscopy

All imaging experiments, except Neurolucida reconstruction and antibody labelling, were performed using a custom-built 2PLSM workstation (Denk, Strickler et al. 1990) built around a SliceScope (Scientifica) microscope with a multiphoton detection unit (MDU; Scientifica). Photomultipliers were in epifluorescence configuration. For excitation, a MaiTai BB (Spectraphysics)

Ti:Sa laser was used, tuned to 800-820 nm for Alexa 594 and 880-900 nm for GFP. Gating of the laser was achieved with Uniblitz LS6ZM2/VCM-D1 shutters. Thorlabs GVSM002/M 5-mm galvanometric mirrors were used as scanners. Laser power was adjusted manually with a Melles Griot PBSH-450-1300-100 with AHWP05M-980 half-wave plate, and monitored with a power meter (Melles Griot 13PEM001/1) with a fraction of the beam picked with a glass slide.

2PLSM fluorescence was collected using an FF665-Di01 or –Di02 dichroic and FF01-680/SP-25 (Semrock) emitter (passing 350-650 nm). Red and green fluorescence was further selected with an FF560-Di01 dichroic (Semrock) and an ET630/75m (Chroma) red emitter, or an ET525/50m (Chroma) or FF01-525/45-25 (Semrock) green emitter.

2.4.2. Laser-scanning Dodt-contrast imaging

For laser-scanning Dodt-contrast imaging, the laser (Ti:Sa) was passed through the preparation and subsequently through the Dodt tube. A portion of the beam was then picked off with a 50/50 beam splitter (Thorlabs BSW17) onto an amplified diode (Thorlabs PDA100A-EC).

2.4.3. Acquisition of imaging data

PCI-6110 boards (National Instruments) were used to acquire imaging data, using modified versions of ScanImage v3.5-3.7 (Pologruto, Sabatini et al. 2003), running in Matlab (MathWorks, Natick, MA). Data was analysed offline using custom software in Igor Pro, as well as MacBioPhotonics ImageJ and Neuromantic.

2.4.4. Spatial resolution of imaging systems

As two imaging systems were used (2PLSM and Neurolucida systems), it may be useful to briefly discuss the spatial resolution of each, as for example in Chapter 3 this may influence the reconstructions generated with either method. For example, the differences in objective numerical aperture and the wavelength of illuminating light will affect resolution in either system.

Numerical aperture (NA) is a measure of an objective's ability to gather light and resolve detail, and is related to the objective aperture angle:

$$NA = \eta \cdot \sin(\alpha)$$

where α is equal to half the objective's opening angle and η is the refractive index of the immersion medium (as this is 1 for air and typically 1.51 for oil, oil immersion objectives are often used to increase numerical aperture).

The theoretical resolution limit of a microscopy system, described by Abbe in 1873, is also related to the wavelength of illuminating light used, and can be described in XY as:

$$d = \frac{\lambda}{2 \cdot NA}$$

where d = diffraction limit, NA = objective numerical aperture and λ = wavelength. As such, one may compare the theoretical resolution of the 2PLSM and Neurolucida systems used in this thesis for Alexa 594 imaging, by considering each case for the wavelength of illuminating light used in each system alongside the specific objectives used. As 2PLSM uses 800 nm illuminating light and a 0.8 NA objective at 40X, d = 500 nm. In the same case, yet using a Neurolucida system with illuminating light of 594 nm and a 1.25 NA oil-immersion objective, d = 237.6 nm. This should illustrate that the use of oil-immersion objectives with higher NA and, for example, confocal systems as opposed to two-photon excitation with longer wavelengths, should increase the resolution of images.

2.5. 3D reconstruction of neurons

2.5.1. Biocytin histology

To enable reconstructions from biocytin histology, 0.1-1% w/v (i.e. 0.1-1 g per 100 ml) Biocytin (Sigma) was included in internal solution. After recording, slices were fixed overnight in 4% paraformaldehyde / 4% sucrose in PBS (pH 7.2-7.4) at 4°C. Slices were permeabilised with immersion in pre-cooled 100% methanol at -20°C for 5-10 mins the following day. Blockade of

endogenous peroxidases was achieved with application of 1% H_2O_2 for 15 mins (room temperature). Slices were incubated overnight at 4°C with Vectastain ABC (avidin-biotin-complex) Elite peroxidase kit (Vector Labs). Following this, slices were incubated with ImmPact SG Peroxidase substrate (Vector Labs) to produce the stain; this was stopped when required (~10 mins) with PBS. At least 3X5 min PBS washes were performed in-between each step above. Slices were mounted in Mowiol (Sigma), coverslipped, and refrigerated until use.

2.5.2. Neurolucida reconstructions

Reconstruction of neurons from biocytin histology was performed using the Neurolucida system (MBF Bioscience) with an Olympus BX61 microscope and 100X oil-immersion objective (1.25 NA). Reconstruction was performed manually with a mouse (as opposed to touchscreen) using the tracing mode of Neurolucida. Somata were defined using contour mode. 3D reconstructions were saved as DAT files and converted to SWC format for analysis using the freeware NLMorphologyConverter (www.neuronland.org). Reconstructions had dendritic, axonal and somatic sections labelled in Neuromantic as for fluorescence reconstructions (see below).

2.5.3. Fluorescence reconstructions

To allow reconstruction of neurons from 2PLSM imaging, 10-40 μm Alexa Fluor 594 was included in internal solutions. 20-60 mins were left between patching the cell and any imaging that was used for reconstruction of morphologies, in order to allow distal areas to fill with dye. Image stacks used for reconstruction were acquired at 2 ms/line with z-steps of 1-2 μm, and saved as 16-bit TIFFs. Slices were 512X512 pixels. Each slice was an average of three captured frames to reduce noise. Multiple XYZ stacks were captured, covering all areas with any noticeable fluorescence signal as monitored online. Stacks were 3D-median filtered and/or contrast and brightness edited in MacBiophotonics ImageJ (www.macbiophotonics.ca).

Registration of image stacks, and manual 3D reconstruction of neurons was performed using the freeware Neuromantic software (http://www.reading.ac.uk/neuromantic). The resulting morphologies were saved as SWC files. Scaling (in pixels/µm) of these reconstructions was determined by comparison to imaging of a graticule. SWC files were transformed in Neuromantic to make scaling equal to 1 pixel/µm prior to analysis. Apical dendrites, basal dendrites, axonal and somatic segments were each assigned separate labels using Neuromantic.

2.6. Morphometric analysis

Quantitative analysis of morphology was performed on all reconstructed neurons, using Neuromantic, qMorph (in-house custom software running in Igor Pro) and the freeware L-measure (Scorcioni, Polavaram et al. 2008). Representative images of reconstructed cells were rendered in NEURON (http://www.neuron.yale.edu).

2.6.1. qMorph analysis

Morphometric analysis using qMorph consisted of three approaches: creation of density maps, convex hulls and Sholl analysis (Sholl 1953). Before analysis with qMorph, all reconstructions were rotated slightly about the soma to align the pia ‘straight up’. Reconstructions were aligned at the soma for comparison of reconstruction methods (as layering information was not available for biocytin reconstructions), and at the L4 / L5 boundary for investigation of preNMDARs. Neocortical layer boundaries were identified from laser-scanning Dodt-contrast stacks acquired simultaneously with fluorescence stacks; these were overlaid in Neuromantic and layer boundaries marked and saved as SWC in the same coordinate space as the relevant reconstruction. Identification of layers was based on large L5 PC somata, a granular and darker L4, and L1 lacking in cell bodies.

Density maps

Density maps were created separately for axon and dendrite by assigning a two-dimensional Gaussian to each compartment (aligned on the XY centre)

of the SWC reconstruction of each cell, with amplitude proportional to compartment length and σ set to a constant 25 μm. For each cell, these Gaussians were then summed to create the individual density map, which is similar to a smoothed 2D projection of the morphology cross-section. To create ensemble density maps for e.g. cell types, each individual density map was normalised and averaging performed.

For figures, ensemble axonal and dendritic density maps were normalised and gamma corrected ($V_{out} = V_{in}^{\gamma}$) with $\gamma = 1/2$ to visualise weaker densities. Axonal and dendritic density maps were assigned colour lookup tables (yellow to white and magenta to white respectively) and merged with logical OR. Colour maps are in arbitrary units and the appearance of symmetry in figures arises from mirroring of reconstructions, however all analyses were performed on non-mirrored data.

Convex hulls

Convex hulls were constructed separately for 2D projections of axon and dendrite for each cell, using the gift-wrapping algorithm, also known as a Jarvis march (Jarvis 1973). Briefly, this begins a point outside of the set of points for which a convex hull is to be formed, from which a radius arm or line is ‘swung’ in either direction until it meets a point of the set to be enclosed. This is chosen as a new origin point and another arm is swung in the same direction to meet the next point. The process is repeated until an enclosing convex hull is formed. In figures, ensemble convex hulls are convex hulls of all convex hulls for e.g. a specific cell type (including mirror images).

Sholl analysis

Sholl analysis (Sholl 1953) is a classical form of quantifying morphology based on counting the number of neurite crossings over (usually soma-centred) concentric circles of increasing radius. In qMorph, this was implemented by aligning reconstructions on somata and, in radial coordinates, moving in 6.5 μm steps from $r = 0$ and counting the number of

axonal or dendritic crossings at each radius *r*. Ensemble Sholl analyses are averaged without normalisation.

qMorph functions

Detailed morphometry based on the three approaches outlined above was performed to obtain measurements for the qMorph functions, outlined in Table 2-1.

Table 2-1: qMorph functions

qMorph function name	**Measure**
Density cloud x-centre (axon or dendrite)	X-coordinate of the qMorph density cloud centre, calculated as the average of all compartment x-coordinates
Density cloud y-centre (axon or dendrite)	Y-coordinate, as above
Euclidean distance to cloud centre	Euclidean distance from 0,0 to density cloud centre (µm)
Angle to density cloud centre (axon or dendrite)	Angle to density cloud centre from 0,0 (e.g. to 1,0 = 0˚, to 0,1 = 90˚)
Most distal compartment (x) (axon or dendrite)	X-coordinate of the most distal (defined by Euclidean distance) axonal or dendritic compartment from 0,0
Most distal compartment (y) (axon or dendrite)	Y-coordinate, as above
Euclidean distance to most distal compartment (axon or dendrite)	Euclidean distance to most distal axonal or dendritic compartment (µm)
Angle to most distal axonal/dendritic compartment	Angle to most distal compartment from 0,0 (e.g. to 1,0 = 0˚, to 0,1 = 90˚)
Convex hull (axon or dendrite) x-centre	X-coordinate of axonal or dendritic convex hull centre
Convex hull (axon or dendrite) y-centre	Y-coordinate, as above
Convex hull (axon or dendrite) width	Maximum axonal or dendritic convex hull width (µm)
Convex hull (axon or dendrite) height	Maximum axonal or dendritic convex hull height (µm)
Sholl maximum value (axon or dendrite)	Maximum observed number of neurite crossings for any single measured radius (i.e: the critical radius) used in Sholl analysis

Sholl critical radius (axon or dendrite)	Radius with the maximum number of neurite crossings (maximum value) in Sholl analysis
Maximum Sholl radius (axon or dendrite)	Furthest radius with at least one crossing in Sholl analysis

2.6.2. L-measure analysis

Morphometric analysis using L-measure was performed on whole cells (axon and dendrite pooled), unless otherwise stated. To reduce ambiguity, L-measure functions are referred to using the names in the software (see http://cng.gmu.edu:8080/Lm/help/index.htm). The L-measure function "Length" refers to average compartment length, and as such this is referred to as "Compartment length" for clarity.

2.6.3. Neurite diameters

Where axonal or dendritic diameters are reported, these were measured in L-measure (treating axon and dendrite separately) for averages. For diameters of individual compartments, used for example in comparison of matched locations between reconstruction methods (Chapter 3), these were measured manually in Neuromantic.

2.6.4. Putative synaptic contacts

Putative synaptic contacts in Chapter 4 were identified manually upon inspection of 2PLSM imaging stacks; neurites of cells filled with Alexa 594 were inspected and putative contacts were defined as axonal-dendritic overlap / crossover separated by less than 1 µm, as described previously (Sjostrom and Hausser 2006). As noted in results text, this method may result in false positives but suffer less from false negatives; as such, the term 'putative' is used.

2.7. Image processing for *Sholl Analysis* software

In Chapter 5, images were processed in Fiji (Schindelin, Arganda-Carreras et al. 2012) prior to analysis. Fluorescence from filling pipettes was removed

manually. Background was removed with 3D median filtering, and segmentation of arbours was performed using built-in thresholding methods. Removal of axons in stacks with a mixture of axonal and dendritic arbours was performed manually by changing the range of thresholded pixel intensities, confirmed with visual inspection.

2.8. Immunohistochemistry

2.8.1. Antibody labelling

Procedures for antibody labelling experiments were adapted from those described previously (Hofer, Ko et al. 2011). Labelling was performed in a mouse line reported to express GFP in PV+ interneurons (Chattopadhyaya, Di Cristo et al. 2004). Transcardial perfusion of 4% PFA in phosphate buffer (pH 7.4) was performed on ketamine / xylazine anaesthetised mice, following perfusion with PBS. The mouse was then decapitated and the brain removed. 60-µm-thick coronal sections containing visual cortex were cut using a DSK DTK-1000 vibratome. These sections were blocked in 10% normal goat serum and 1% Triton to prevent non-specific binding. Sections were then incubated at 4°C for 24 hours with the following primary antibodies: Alexa 488-conjugated rabbit anti-GFP (1:2000, Invitrogen) and anti-PV (monoclonal antibody, 1:1000, Sigma, IgG) in 10% NGS and 0.1% Triton at 4°C for 48 hours. Following this, free-floating sections were incubated with Alexa 568-conjugated goat anti-mouse IgG at 4°C for 24 hours. Mounted sections were imaged with a confocal microscope (Leica SP1) with a 20X or 40X oil-immersion objective and channels with appropriate filters for Alexa 488 and 568 fluorescence. Images were obtained in L5 of primary visual cortex (identified by the presence of a granular layer 4). No bleed through was observed between channels. Scans were performed in sequential mode, and subsequently merged for analysis. Settings and gains were invariant between samples. Images were saved as TIFFs.

2.8.2. Analysis

Analysis of GFP / PV colocalisation was performed manually using MacBioPhotonics ImageJ. Within matched image stacks from Alexa 488 and 568 channels, all visible cell bodies (with signal) were marked, and the XYZ coordinates of these compared. “Specificity” is defined as the percentage of GFP+ cells that also expressed PV. “Sparsity” indicates the percentage of PV+ cells that expressed GFP, as the mouse line used labels only a subset of PV+ cells (Chattopadhyaya, Di Cristo et al. 2004). Statistical significance was determined with a χ^2 test.

2.9. Simulations

All simulations were implemented in NEURON 7.2 by Stefan Grabuschnig (Blackman, Grabuschnig et al. 2014) or in Matlab by Rui Costa (Buchanan, Blackman et al. 2012). Figures were created using Matlab and Igor Pro.

2.9.1. Basic cable theory and compartmental models

Cable theory

Cable theory originates with the mathematical models of signal decay in telegraphic cables developed by Lord Kelvin (Thomson 1854). Cable theory was applied to dendrites by Rall (Rall 1957, Rall 1959). Classical cable theory can utilise the simplifying assumption that as dendrites may be described as a core conductor surrounded by a relatively good insulator (membrane), current will mostly flow parallel to the cylindrical axis. As such, cable theory can consider only one spatial dimension (x), being that along the axis of the cylinder (dendrite). For a passive and uniform membrane, the one-dimensional cable equation can be solved analytically. A full description and derivation of the cable equation can be found in (Jack, Noble et al. 1975), however considering a length of cable with some fixed diameter it is often stated as

$$\frac{1}{r_i}\frac{\partial^2 V}{\partial x^2} = c_m \frac{\partial V}{\partial t} + \frac{V}{r_m}$$

a second-order partial differential equation, where r_i = resistance per unit length along the x-axis, c_m = membrane capacitance per unit length, r_m = membrane resistance for a unit length, and V = voltage.

Compartmental models

In order to reduce computational cost and to maximise the relationship between effort and potential insight, compartmental computational models are often employed in neuroscience. These are typically created by creating a realistic morphological model (utilising biocytin reconstruction or similar), and using this as a basis to generate a computational model divided into a series of isopotential compartments with passive and active properties that should match the actual properties of the simulated cell as closely as possible. For example, one may approach this by assuming that the passive properties of a cell are constant, and optimising values of $R_{M,}$ $C_{M\ and}$ R_A (see below) to fit data obtained from dual dendritic and somatic recordings (Carnevale and Hines 2006). Further complexity is added by active properties, which in the case of the cable equation, introduce nonlinearities which significantly complicate solutions (Jack, Noble et al. 1975).

Compartmental modelling can approximate the non-linear cable equation by treating short segments of dendrite as discrete isopotential R-C compartments (Rall 1964, Jack, Noble et al. 1975, Carnevale and Hines 2006). Here, differences in, for example, diameter and membrane properties occur between compartments instead of within them, as compartments are isopotential. Therefore, a continuous cable equation may be replaced by a set of ordinary differential equations which can be solved for each time step (Jack, Noble et al. 1975, Carnevale and Hines 2006). Such an approach can easily accommodate a branched structure with N compartments, which would imply N coupled equations that would be solved simultaneously for a particular time point. Using such an approach, environments such as NEURON can compute the voltage in a particular compartment given particular nonlinear inputs, and voltage and time-dependent membrane properties (Carnevale and Hines 2006).

2.9.2. NEURON simulations

NEURON (Carnevale and Hines 2006) simulations were employed to quantify differences between FI and BH reconstructions of the same original cells in Chapter 3. Simulations of both active back propagation of action potentials and passive forward propagation of EPSPs along the apical dendrite were performed. Distance is measured as the Euclidean distance between the origin of the apical dendrite at the soma and the recording site. Analysis is performed on a path from the soma to apical tuft, selected manually to be straight. Plots are of peak potential recorded at points along this path against Euclidean distance, as described above. Compartmentalisation of models was performed using nseg=100 (Carnevale and Hines 2006), and increasing this number had no effect on results. The model contained only sodium and potassium conductances (Stuart and Hausser 2001). For the purposes of the study presented here, it was more important to highlight any potential differences in modelling results due to reconstruction method alone than any other objective. Therefore, a single, previously published simple model based on electrophysiological data was chosen and kept constant throughout all simulations (Stuart and Hausser 2001). Furthermore, it should be stressed that the intention of the modelling performed was simply to highlight any potential differences in results that may derive from reconstruction method choice, and not to accurately simulate the electrophysiological properties of the specific cells used, therefore no attempt was made to fit the model properties to recordings of the exact cells used for reconstruction, nor was an attempt made to include all possible channel types in the simulation, instead restricting modelling to a reasonable minimal subset required to achieve active propagation. If differences in simulation results are seen in reconstructions of the exact same cells using the exact same model, this can be taken as evidence that these differences are due to reconstruction method choice. This said, the model employed here has been validated elsewhere (Stuart and Hausser 2001).

Model initialisation

Active and passive membrane conductances used matched those in the model of (Stuart and Hausser 2001). Uniform specific membrane and axial resistivities R_M = 12000 Ωcm^2, R_A = 150 Ωcm and a specific membrane capacitance C_M = 1 $\frac{\mu F}{cm^2}$ were used. Uniform distribution of active conductances (fast sodium and slow potassium) over the membrane in dendrites and soma was used with $\bar{g}_{Na}$ = 30 $\frac{pS}{\mu m^2}$ and $\bar{g}_{Kv}$ = 50 $\frac{pS}{\mu m^2}$. As end-effects were observed, sodium conductances were reduced in basal and apical oblique dendrites to $\bar{g}_{Na}$ = 8 $\frac{pS}{\mu m^2}$. Dendritic conductances and capacitance were multiplied by 2 to account for spines (Bush and Sejnowski 1993). A completely myelinated axon was used, with $\bar{g}_{Na}$ = 10 $\frac{pS}{\mu m^2}$, and $\bar{g}_{Kv}$ = 0 $\frac{pS}{\mu m^2}$, a reduced C_M of 0.04 $\frac{\mu F}{cm^2}$ and no spike initiating regions.

Action potential backpropagation

Backpropagating action potentials were simulated with a rheobase spike initiated at the soma. The reconstruction PC FI 2 (20130205) had a spike-initiating hillock added for spike generation, with $\bar{g}_{Na}$ = 10000 $\frac{pS}{\mu m^2}$ and $\bar{g}_{Kv}$ = 500 $\frac{pS}{\mu m^2}$. A rheobase spike was initiated with 5 ms current injection of 1.0215 nA.

EPSP forward propagation

Alpha-synapses were used for EPSP generation, with a maximum conductance of 5 nS, a τ_{rise} of 0.3 ms and a τ_{fall} of 3 ms. Synapses were placed at matched locations on reconstructions of the same cell using either method, identified by clearly identifiable surrounding morphology.

Length constants

To determine potential effects of reconstruction method choice on spatial filtering, length constants were measured in simulations. This was performed by injecting a 300-ms-long current of 50 pA at visually matched locations

(using the same method as for EPSPs); as the model employed had no active conductances that were appreciably gated at the resulting level of depolarisation (the compartment with maximum depolarisation was depolarised ~2mV from rest), this provided a reasonable approximation. Membrane voltage was plotted against distance from the injection site at an arbitrary time (t = 149 ms) after steady state was reached. Length constants, λ, were then approximated by fitting decaying exponentials to these plots in Igor Pro.

2.10. Principal component analysis

Principal component analysis is a technique that is used to reduce the data set to one with fewer components or variables, which are ordered by their contribution to the total variance. Conceptually, for its use here, the components which cover the most total variance should better account for differences between cell types; therefore, the first two principal components were selected for clustering in Chapter 3, and the first principal component for Chapter 5. PCA was performed in JMP (SAS), on standardised data to remove differences due to units.

Principal component analysis relies on a number of assumptions, briefly stated here. Firstly, measurements must use an interval or ratio scale. Each case should contribute one score for each variable and these should represent a random sample. The relationship between variables should be linear, each variable should be normally distributed, and pairs of observed variables should have a bivariate normal distribution (O'Rourke, Hatcher et al. 2005).

2.11. Data clustering

2.11.1. Method comparisons

For comparison of morphometric performance of reconstruction methods (Chapter 3), automated multidimensional hierarchical data clustering was used. In cluster analysis, it is assumed that the distance between pairs of

objects reflects inter-object similarity, and that a representative sample was chosen. Use of non-standardised data may adversely affect similarity measures due to differing scales. Cluster analysis was performed on the first two principal components of standardised data and implemented in JMP (SAS), using Ward's method, which joins clusters in a manner that minimises the total variance within-cluster at each step. Euclidean distance was used as the linkage metric.

Before hierarchical clustering, some variables were excluded in order to achieve fair weighting of morphological features, as described previously (Tsiola, Hamzei-Sichani et al. 2003). Principal component analysis was performed on all morphological variables measured, and pairs of variables with correlation $r > 0.8$ were identified. Of these pairs, the variable with the lower loading value in PCA was excluded from further analysis; therefore, hierarchical clustering was performed on the first two principal components (to increase case/variable ratio and stability) of 27 morphological variables, which are listed below:

Selected L-measure functions

- Diameter
- Length
- PathDistance
- Branch_Order
- Taper_1
- Contraction
- Daughter_Ratio
- Parent_Daughter_Ratio
- Partition_asymmetry
- Bif_ampl_local
- Helix
- Fractal_Dim

Selected qMorph variables

- Distance to axonal cloud centre
- Angle to axonal cloud centre
- Most distal axonal compartment (x-coordinate)
- Most distal axonal compartment (y-coordinate)
- Most distal dendritic compartment (x-coordinate)
- Angle to most distal dendritic compartment

- Axonal hull x-centre
- Axonal hull width
- Dendritic hull x-centre
- Dendritic hull y-centre
- Dendritic hull width
- Axonal Sholl max value
- Axonal Sholl critical radius
- Dendritic Sholl critical radius
- Axonal maximum Sholl radius

Normal mixtures clustering

Data clustering was also performed using the normal mixtures iterative clustering function in JMP (http://www.jmp.com/support/help/Normal_Mixtures.shtml; set to identify two clusters). This is based on the expectation-maximisation algorithm, which estimates the probability that each case is in each cluster (Do and Batzoglou 2008).

2.11.2. preNMDARs

Data clustering was also performed to aid investigation of preNMDAR expression (Chapter 4). Here, in-house software running in Igor Pro was used – classification was performed with agglomerative single-linkage hierarchical clustering, as described in (Buchanan, Blackman et al. 2012). The squared Euclidean distance was used as the linkage metric. As a selection criterion for the optimum number of found clusters, a 25% linkage threshold was used, normalised to the greatest separation in the data set. Fuzzy c-means clustering built-in to Igor Pro 6.2 always gave the same classification of data points as the above, but is set to find two clusters by default.

2.11.3. Sholl Analysis

For verification of the performance and utility of *Sholl Analysis* software (Chapter 5), clustering was performed to classify PV INs on the first principal component of all 18 metrics extracted by the software. Hierarchical clustering using Ward's method was used, with a 25% linkage cutoff (normalised to the greatest linkage separation in the dataset) as a selection criterion for the

number of found clusters. Squared Euclidean distance was used as the linkage metric.

2.12. Statistical comparisons

All statistical tests were carried out in Igor Pro, Microsoft Excel and/or JMP (SAS). To reduce type 1 and 2 errors, at least 3 animals were used for each group analysed, and typically $n_{cell} = n_{animal}$ (Aarts, Verhage et al. 2014). Significance levels $p<0.05$, $p<0.01$ and $p<0.001$ are indicated by one, two or three asterisks respectively, whilst n.s. indicates $p>0.05$. Results are reported as mean ± SEM unless otherwise stated.

2.12.1. Method comparisons

Statistical comparisons (Chapter 3) of sample means were made using student's *t*-test for paired samples, unless otherwise stated. No corrections for multiple comparisons were made here, as highlighting potential differences between methods was deemed more important and preferable than overlooking them.

2.12.2. preNMDARs

All statistical comparisons (Chapter 4) were to compare sample means using unpaired students *t*-test, unless otherwise stated. Multiple comparisons were corrected using Bonnferoni-Dunn's method, requiring an adjusted α of $\frac{\alpha}{n}$ where n = number of comparisons. Unequal variances *t*-test was used if equality of variances F-test gave $p < 0.05$. Wilcoxon-Mann-Whitney's non-parametric test gave similar p values for all comparisons.

3. Effects of reconstruction method choice on morphometry, cell-type classification and computer modelling

3.1. Overview

The following chapter is based on a study recently published in *Frontiers in Neuroanatomy*, of which I am first author (Blackman, Grabuschnig et al. 2014). Reconstructions of the same cells were created using both a common method (biocytin histology) and one gaining in popularity (2PLSM fluorescence imaging) and compared as to performance in morphometry, cell classification and single-cell multicompartmental simulations in NEURON – in order to assess the suitability of each method for these purposes. FI reconstructions are deemed suitable for cell classification, whilst BH reconstructions are preferred for single-cell modelling and long-range tracing.

3.2. Authorship

I completed all experiments, reconstructions and morphometry. NEURON simulations were implemented by Stefan Grabuschnig with design input from myself, Robert Legenstein and P. Jesper Sjöström. Input and advice regarding experimental design and analysis was provided by all authors. I performed analyses with input from co-authors.

3.3. Introduction

3.3.1. Reconstructions of neuronal morphology

Investigations and reconstructions of neuronal morphology have been integral to neuroscience since it's beginnings – perhaps most famously in Ramón y Cajal's use of the Golgi stain to form the neuron doctrine (Ramón y Cajal 1911, Senft 2011). Since then, the increasing drive to link neural structure and function has required the development of more accurate and quantifiable methods to model morphology, reflected in the neuroanatomical

credo *"the gain in brain is mainly in the stain"* (Osten and Margrie 2013). Reconstructions of neuronal morphology are vital aspects of many sub-fields of modern neuroscience, such as circuit reconstruction (Helmstaedter 2013), computer modelling (Vetter, Roth et al. 2001, Gidon and Segev 2012), cell-type classification (Ascoli, Alonso-Nanclares et al. 2008, DeFelipe, Lopez-Cruz et al. 2013) and anatomy itself (Cannon, Wheal et al. 1999). Efforts to link anatomy and physiology in particular have benefited from the development of techniques such as biocytin labelling in conjunction with electrophysiology, genetic labelling of cell types, 2-photon and confocal microscopy, and digital analyses of morphology (Ascoli 2006, Svoboda 2011, Thomson and Armstrong 2011); these approaches have provided valuable insight into the structure and function of neural circuits (Douglas and Martin 2004). According to the particular requirements of a study, there may be different requirements for resolution, accuracy, throughput and completeness – and as such the experimenter may choose from a number of imaging and reconstruction methods, from histological techniques to electron microscopy. As the number and availability of digital reconstructions increases, new approaches become possible, such as data mining of large interlinked datasets of morphologies from published studies (such as those available at NeuroMorpho.Org) and subsequent use in large-scale projects such as the Human Brain Project, or any other project intended to simulate the brain (Ascoli, Donohue et al. 2007, Markram 2013).

3.3.2. Reconstruction method choice

Whilst electron microscopy may be required for circuit reconstruction at spine and synapse-level resolution (Kleinfeld, Bharioke et al. 2011), most applications requiring reconstruction of single cells rely on optical techniques (Halavi, Hamilton et al. 2012). Of these, the most popular current method uses the Neurolucida system to reconstruct biocytin labelled cells. Briefly, this involves filling recorded cells with biocytin and performing histological processing in fixed tissue, exploiting the affinity of avidin (usually in complex with a biotinylated enzyme such as a peroxidase) for biotin to produce the stain (see 2.5.1). Whilst the majority of published reconstructions at present

have been produced with this method, there is a trend for increasing use of alternative methods such as the use of fluorescent markers; recent studies also utilise technologies such as 2PLSM and alternative freeware reconstruction software such as Neuromantic (Buchanan, Blackman et al. 2012, Halavi, Hamilton et al. 2012, Myatt, Hadlington et al. 2012). Importantly, the use of different reconstruction methods may yield differing results; for example, BH reconstructions may exhibit distortions and shrinkage – particularly in the z-axis – when compared to 2PLSM FI counterparts (Egger, Nevian et al. 2008). Effects such as these may influence the results of morphological and modelling studies, introducing variation due to reconstruction method choice alone. Despite this possibility, there has until now been little quantification of the potential effects of method choice on morphometry, cell classification and single-cell modelling. Here, 16 reconstructions of the same 8 cells, created from both biocytin histology and 2PLSM fluorescence imaging, are directly compared. In this process, their relative strengths and weaknesses are identified, and recommendation made as to the appropriate method choice for particular applications.

3.4. Results

3.4.1. Experimental approach

Neocortical L5 pyramidal (PC) and basket (BC) cells were targeted visually for whole-cell recordings in wild-type mice based on large, ovoid and small, round somata respectively. Cell types were further identified online with inspection of morphology from 2PLSM fluorescence imaging (FI) – PCs had a characteristic apical dendrite branching in L1, whilst BCs exhibited dense local axonal arborisation staying mainly within L5. Rheobase current injection resulted in a fast, non-accommodating response in BCs and a regular spiking response in PCs. Both biocytin and Alexa 594 were included in internal solutions, allowing reconstruction of recorded cells (Figure 3-1) from acquired 2PLSM FI stacks using Neuromantic and also with Neurolucida following biocytin histology (BH). With this approach, it was possible to obtain

and directly compare two paired reconstructions using the BH or FI methods from each cell.

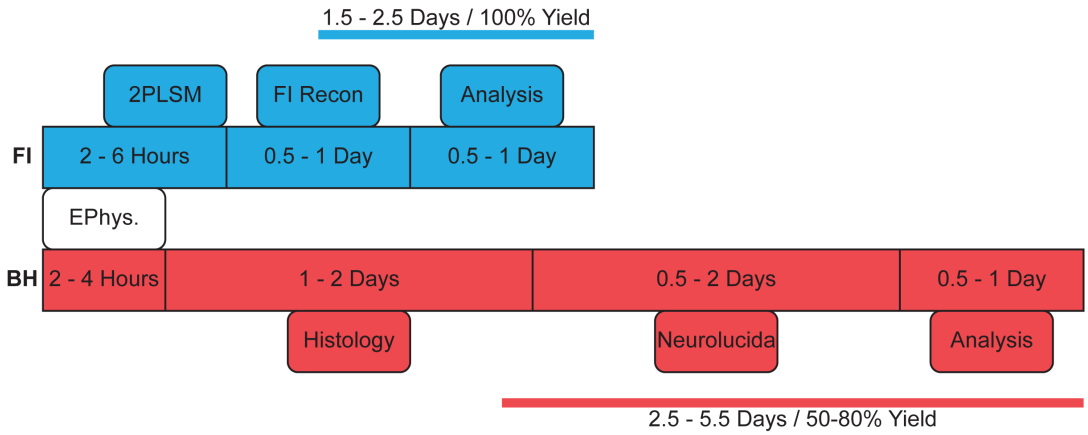

Figure 3-1: Overview of reconstruction steps for FI and BH reconstructions.

BH reconstructions require more time due to the processing steps and multiple setups required. Online monitoring of FI results in effectively 100% yield. Depending on the particular protocol used and expertise of experimenter, BH histology occasionally fails, resulting in a 50-80% yield in the experience of our lab. Figure as originally published in Blackman AV, Grabuschnig S, Legenstein R and Sjöström PJ (2014) A comparison of manual neuronal reconstruction from biocytin histology or 2-photon imaging: morphometry and computer modeling. Front. Neuroanat. 8:65. doi: 10.3389/fnana.2014.00065.

3.4.2. Morphometry

Qualitative visual comparison of reconstructed cells revealed similarity between methods, although BH reconstructions exhibited longer thin distal processes (Figure 3-2). These differences could be the result of both slow dye-filling of such processes in FI reconstructions (affecting area imaged whilst viewing online, see Figure 3-2) and the amplification step in BH processing that potentially allows better visualisation of smaller, less well-labelled processes. BH reconstructions, however, appeared to exhibit compression (shrinkage in Z and expansion in XY) and distortion artefacts as compared to FI reconstructions.

Quantitative comparison of morphologies was performed using the freeware L-measure (Scorcioni, Polavaram et al. 2008) to analyse whole cells (axon and dendrite pooled) and in-house custom software, qMorph, running in Igor Pro to analyse axonal and dendritic arbours separately. Full details and significance levels are available in Table 3-1.

Measurements obtained from L-measure revealed that BH reconstructions of BCs had a wider arbour width than FI reconstructions ($p<0.05$), which appears to reflect the greater ability of BH to reveal thin distal arbours. BH reconstructions of PCs, on the other hand, resulted in a smaller depth ($p<0.01$) and somatic surface area ($p<0.05$) than FI counterparts (full detail in Table 3-1). This perhaps reflects shrinkage during the fixation process and differences in soma modelling (between Neurolucida and Neuromantic) respectively.

Branch and bifurcation-level morphometry was also examined using L-measure. Here, most measures were indistinguishable (Table 3-1), indicating that both reconstruction methods were comparable. However, local bifurcation amplitude, defined as the angle between the two new branches at a bifurcation point, was larger for BH BC reconstructions ($p<0.05$). Parent-daughter ratio, defined as the ratio of neurite diameter between parent and daughter at a bifurcation point, was in addition lower for BH PC reconstructions ($p<0.05$).

In many applications of morphometry, it is useful to treat axonal and dendritic arbours separately – for example, axonal morphology is a key determinant of cortical IN classification, whilst dendritic morphology is not (Markram, Toledo-Rodriguez et al. 2004, Ascoli, Alonso-Nanclares et al. 2008, DeFelipe, Lopez-Cruz et al. 2013). As such, morphology was quantified separately for axon and dendrite using convex hulls, density maps and Sholl analysis (see 2.6), as described in (Buchanan, Blackman et al. 2012).

Comparison of convex hulls generated using qMorph indicated the greater ability of BH to reveal thin distal arbours (Figure 3-2): axonal hull width was larger for BH PC reconstructions ($p<0.01$), and both axonal and dendritic hull widths were larger for BH BC reconstructions ($p<0.05$ for both). However, all other measured features of convex hulls were indistinguishable, indicating the similarity of methods to reveal the majority of morphology – importantly, this included hull centres.

As convex hulls describe the extent of neuronal arborisation without taking into account the density of branching within this, qMorph was also used to create and compare density maps of axonal and dendritic branching (Figure 3-2). Here, the only significant difference between methods was the angle to the centre of the dendritic density cloud, which was larger for BH reconstructions of PCs ($p<0.05$). However, this may be a spurious finding as reconstructions were rotated manually to a subjective 'straight up' position. This result remained significant even when carefully controlling this process, so it is reported as is. There is additionally a possibility that distortion of BH reconstructions during the fixation process may introduce curvature that would affect this result. That this was the only significant difference in density clouds again provides evidence that both methods are comparable in revealing the majority of tree-level morphology for the reconstructed cells.

When the distance to the most distal axonal and dendritic compartments were compared between methods, this again indicated that BH was superior in revealing the most distal processes. Euclidean distance to the most distal axonal compartment was higher for BH PCs ($p<0.05$), and Euclidean distance to the most distal dendritic compartment was higher for BH BCs ($p<0.05$). Compartment coordinates and angles to the most distal compartments were not significant between methods, perhaps as these differences were non-systematic between cells.

Reconstructions were finally analysed using Sholl analysis (Sholl 1953), as this is a widely used classical method to quantify morphology (Figure 3-2). This is based on counting the number of crossings made by e.g. dendritic arbours over soma-centred concentric circles of increasing radius. In Sholl analysis, three measures were compared: critical radius (the radius with the most crossings), maximum value (maximum number of crossings) and maximum Sholl radius (furthest radius with at least one crossing). In agreement with previous analyses, significant differences were found only in maximum Sholl radii, which were larger for BH PC axon ($p<0.05$) and BH BC dendrite ($p<0.05$). This, along with previous measurements indicating that

BH reconstructions span a wider area, perhaps reflects both the ability of BH to reveal more distal processes, and the effects of shrinkage and compression after coverslipping, which leads to reduced depth and XY expansion in BH reconstructions.

Taken together, these analyses show that whilst BH reconstructions facilitate visualisation of thin distal processes (indicated by e.g. wider arbour extents and greater distance to the most distal compartments), the majority of neural morphology was represented similarly between methods. Additionally, as FI / 2PLSM reconstructions are limited by the extent of imaging captured during recording, it may be possible to increase the extent of morphology available for reconstruction by imaging a greater area, even if there is no signal when viewing online.

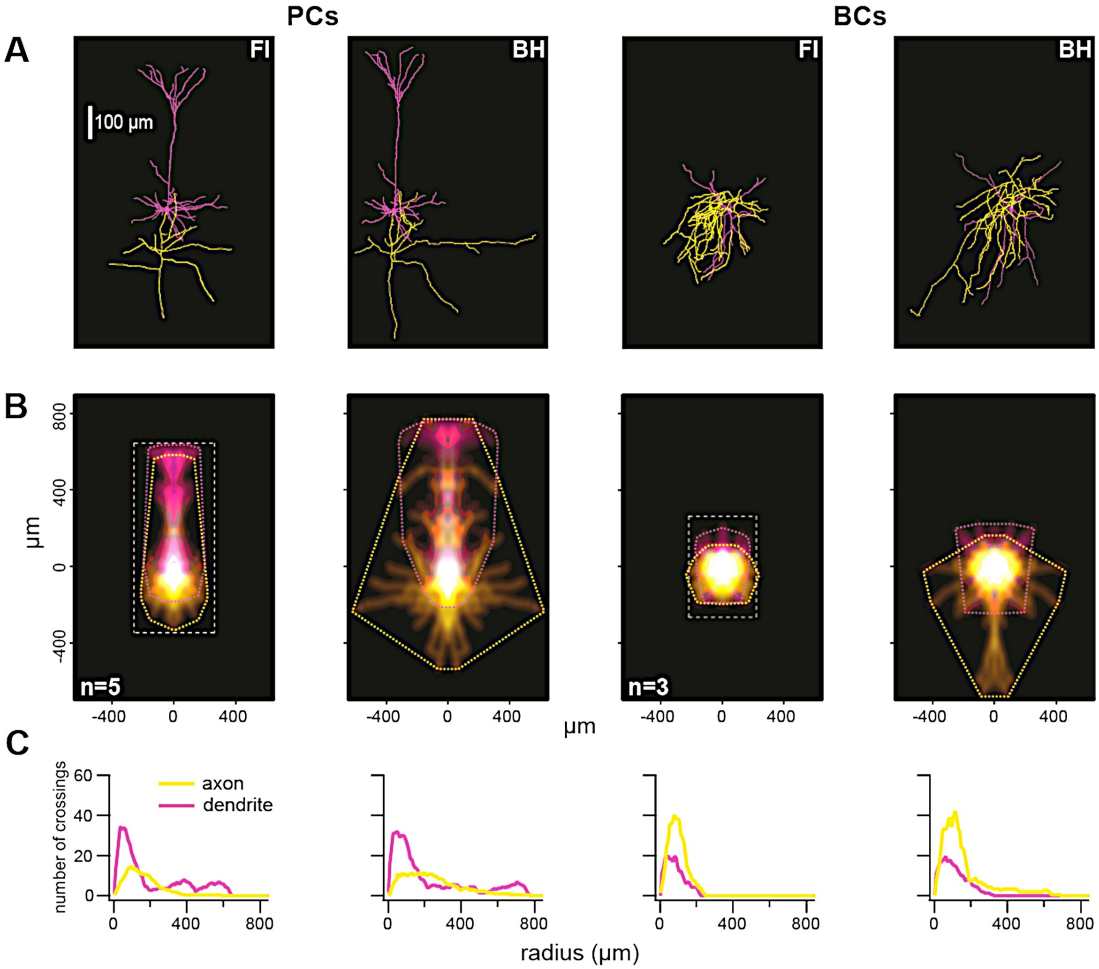

Figure 3-2: BH reconstructions reveal thin distal arbours.

A: Representative reconstruction pairs of a single pyramidal (PC; left) and basket (BC; right) cell reconstructed from fluorescence imaging (FI) or biocytin histology (BH). Whilst reconstructions appeared subjectively similar, note that BH reveals longer distal collaterals. BH also was affected by expansion in XY due to compression. B: Density maps and convex hulls created separately for axon (yellow) and dendrite (magenta) using qMorph. Axonal convex hull widths were larger for BH PCs ($p<0.01$) and BCs ($p<0.01$). Dendritic hull widths were larger for BH BCs ($p<0.05$). Euclidean distance to the furthest axonal compartment was larger for BH PCs ($p<0.05$), and Euclidean distance to the furthest dendritic compartment was larger for BH BCs ($p<0.05$). Angle to the centre of the dendritic density map was larger for BH PCs ($p<0.05$). All other measures were non-significant. For FI reconstructions, area imaged is indicated by the white dotted line. Reconstructions are aligned on soma. C: Sholl analysis. Comparisons were indistinguishable between methods, except maximum Sholl radii, which were larger for BH PC axon ($p<0.05$) and BH BC dendrite ($p<0.05$). Paler hues indicate ±SEM. Figure as originally published in Blackman AV, Grabuschnig S, Legenstein R and Sjöström PJ (2014) A comparison of manual neuronal reconstruction from biocytin histology or 2-photon imaging: morphometry and computer modeling. Front. Neuroanat. 8:65. doi: 10.3389/fnana.2014.00065.

3.4.3. Cell-type classification

Many features of interest, such as synaptic properties, may vary according to cell type – and a key indicator of cell type, particularly for cortical interneurons, is morphology (Ascoli, Alonso-Nanclares et al. 2008, Blackman, Abrahamsson et al. 2013, DeFelipe, Lopez-Cruz et al. 2013). This

being the case, it is vital to properly identify cell type using morphological analysis when investigating the properties of neural circuits.

The differences in morphometric results obtained with BH and FI reconstruction methods described above may affect the ability to reliably classify cells based on morphology. This possibility was assessed with multidimensional hierarchical clustering of many morphological variables (see 2.6 and 2.11), including all reconstructions from both methods. Clustering of the first two principal components of identified uncorrelated morphological variables independently segregated reconstructions into two major clusters containing exclusively PCs or BCs; however, distinct subclusters composed of BH and FI reconstructions were not formed (Figure 3-3). This indicates that both reconstruction methods can be used successfully to classify different neuronal types, whilst having such similar outcomes that reconstruction method does not appreciably affect cell classification. This said, in only one case did a reconstruction pair (that is, BH and FI reconstructions of the same original cell) form a nearest-linkage neighbour, highlighting the fact that whilst FI and BH methods exhibit similar classification performance, they do generate reconstructions with some appreciable morphological differences (as identified in 3.4.2).

An alternative approach to clustering all reconstructions from both methods was taken with the use of the expectation-maximisation algorithm, set to identify two groups (as described in 2.11). Here, PCs and BCs were also segregated with no errors (Figure 3-3), further indicating the similarity in cell classification performance between BH and FI. Whilst this method is set to find two clusters, the possibility that both PCs (Groh, Meyer et al. 2010) and BCs (Markram, Toledo-Rodriguez et al. 2004) may be composed of further subtypes should be noted.

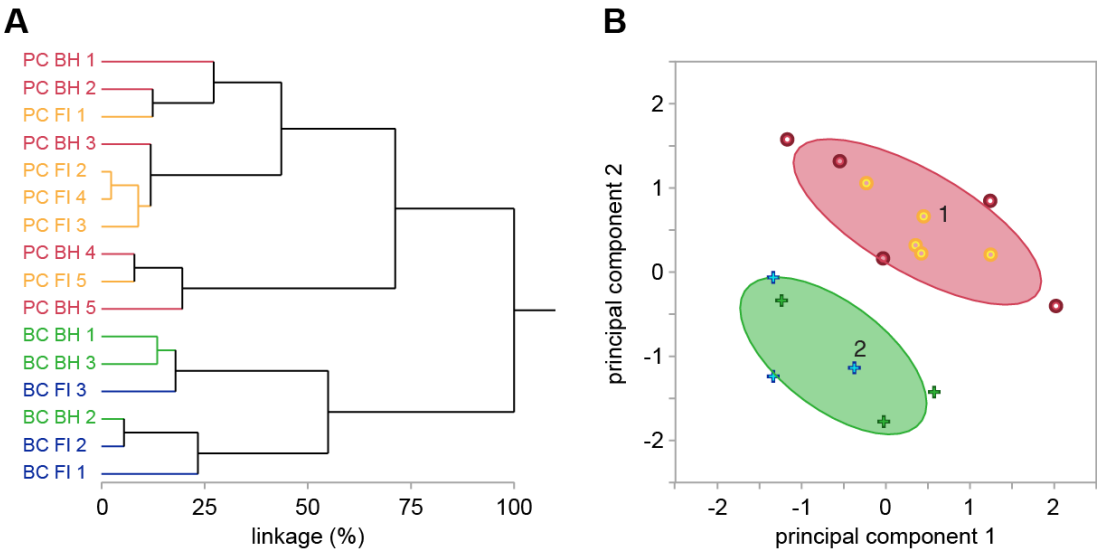

Figure 3-3: BH and FI reconstruction methods have similar overall morphometric performance.

A: Hierarchical clustering performed on the first two principal components of 27 uncorrelated morphological variables (see 2.10 and 2.11) independently segregated all reconstructions into two major clusters containing exclusively PCs or BCs. Within these clusters, further subclusters segregating FI and BH reconstructions were not formed. Overall, this reflects the similarity of FI and BH reconstructions when used for morphological cell-type classification. Each label on the y-axis represents a single reconstruction, with colouring indicating cell and method type. Linkage distance, indicating the level of similarity between clusters, is plotted on the x-axis. B: Similarly, expectation-maximisation clustering of all reconstructions into two groups segregated BCs and PCs with no errors. As in A, colouring indicates reconstruction method (blue or yellow = FI; green or red = BH). Crosses denote BCs and dots PCs. Ovals mark the region where 90% of observations in each cluster are expected to fall. Figure as originally published in Blackman AV, Grabuschnig S, Legenstein R and Sjöström PJ (2014) A comparison of manual neuronal reconstruction from biocytin histology or 2-photon imaging: morphometry and computer modeling. Front. Neuroanat. 8:65. doi: 10.3389/fnana.2014.00065.

3.4.4. Neurite diameters

In computer modelling applications particularly, it is important for all aspects of 3D reconstructions of morphologies to be as accurate as possible, as even subtle differences can have quite large effects on biophysical properties such as propagation of electrical potentials (Vetter, Roth et al. 2001, Schaefer, Larkum et al. 2003). Simple differences in process diameter would be expected to affect modelling of membrane surface area, neurite volume, axial resistance, number of ion channels, membrane length constant, and in turn propagation of potentials. Inherent differences between BH and FI reconstruction methods potentially lead to differences in reconstructed neurite diameter. As an example, 2PLSM FI imaging suffers from a worse resolution limit than BH due to the use of longer wavelength illumination. Furthermore, image processing of 2PLSM FI stacks before reconstruction may exacerbate any potential overestimation of process diameters, as

altering e.g. brightness and contrast to better visualise weakly stained processes invariably leads to a perceived thickening of all processes in that stack.

As, for the above reasons, the effect of method choice on reconstructed neurite diameter may have significant effects and introduce errors in modelling, process diameters were compared between methods, both on average and for individually matched compartments. The software L-measure was used to compare whole-cell averages for axonal and dendritic process diameter between BH and FI reconstructions of the same original PCs. Diameters were consistently and systematically larger in FI reconstructions, both for axon and dendrite (Figure 3-4), confirming that the differences in reconstruction processes are enough to have significant effects on model neuron structure.

To investigate the identified differences in process diameter between methods in more detail, the diameters of many individually visually matched compartments for each PC dendrite were compared between reconstruction methods, using manual measurements obtained in Neuromantic. Here, all but one of these matched segments were found to have a larger diameter in the 2PLSM FI reconstruction (n=25; n=5 cells; FI vs. BH, 1.80 ± 0.15 µm vs. 0.91 ± 0.09 µm, $p<0.001$). Linear regression on a Bland-Altman plot (Bland and Altman 1986) of these results identified a significant slope (0.56, $p<0.05$), indicating that this overestimation is worse for larger average diameters. Alongside whole-cell average measurements, these results indicate that FI reconstructions systematically overestimate process diameters for all aspects of reconstructed neurons.

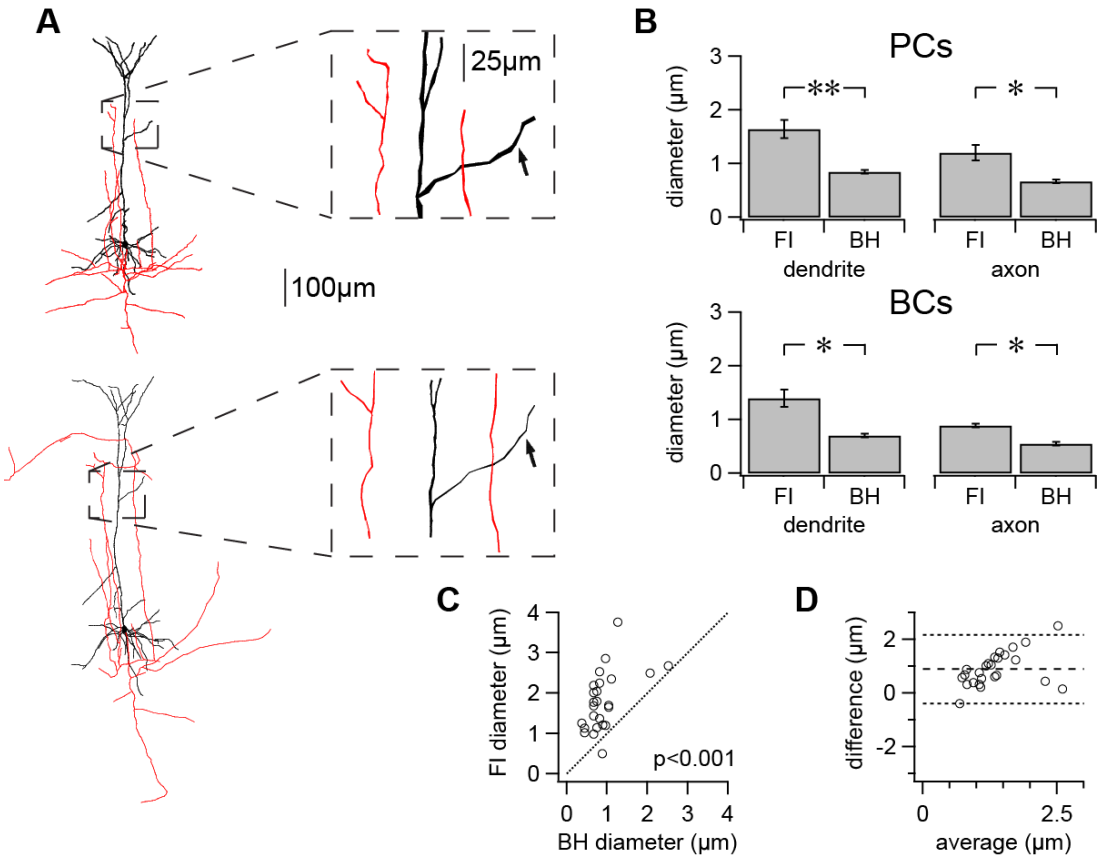

Figure 3-4: FI reconstructions systematically overestimate neurite diameters

A: FI (top) and BH (bottom) reconstructions of the same original cell. Inset: enlarged section of reconstruction highlighting differences in both axonal (red) and dendritic (black) diameters. Arrows indicate an example of visually matched compartments as described in text and analysed in figures C and D. B: Whole-cell axonal and dendritic average differences in neurite diameter for reconstructed PCs and BCs using BH or FI. FI reconstructions exhibited consistently larger diameters in all comparisons for PCs (n=5 cell pairs; FI vs. BH; axon 1.20 ± 0.14 µm vs. 0.67 ± 0.04 µm, $p<0.05$; dendrite 1.65 ± 0.17 µm vs. 0.84 ± 0.03 µm, $p<0.01$) and BCs (n=3 cell pairs; FI vs. BH; axon 0.89 ± 0.04 µm vs. 0.55 ± 0.04 µm, $p<0.05$; dendrite 1.40 ± 0.16 µm vs. 0.71 ± 0.03 µm, $p<0.05$). Pooled whole-cell diameters are found in Table 3-1. C: Individually visually matched compartment diameters (see methods and text) were also systematically larger in FI reconstructions of PCs. All but one matched compartment diameters were plotted above the line of equality (n=5 cell pairs; n=25 segment pairs; FI vs. BH; mean 1.80 ± 0.15 µm vs. 0.91 ± 0.09 µm, $p<0.001$). D: Bland-Altman difference plot (also known as a Tukey mean-difference plot) indicating the degree of agreement between BH and FI reconstruction methods (Bland and Altman 1986). The difference (FI diameter – BH diameter) was plotted against the mean diameter of a compartment between methods (FI+BH diameters / 2). There was a positive mean difference (middle dotted line; 0.89 ± 0.13 µm), indicating that FI systematically overestimates diameters. Top and bottom dotted lines indicate ± 2SD (95% limits of agreement; SD = 0.64 µm). Linear regression (not shown) indicated that FI overestimates diameters more for larger compartments (slope 0.56; $p<0.05$). Figure as originally published in Blackman AV, Grabuschnig S, Legenstein R and Sjöström PJ (2014) A comparison of manual neuronal reconstruction from biocytin histology or 2-photon imaging: morphometry and computer modeling. Front. Neuroanat. 8:65. doi: 10.3389/fnana.2014.00065.

3.4.5. Multicompartmental single-cell modelling

In addition to anatomical applications, a major use of detailed 3D reconstructions of neuronal morphologies is in single-cell and network modelling using software such as NEURON (Carnevale and Hines 2006).

For example, single cell modelling has been used to show that morphology alone can determine efficacies of action potential propagation (Vetter, Roth et al. 2001), and that coincidence detection in L5 PCs is up or down-regulated by the addition of proximal or distal oblique dendritic branches respectively (Schaefer, Larkum et al. 2003). In such studies, the accuracy of reconstructed morphologies is paramount. The choice between reconstruction methods may lead to systematic differences in reconstructed morphologies – particularly in features such as neurite diameter – which may have considerable effects on the results of such modelling studies (Vetter, Roth et al. 2001, Tsay and Yuste 2002, Acker and White 2007, Sarid, Feldmeyer et al. 2013). It is therefore important to quantify such effects, in order to understand if method choice may alter the results of modelling studies on a level that may obscure differences caused by variation in the true underlying morphology of cells.

To address the issues discussed above, single-cell modelling of action potential backpropagation (bAP) and EPSP forward propagation was performed using FI and BH reconstructions of the same original PCs in the NEURON simulation environment (Figure 3-5). As the parameters of the model (Stuart and Hausser 2001) were invariant throughout experiments (see 2.9), systematic discrepancies in results should reflect differences in reconstructed morphology caused by method choice.

Investigation of bAP simulations was performed by generation of a rheobase spike at the soma of each model (Figure 3-5). The resulting changes in potential were measured throughout the dendritic tree, and the measured peak potentials (bAP amplitudes) at each location were plotted against distance from the soma. Perhaps unexpectedly, although FI reconstructions exhibited a small trend for weaker depolarisation, simulated bAP propagation was indistinguishable between methods at all locations. Whilst this may indicate that reconstruction method choice may have only subtle effects on modelling, it is also important to mention that these findings might also depend on the model parameters used – for example active properties of dendrites.

Comparison of simulated EPSP forward propagation was achieved by placing a model synapse at visually matched locations on FI and BH reconstructions of the same cells (Figure 3-5). As with bAP simulations, the resulting peak depolarisation (EPSP amplitude) due to activation of this synapse was measured across the morphology. FI reconstructions consistently resulted in smaller depolarisations. Due to synapse locations varying between cells (but not between reconstructions of the same cells using different methods), averaging was performed on somato-synaptic distance normalised data. Comparison of these data indicated that FI reconstructions exhibited systematically lower depolarisations in response to the same stimulation (peak amplitude; FI vs. BH; 6.27 ± 0.33 mV vs. 15.65 ± 1.63 mV, $p<0.01$; other areas of significance where $p<0.05$ indicated by black bar in Figure 3-5 C).

Although no systematic differences were identified between methods for bAP simulations, the large differences in process diameter between FI and BH reconstructions may be expected to affect the spatial rate of voltage decay in both active and passive processes (Segev 1998). To assess this possibility, the length constant (λ) was approximated (see methods) in each reconstruction using the voltage response during the steady-state period of a small current injection at matched locations between FI and BH reconstructions of the same cells (see 2.9). At least for passive propagation, as $\lambda = \sqrt{\frac{R_m}{R_a}}$, where R_m = membrane resistance and R_a = axial resistance, increases in neurite diameter would be expected to lead to increases in λ. Surprisingly, given the large and systematic differences in neurite diameter between reconstructions (Figure 3-4), differences in λ were indistinguishable between methods (λ_{FI} = 321.128 ± 65.185 μm vs. λ_{BH} = 308.518 ± 46.319 μm, $p=0.80$). The lack of measurable systematic differences in λ was presumably due to other non-systematic differences between reconstruction methods that also affected length constants. For example, the branching patterns and local variations in diameter may well have differed non-

systematically, despite general and individual compartment diameters being larger in FI reconstructions.

Overall, whilst some effects of method choice on modelling results (such as in bAPs or λ measurements) may be too subtle to be significant, there was a consistent and dramatic reduction in simulated EPSP depolarisations in FI reconstructions in response to the same synaptic stimulation. As such, FI reconstructions may not be suitable for single-cell modelling applications.

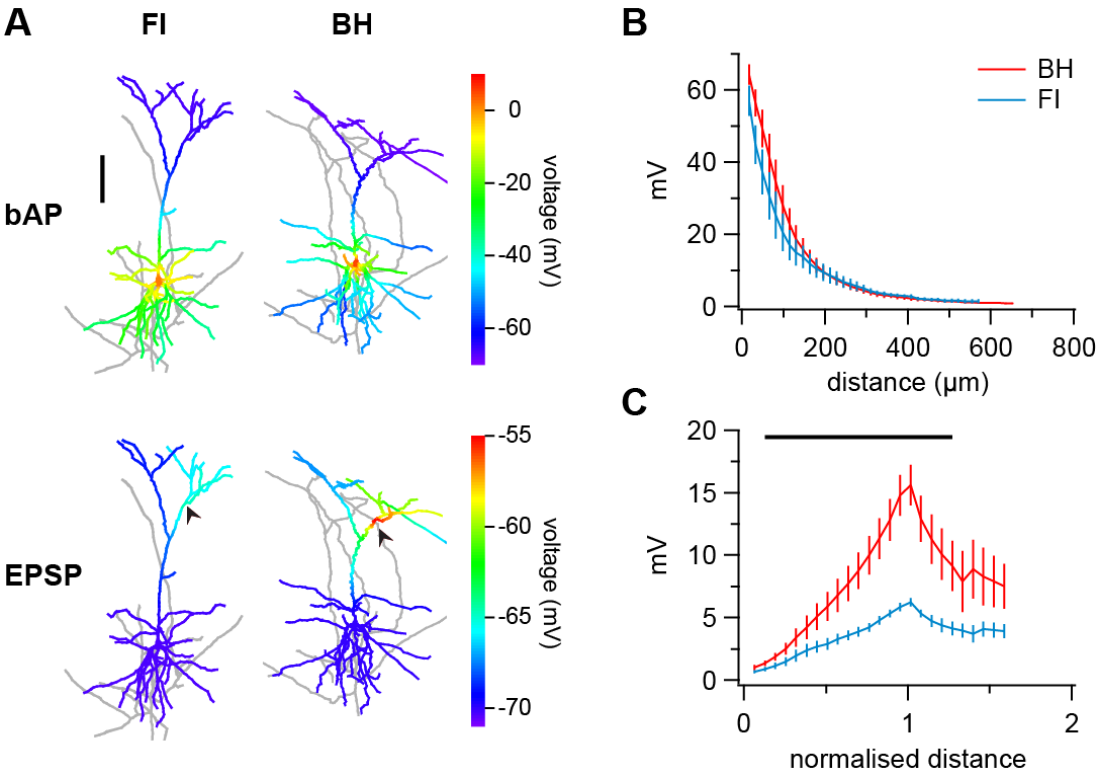

Figure 3-5: FI reconstructions introduce errors in single-cell modelling

A: Example of the same PC reconstructed with FI (left column) and BH (right column) methods, indicating peak potentials (mV; colour bars to right of examples) recorded during simulated backpropagating action potentials (bAP; top row) or forward propagating EPSPs (EPSP; bottom row). Whilst peak potentials in bAP simulations appeared similar, depolarisations due to simulated EPSPs were smaller in FI reconstructions. For EPSP, arrows indicate matched location of synapse. Distal branches of morphologies are slightly cropped to increase clarity. B: Ensemble averages of bAP simulations (n=5 cell pairs), indicating peak amplitudes vs. distance from soma. Peak voltages were indistinguishable at all locations between FI and BH methods. Vertical bars indicate ± SEM. C: Somato-synaptic distance normalised ensemble averages of peak amplitudes resulting from EPSP simulation (n=5 cell pairs). FI reconstructions exhibit a striking reduction in depolarisations. Distance is normalised to somato-synaptic distance. Black bar indicates region of significance (paired *t*-test, $p<0.05$). Figure as originally published in Blackman AV, Grabuschnig S, Legenstein R and Sjöström PJ (2014) A comparison of manual neuronal reconstruction from biocytin histology or 2-photon imaging: morphometry and computer modeling. Front. Neuroanat. 8:65. doi: 10.3389/fnana.2014.00065.

Morphometric Measure	PC (FI)	PC (BH)	P value (paired t-test; n=5 cells)	BC (FI)	BC (BH)	P value (paired t-test; n=3 cells)
X-Center of axonal density cloud	-7.20 ± 7.28	6.96 ± 15.58	0.272	-13.95 ± 17.76	7.57 ± 16.53	0.260
Y-Center of axonal density cloud	-30.13 ± 30.50	-7.25 ± 44.83	0.413	-29.09 ± 7.39	-57.21 ± 36.28	0.532
Euclidean distance to axonal cloud center (µm)	59.60 ± 18.31	87.60 ± 18.94	0.244	44.31 ± 9.65	75.88 ± 29.36	0.455
Angle to axonal cloud center (°)	-15.59 ± 47.87	39.83 ± 45.46	0.284	-116.37 ± 21.78	-73.23 ± 33.52	0.468
X-Center of dendritic density cloud	2.65 ± 4.79	-8.17 ± 6.28	0.058	-19.78 ± 8.01	-9.28 ± 11.07	0.132
Y-Center of dendritic density cloud	159.08 ± 32.28	189.65 ± 50.31	0.212	12.21 ± 10.25	-4.40 ± 15.38	0.218
Euclidean distance to dendritic cloud center (µm)	159.43 ± 32.23	190.55 ± 50.02	0.201	31.24 ± 6.22	35.11 ± 4.56	0.754
Angle to dendritic cloud center (°)	89.05 ± 1.98	94.43 ± 2.79	0.046	27.07 ± 69.31	33.41 ± 61.84	0.820
Most distal axonal compartment (X)	-31.83 ± 18.68	196.39 ± 184.98	0.278	-100.11 ± 48.27	-19.63 ± 158.43	0.685
Most distal axonal compartment (Y)	259.49 ± 154.65	217.77 ± 182.32	0.791	-188.26 ± 3.11	-284.15 ± 158.60	0.691
Euclidean distance to most distal axonal compartment (µm)	394.73 ± 48.99	580.31 ± 69.04	0.024	229.51 ± 13.28	468.62 ± 93.33	0.152
Angle to most distal axonal compartment	58.00 ± 37.47	44.22 ± 29.24	0.717	-115.07 ± 12.50	-79.13 ± 35.37	0.393
Most distal dendritic compartment (X)	-65.98 ± 43.90	-130.45 ± 49.65	0.360	15.03 ± 63.92	-52.30 ± 119.22	0.527
Most distal dendritic compartment (Y)	537.10 ± 43.13	556.52 ± 70.89	0.695	55.69 ± 94.62	37.19 ± 107.44	0.637
Euclidean distance to most distal dendritic compartment (µm)	547.91 ± 44.08	581.67 ± 67.72	0.454	216.10 ± 5.18	299.08 ± 12.59	0.013
Angle to most dital dendritic compartment (°)	97.08 ± 4.45	103.57 ± 6.07	0.406	3.65 ± 49.96	18.47 ± 61.80	0.537
Axon hull X center	-9.68 ± 13.67	48.22 ± 39.77	0.112	-16.11 ± 18.00	-4.28 ± 39.89	0.727
Axon hull Y center	5.14 ± 56.98	-21.62 ± 57.86	0.523	-42.23 ± 8.59	-90.65 ± 57.26	0.536
Axon hull width (µm)	348.21 ± 39.72	672.47 ± 55.36	0.004	357.46 ± 12.82	572.72 ± 30.10	0.011
Axon hull height (µm)	587.62 ± 58.75	751.04 ± 171.29	0.281	281.82 ± 10.25	475.71 ± 121.74	0.356
Dendrite hull X center	-5.38 ± 9.99	-8.95 ± 12.44	0.633	-15.75 ± 12.70	-21.95 ± 23.87	0.736
Dendrite hull Y center	198.48 ± 25.84	203.68 ± 47.22	0.835	25.26 ± 11.10	17.30 ± 16.88	0.685
Dendrite hull width (µm)	284.90 ± 11.56	392.02 ± 70.34	0.188	299.56 ± 11.55	398.70 ± 17.58	0.044
Dendrite hull height (µm)	672.59 ± 48.90	736.56 ± 80.09	0.324	291.05 ± 28.34	335.77 ± 52.82	0.402
Sholl Maximum value (axon)	16.60 ± 2.50	15.00 ± 1.90	0.538	42.33 ± 8.69	43.67 ± 3.14	0.899
Sholl Critical radius (axon)	96.05 ± 8.24	102.85 ± 28.52	0.859	80.75 ± 11.40	106.25 ± 6.58	0.374
Sholl Maximum value (dendrite)	36.20 ± 1.62	36.80 ± 4.94	0.874	21.00 ± 1.61	21.67 ± 2.91	0.826
Sholl Critical radius (dendrite)	45.05 ± 4.96	48.45 ± 12.72	0.717	49.58 ± 12.22	60.92 ± 13.35	0.762
Maximum / enclosing Sholl radius (axon)	388.45 ± 49.52	573.75 ± 67.68	0.021	225.25 ± 13.17	466.08 ± 93.45	0.154
Maximum / enclosing Sholl radius (dendrite)	541.45 ± 44.93	578.85 ± 67.45	0.406	211.08 ± 4.39	296.08 ± 11.61	0.013

L-measure Function						
Soma_Surface (µm²)	317.40 ± 56.87	138.98 ± 19.97	0.032	240.08 ± 19.11	132.67 ± 24.57	0.124
Width (µm)	306.76 ± 21.79	537.38 ± 80.28	0.078	301.10 ± 18.59	406.52 ± 17.76	0.024
Height (µm)	684.17 ± 39.19	807.29 ± 89.55	0.115	298.58 ± 12.11	484.32 ± 153.62	0.372
Depth (µm)	83.00 ± 4.25	57.20 ± 8.68	0.008	80.33 ± 6.77	46.61 ± 6.40	0.108
Diameter (µm)	1.49 ± 0.15	0.83 ± 0.02	0.008	1.03 ± 0.07	0.60 ± 0.02	0.041
Length (µm)	6.16 ± 0.58	5.12 ± 0.55	0.127	4.69 ± 0.42	3.54 ± 0.43	0.149
EucDistance (µm)	182.06 ± 20.44	219.98 ± 35.73	0.119	89.66 ± 4.42	120.49 ± 20.96	0.270
PathDistance (µm)	245.02 ± 24.46	296.27 ± 48.19	0.121	187.87 ± 14.84	259.50 ± 48.38	0.326
Branch_Order	6.02 ± 1.43	5.93 ± 1.37	0.779	5.22 ± 1.37	7.70 ± 2.17	0.224
Taper_1	0.04 ± 0.01	0.04 ± 0.00	0.302	0.03 ± 0.01	0.02 ± 0.00	0.647
Contraction	0.93 ± 0.00	0.91 ± 0.01	0.275	0.90 ± 0.01	0.91 ± 0.01	0.706
Daughter_Ratio	1.75 ± 0.10	1.72 ± 0.10	0.858	1.68 ± 0.16	1.38 ± 0.13	0.296
Parent_Daughter_Ratio	0.97 ± 0.02	0.86 ± 0.02	0.021	1.04 ± 0.02	0.93 ± 0.01	0.073
Bif_ampl_local (°)	69.24 ± 3.01	74.57 ± 7.23	0.356	75.40 ± 2.77	88.84 ± 3.75	0.038
Helix (µm)	0.00 ± 0.00	0.00 ± 0.00	0.114	0.00 ± 0.00	0.00 ± 0.00	0.620
Fractal_Dim	1.02 ± 0.00	1.02 ± 0.00	0.553	1.03 ± 0.00	1.02 ± 0.01	0.499

Table 3-1: Comparison of morphometric measures between FI and BH reconstructions

Measures are those used in Figure 3-2 and Figure 3-3 for comparison of FI and BH reconstructions of PCs and BCs. Measurements were obtained with in-house software (qMorph) or L-measure. Comparisons with significance levels $p<0.05$ and $p<0.01$ are highlighted in green and yellow, respectively. Unitless measures such as counts and ratios are indicated with (-). Table as originally published in Blackman AV, Grabuschnig S, Legenstein R and Sjöström PJ (2014) A comparison of manual neuronal reconstruction from biocytin histology or 2-photon imaging: morphometry and computer modeling. Front. Neuroanat. 8:65. doi: 10.3389/fnana.2014.00065.

3.5. Discussion

In this chapter, the relative merits and effects of reconstruction method choice (between two commonly used reconstruction methods) on studies involving morphometry and computer modelling have been quantified and assessed. This analysis is timely as whilst one method, BH is well established and considered state of the art, the other, FI, is rapidly gaining in popularity (Halavi, Hamilton et al. 2012). As such, it is important for the design of future experiments to know the strengths and pitfalls of either method. By direct comparison of reconstructions of the same individual cells using either method here, it has been possible to identify such strengths and limitations, and in turn make recommendations as to the suitability of FI or BH for particular applications. According to the results presented in this chapter, FI is preferable for cell-type classification scenarios and studies requiring distortion-free representation of local morphology, whilst BH is superior for multicompartmental modelling, detailed tracing of thin arborisations over a long range, and applications requiring accurate measurements of neurite diameter.

3.5.1. Quantitative morphometry and cell-type classification

A key use of 3D reconstructions of neurons is to enable quantification of morphology. In studies of neural circuit properties, this is often with the aim of defining cell type; axonal morphology is currently widely regarded as the best way to determine cortical interneuron cell type (Markram, Toledo-Rodriguez et al. 2004, Wang, Toledo-Rodriguez et al. 2004, Toledo-Rodriguez, Goodman et al. 2005, Ascoli, Alonso-Nanclares et al. 2008). The importance of accurately identifying neuronal cell type during studies investigating neural circuits is supported by increasing evidence that many properties – such as short-term plasticity, synapse type and ion channel expression – are dependent on anatomical cell class, even at connections from a single presynaptic cell (Blackman, Abrahamsson et al. 2013). As such, it is important to verify the performance of emerging reconstruction methods such as 2PLSM FI when used for cell classification. If, for example,

FI offers comparable classification performance to BH, then its other benefits (lower cost, higher yield, higher throughput etc.) could be used to the advantage of studies investigating cell-type specific circuit properties. On the other hand, if FI reconstructions adversely affect classification performance, then studies relying on this method may be subject to errors.

The results presented here indicate that FI and BH reconstructions are comparable in revealing the majority of neuronal morphology, with most morphological measures being indistinguishable between the two methods (Table 3-1). For the purposes of cell-type classification, both methods appear to exhibit similar performance; unsupervised clustering segregates pyramidal and basket cells from both methods, but does not form subclusters composed of reconstructions from a particular method type (Figure 3-3). As touched upon above, whilst FI and BH appear equivalent for classification applications, FI confers a number of benefits, which make it a preferable method choice. Firstly, FI offers a near 100% yield, as the experimenter can monitor imaging online and adjust parameters such as laser power when acquiring images. This is in contrast to the 50-80% yield of BH (in the experience of the author), which is dependent on the outcome of histological processing. The yield of BH is highly dependent on experience and the refinement of the process, as well as other factors such as cell type, tissue age, etc.; whilst the yield of BH can clearly be improved with training (as it has in the experience of the author), it will never reach 100%. On the other hand, FI reconstructions are straightforward from initial attempts, and as such are suitable even for untrained or novice lab members such as undergraduates. Furthermore, FI offers some particular advantages for experiments where morphology is used to identify cell-type in neural circuits; morphology can be examined subjectively online with FI, increasing the throughput of electrophysiology experiments where e.g. a particular IN type is targeted. Additionally, FI does not suffer from the unwanted distortions, compression and shrinkage seen with BH – this would be a particular advantage in studies focusing on detailed 3D morphometry requiring models with accurate depth (in the z-axis). Whilst shrinkage in the Z-axis is well documented with BH (Egger, Nevian et al. 2008), as are nonlinear distortions

when embedding with Mowiol (Marx, Gunter et al. 2012), the expansion in XY seen here may be due to further compression from coverslipping. Because of these factors, FI reconstructions may in some ways better represent the true 3D morphology.

A further important consideration (as with all methods) is the cost incurred by the choice of either FI or BH. Here, provided one already has two-photon imaging set up, FI may offer a distinct advantage. Firstly, FI does not require the histological processing step or dedicated Neurolucida setup needed for BH reconstructions; the use of less auxiliary equipment and consumables results in lower cost per reconstruction. Additionally, FI image stacks are collected at the same time as electrophysiological recording, saving running costs. As mentioned above, FI is dependent on the ability to perform 2PLSM or confocal imaging – if a lab does not already have access to these technologies the high setup costs may be prohibitive. In the opinion of the author, as many labs are already using 2PLSM or confocal imaging, the cost savings of FI, coupled with its equal performance in cell classification and representation of local morphology, and lack of distortions, render FI the preferred method for studies focussing on morphological cell-type classification. This said, there may still be some scenarios where BH is preferable for this purpose, such as when cell-types extend over far greater areas than those described here (Lichtman and Denk 2011). Whilst the extent of morphology revealed by FI may be improved by increasing fluorophore concentration, fill time and area imaged (see Figure 3-2), the results presented here indicate that BH is indeed superior in revealing more distal processes (see Table 3-1; hull widths, maximum Sholl radius, etc.). As such, BH may be preferable when long-distance tracing is required. This said, successful long-range tracing of axonal arbours using FI has been successfully reported (Pressler and Strowbridge 2006, Williams, Larimer et al. 2007). Indeed, FI may be used to map large-scale connectivity using methods such as serial two-photon tomography (Ragan, Kadiri et al. 2012, Osten and Margrie 2013).

3.5.2. Single-cell multicompartmental computer modelling

3D reconstructions of neurons find another major use in single-cell modelling studies, where realistic model neurons are used as the basis of simulations in environments such as NEURON. Here, reconstructions must be as accurate as possible, as even small differences in morphology can exert significant effects on passive and active properties of neurons (Rall, Segev et al. 1995, Vetter, Roth et al. 2001). To illustrate, the number and position of oblique dendrites is thought to affect the degree of coupling (that is, the reduction in threshold for a dendritic Ca^{2+} spike caused by a coincident bAP) in L5 PCs, an effect replicated with modelling (Schaefer, Larkum et al. 2003). As described in that study, modelling places particular constraints on the quality and accuracy of reconstructions; omission of dendritic branches, for example, is likely to have a much greater effect than compression or distortion of a fully described morphology. Here, results revealed that differences in reconstructed morphologies, resulting purely from reconstruction method choice, have large and significant effects on multicompartmental simulations. FI reconstructions consistently exhibited much smaller simulated EPSP amplitudes than BH reconstructions of the same cells (see Figure 3-5).

As described in Figure 3-4, a key contributor to the observed differences in EPSP simulation between FI and BH reconstructions is likely the large differences in dendritic diameter observed between the two methods, where FI consistently overestimated diameters as compared to BH. These differences alone would be expected to affect models of synaptic efficacy (Holmes 1989) and voltage attenuation (Stuart and Spruston 1998), amongst others. As FI exhibits larger process diameters both on average and for matched compartments, this is likely a major factor in the observed differences in modelling results. A lack of spine detection is unlikely to be the cause of this effect, as spines and axonal varicosities can be visualised with both FI and BH. There are however a number of plausible and expected factors that may have contributed to the overestimation of diameters in FI.

For example, increasing laser power during 2PLSM image acquisition typically results in a noticeable thickening of dendrites and axons; the experimenter may increase power to an extent revealing thinner neurites when monitoring imaging online, also increasing the perceived diameter of all other processes. Furthermore, when performing manual reconstruction in e.g. Neuromantic, the experimenter may adjust brightness and contrast settings to compensate for weak fluorescence, in the process broadening diameters. With BH, such compensations appear not to be required, presumably because the contrast produced during the staining procedure is in itself sufficient. BH, due to the wavelength of illuminating light and typical usage of high numerical aperture oil-immersion objectives, also benefits from a higher resolution limit than that of 2PLSM. For the same reasons, it may be expected – although this has not been tested – that confocal microscopy may suffer less from neurite thickening than 2PLSM, as it benefits from a better resolution limit.

If differences in diameter between FI and BH reconstructions are systematic, it may be possible to determine a procedure to correct for this and in turn correct simulation results to match those seen with BH reconstructions. In order to explore this, a preliminary multiplicative correction factor with an additive offset was determined using linear regression performed on data shown in panel C of Figure 3-4: BH diameter = 0.33 • FI diameter + 0.32 ($p<0.01$). Using these parameters, the diameters of all FI compartments were adjusted on a node-wise basis (100 nodes per compartment) in an attempt to match those of the corresponding BH reconstruction. Using these adjusted morphologies, simulations were performed and compared to those using BH reconstructions. After this adjustment, simulated EPSP amplitudes were recovered to the levels seen with BH (Figure 3-6; $p>0.05$ at all locations). However, bAP simulations now exhibited several regions of significant difference, with adjusted FI bAPs failing earlier than their BH counterparts. The difficulties encountered in attempting to correct for differences in diameter between FI and BH presumably stem from the presence of non-systematic differences between the methods and

reconstructions; indeed, this may have been indicated previously by the similarity of length constants between methods (see 3.4.5).

Further to these caveats, there are a number of reasons to exert caution when considering the determination of a correction factor for FI. Firstly, whilst it may be possible with further analysis to determine correction parameters for a particular experimenter and setup by directly comparing BH and FI diameter differences, there is reason to believe that these parameters may not hold in alternate situations. For example, wide variation in neurite diameters and simulation results has been described between experimenters when reconstructing the same cell from multiphoton imaging (Losavio, Liang et al. 2008). Furthermore, whilst there are several good reasons to treat BH as preferable for single-cell modelling, without technically demanding dendritic recordings it is difficult to ascertain completely the ground truth (whether FI or BH reconstructions produce simulations closer to reality). Here, the higher resolution and better signal-to-noise ratio of BH provide evidence to support its use for single-cell modelling over FI..

Due to the difficulties in determining generalisable correction parameters, and the other factors described above, the usage of BH is recommended in all multicompartmental modelling applications. BH has been shown in this chapter to reveal greater morphological detail – this is of importance as even small differences in dendritic branching may result in large effects on e.g. the physiological properties of cortical pyramidal cells (Schaefer, Larkum et al. 2003). As such, simulations of properties such as synaptic integration and coincidence detection should be based on the most accurate representations of morphology – in particular branching and process diameters – possible. In contrast, the compression and distortions found with BH reconstructions are actually not likely to have a major effect on simulations (Schaefer, Larkum et al. 2003), and as such are less of an issue for modelling than they may be in morphometric applications. Until resolution-limit breaking FI methods (see below) become standard in many labs, BH reconstructions should be considered superior for all light microscopy based computer modelling studies.

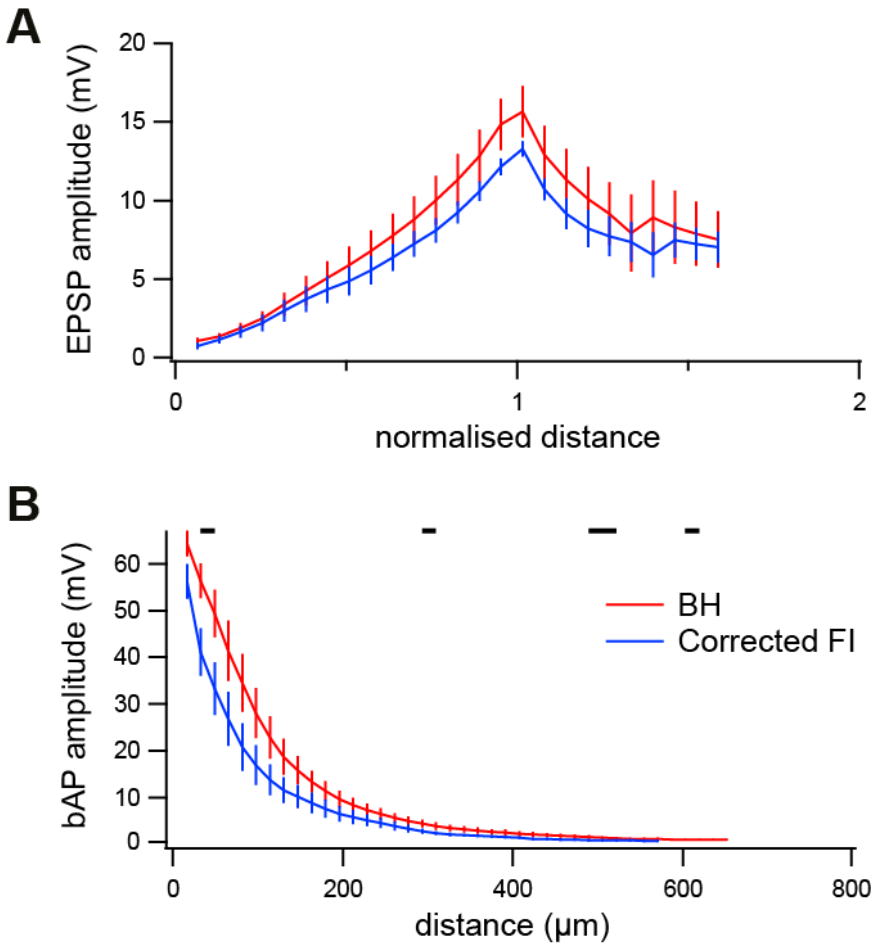

Figure 3-6: Adjustment of FI neurite diameters recovers simulated EPSP amplitude but introduces errors in bAPs

A: Adjustment of FI process diameter alone based on comparison with BH diameter (n=5 PC cell pairs; see text; compare with Figure 3-5) resulted in reconstructions with indistinguishable simulated EPSP amplitude to BH equivalents. Vertical bars indicate ± SEM B: FI diameter adjustment however introduced significant differences in simulated bAPs when compared to BH reconstructions (vertical bars indicate ± SEM; black bars indicate regions where $p<0.05$; compare to Figure 3-5 where no distinguishable differences are seen).

3.5.3. Future directions, improvements and alternative approaches

In this chapter the focus has been on two commonly used methods to reconstruct neurons with light microscopy; the choice of methods to compare was made with the aim of providing a broadly applicable quantitative comparison of the strengths and weaknesses of fluorescence and histology based reconstructions. However, this is not to say that these are the only viable reconstruction methods; a range of alternative methods are becoming increasingly available, and some of these may offer ways to address and

improve upon issues identified with FI and BH. This said, these methods are often far more technically demanding, expensive and time consuming.

Improvements to fluorescence imaging

For FI imaging and reconstructions, perhaps the largest issues identified in this chapter are a lack of accuracy at high detail levels (diameters, smaller and distal neurites), presumably due to the effects of image processing, scattering of laser light in brain tissue, and, importantly, a worse resolution limit than other forms of light microscopy.

Recent advances in fluorescence imaging have, however, made it possible to use FI to image structures under the resolution limit with 2PLSM (Hell 2007). An example of this is stimulated emission depletion microscopy (STED), which relies on a spatially selective deactivation of fluorophores (through stimulated emission) with a depletion laser – usually a doughnut shape around the excitation laser – thus reducing the area from which detectable fluorescence can be emitted (Ding, Takasaki et al. 2009). Methods such as this offer the potential to produce reconstructions using 2PLSM FI with the detail required for accurate diameters and usage in NEURON modelling, albeit requiring systems which have not yet been widely adopted and may be highly expensive. If information from electrophysiological recording is not required alongside detailed reconstructions, an alternative method to create accurate models may be to use microinjection of fluorescent dyes in fixed tissue and subsequent confocal microscopy with deconvolution (Dumitriu, Rodriguez et al. 2011). Confocal microscopy in general may produce reconstructions with different properties to the 2PLSM FI reconstructions shown here, as previously noted.

Issues and potential improvements using biocytin histology

Whilst for many measures such as diameters and completeness the BH reconstructions compared here appear superior to those generated with FI, there are still some identifiable issues with BH. A key shortcoming is perhaps the propensity of BH reconstructions to be affected by distortions and

deformations, or by shrinkage introduced in the fixation process. These artefacts are potentially more of an issue for morphometry than for modelling, as discussed in 3.5.2. Additionally, BH requires more time to refine and set up for the novice experimenter, introducing a risk of including reconstructions from incompletely processed tissue.

A recent improved biocytin protocol has been shared which may address some of these issues; here, slow dehydration and the embedding medium Eukitt are used – this appears to preserve some cytoarchitectonic features and allows for a consistent correction for shrinkage to be applied in all directions (Marx, Gunter et al. 2012). This may allow for more realistic and accurate morphologies to be constructed than with the far more common BH method used here, and may alleviate issues with distortions for demanding morphometric applications. This said, this method is not currently widely used and requires many more reagents than the standard BH protocol used here.

3.5.4. Conclusions

In this chapter, a quantitative comparison of reconstructions created with two popular methods (FI and BH) has been completed, and significant systematic differences in aspects of performance in morphometry and computer modelling have been identified. This is a timely exploration of these issues due to the recent increase in FI reconstructions (Halavi, Hamilton et al. 2012), and should influence the design and interpretation of future experiments and modelling studies. Whilst both methods are comparable for many morphological applications, including cell classification, BH reconstructions provide more detail and completeness but suffer from compression and distortion. For single-cell modelling, simulated EPSPs had consistently smaller amplitudes in FI reconstructions, an effect resulting from systematically enlarged diameters when compared to BH.

Recommendations for future experiments

Due to the issues described above, it is important to take into account reconstruction method and its potential effects when designing or interpreting experiments. Particularly for simulations, there is a danger of introducing non-physiological variability caused solely by the effect of method choice, especially if reconstructions from different methods are mixed. This is a consideration that should be emphasised when the use of large amounts of reconstructions from third parties or databases such as NeuroMorpho.org (Ascoli, Donohue et al. 2007) is considered. According to the results in this chapter, BH reconstructions are a benchmark for accuracy (particularly in modelling applications). However, FI reconstructions confer many benefits that make them preferable for cell classification (such as a lack of compression and distortion), where they offer equal performance with higher throughput, lower cost and technical difficulty. As such, for many physiological studies (such as that described in Chapter 4), where reconstruction is used primarily for cell-type identification, FI reconstructions are indeed a superior choice.

4. Target-cell-specific expression of presynaptic NMDA receptors in neocortical microcircuits

4.1. Overview

This chapter is based on a study published in *Neuron* (Buchanan, Blackman et al. 2012), of which I am co-first author. NMDA receptors (NMDARs) are ionotropic glutamate receptors that classically are found postsynaptically where their dual requirement for glutamate binding and depolarisation-mediated relief of Mg^{2+} block allows them to act as Hebbian coincidence detectors (MacDermott, Mayer et al. 1986, Ascher and Nowak 1988). However, more recent evidence suggests the existence of putatively presynaptic NMDA receptors (preNMDARs) (Corlew, Brasier et al. 2008, Duguid and Smart 2009, Duguid 2013), including in cortical L5 PCs (Sjostrom, Turrigiano et al. 2003), where their location has proved controversial (Christie and Jahr 2009). As discussed earlier in this thesis, many (pre-) synaptic properties of cortical circuits are target and cell-type specific, including preNMDAR expression (Brasier and Feldman 2008). Using the methods validated in chapter 3 to identify and classify type for cells used in paired electrophysiological recordings and imaging experiments, it is shown that in L5 of developing mouse visual cortex, preNMDARs are expressed specifically at synapses between PCs onto other PCs and Martinotti interneurons (MCs), whilst synapses onto basket cells (BCs) lack preNMDARs. Furthermore, a novel fast-spiking IN type that mediates ascending inhibition is described, for which PC-IN synapses express preNMDARs. PreNMDARs are found to upregulate synaptic transmission during high frequency PC firing, working in conjunction with synapse-specific differences in short-term plasticity to reroute information flow and remap inhibition across the somato-dendritic axis.

4.2. Authorship

I completed all morphological reconstructions and analysis, identification of synaptic contacts, antibody labelling experiments, and, where noted, extracellular stimulation experiments and paired recordings. Other paired recordings were performed by Katherine A Buchanan, Txomin Lalanne and Dale Elgar. Imaging experiments were performed by Katherine A Buchanan, Txomin Lalanne and Alexandre W Moreau. Computer models were implemented by Rui Costa. Some extracellular stimulation experiments were performed by Dale Elgar and Julia Oyrer. MiniEPSC recordings were performed by Katherine A Buchanan and Adam A Tudor-Jones.

4.3. Introduction

4.3.1. The NMDA Receptor

NMDA receptors are heterotetrameric ionotropic glutamate receptors, which are nonselectively permeable to cations and are blocked by Mg^{2+} at the typical resting potential of neurons (Nowak, Bregestovski et al. 1984, Cull-Candy, Brickley et al. 2001, Lee, Lu et al. 2014). NMDARs are known to play a number of roles in e.g. synaptic transmission (Salt 1986), dendritic integration and computation (Schiller, Major et al. 2000) and excitotoxicity (Choi, Koh et al. 1988). Perhaps the most well known function of the NMDAR is its canonical role as a coincidence detector in Hebbian long-term plasticity (Hebb 1949, Bliss and Lomo 1973, Herron, Lester et al. 1986, Bliss and Collingridge 1993), where the dual requirement for glutamate binding and postsynaptic depolarisation is key to its function in detecting coincident pre- and postsynaptic activity; as such, NMDARs must be located postsynaptically. However, recent and increasing evidence suggests the existence of putatively presynaptic NMDA receptors across a variety of brain areas (Corlew, Brasier et al. 2008), the existence of which has proved controversial (Duguid 2013).

4.3.2. Presynaptic NMDA receptors

Although a presynaptic location of NMDARs may at first seem counterintuitive, as it appears to prevent e.g. their function as coincidence detectors without retrograde signalling from the postsynapse, preNMDARs have been reported in many recent studies (Duguid and Sjostrom 2006, Corlew, Brasier et al. 2008, Duguid and Smart 2009). Such presynaptic receptors are perhaps ideally situated to modulate transmitter release at the presynapse; evidence for NMDA-dependent facilitation of neurotransmitter release from noradrenergic synaptosomes prepared from terminals in cortex and other areas provided the first evidence for the existence of putative preNMDARs (Fink, Bonisch et al. 1990, Duguid and Smart 2009). Further physiological studies have implicated putative cortical preNMDARs in spontaneous release (Berretta and Jones 1996, Woodhall, Evans et al. 2001), evoked release and short-term plasticity (Sjostrom, Turrigiano et al. 2003, Brasier and Feldman 2008) and spike-timing dependent plasticity (Sjostrom, Turrigiano et al. 2003, Bender, Bender et al. 2006). Physiological evidence for preNMDARs has been obtained across many additional brain areas such as hippocampus (Mameli, Carta et al. 2005), cerebellum (Glitsch and Marty 1999, Duguid and Smart 2004) and others (Duguid and Sjostrom 2006, Corlew, Brasier et al. 2008).

In the majority of studies mentioned above, evidence for putative preNMDARs is provided by identifying a presynaptic locus of effect, for example based on the observation that the NMDAR antagonist APV reduces frequency but not amplitude of miniEPSCs (Berretta and Jones 1996), or alters short-term plasticity during evoked release (Sjostrom, Turrigiano et al. 2003). Whilst the most parsimonious explanation for these effects would be a presynaptic location of NMDARs, and this is supported by the e.g. the lack of effect of postsynaptic NMDAR blockade (Berretta and Jones 1996) or the prevention of effect by inclusion of MK801 in the presynaptic (Rodriguez-Moreno and Paulsen 2008) but not postsynaptic patch pipette (Bender, Bender et al. 2006), it remains possible that putative preNMDARs may not be located precisely at axonal terminals. Although anatomical evidence for

axonal preNMDARs exists (Liu, Wang et al. 1994), including in visual cortex (Aoki, Venkatesan et al. 1994), their precise subcellular location remains controversial. It has been suggested that presynaptic NMDAR-mediated effects may be caused by activation of dendritic NMDARs on the presynaptic cell (Christie and Jahr 2008). In cerebellar basket cells (Pugh and Jahr 2011) and L5 PCs of the visual cortex (Christie and Jahr 2009), a failure to detect NMDAR-mediated Ca^{2+} transients in axons with iontophoresis of L-aspartate has been reported as evidence for the absence of axonal preNMDARs, perhaps suggesting that presynaptic NMDAR-mediated effects in these cells may be due to activation of dendritic NMDARs (Christie and Jahr 2008, Christie and Jahr 2009). This said, as opposed to in cerebellum, NMDAR-like somatic subthreshold depolarisations did not result in axonal Ca^{2+} transients. An alternative possibility is that preNMDAR expression is synapse-specific, and as such not all terminals express preNMDARs, complicating their detection. It has been reported that synapses between L4 and L2/3 PCs express preNMDARs, whilst L4-L4 or L2/3-L2/3 synapses do not (Brasier and Feldman 2008); compartment-specific release of a novel caged form of MK801 in the presynaptic cell at L4-L2/3 synapses strongly suggests that these putative preNMDARs are indeed located in the axon (Rodriguez-Moreno, Kohl et al. 2011), a result supported by EM localisation of presynaptic NR1 in L2/3 (Corlew, Wang et al. 2007).

If preNMDAR expression is pathway-specific, this suggests that these receptors are responsible for specific functional roles in the cortical microcircuit. The apparent developmental regulation of preNMDAR expression also implies preNMDARs play a role in the postnatal emergence and development of cortical circuits (Corlew, Wang et al. 2007). As such, determining precisely when and where preNMDARs are expressed may be key to understanding their function in the local circuit. As discussed in chapters 1 and 3, many synaptic properties may be specific to cell-type, including postsynaptic target cell-type; it remains a possibility that preNMDAR expression in L5 is target-cell-specific, and as such it is important to properly identify cell-type when investigating this. Importantly, whilst preNMDAR expression has been investigated in many different cortical

excitatory-excitatory pathways (Sjostrom, Turrigiano et al. 2003, Bender, Bender et al. 2006, Corlew, Wang et al. 2007, Brasier and Feldman 2008, Corlew, Brasier et al. 2008), there has been a lack of investigation of potential preNMDAR expression at cortical PC-IN connections; the huge variety of cortical IN types (Markram, Toledo-Rodriguez et al. 2004, Ascoli, Alonso-Nanclares et al. 2008), connections to which exhibit a number of cell-type-specific properties (Blackman, Abrahamsson et al. 2013), suggest the possibility of differences in presynaptic ion channel expression at distinct PC-IN synapses.

4.3.3. Evidence for the presynaptic location of NMDA receptors discussed in this chapter

Whilst, as discussed above, the exact location of preNMDARs has been a controversial topic, complementary experiments to those presented in this chapter, both forming part of (Buchanan, Blackman et al. 2012), have addressed this in neocortical L5 PCs. Firstly, the inclusion of the NMDAR channel blocker MK801 in the presynaptic, but not postsynaptic pipette was observed to supress neurotransmission at PC-PC but not PC-IN synapses, suggesting that the NMDARs involved are indeed presynaptic (Buchanan, Blackman et al. 2012). However this may not preclude a dendritic location for these receptors in the presynaptic cell (Christie and Jahr 2008) – to address this possibility, uncaging of MNI-NMDA directly onto axon was utilised; when this was paired with a train of presynaptic action potentials, supralinear calcium signals were observed in a subset of axonal boutons. Similarly, action potential-mediated calcium signals in a subset of axonal boutons were reduced by local puff of the NMDAR antagonist AP5 (Buchanan, Blackman et al. 2012). Taken together, this evidence supports a presynaptic location of preNMDARs (Duguid 2013), similar to that demonstrated in barrel cortex (Rodriguez-Moreno, Kohl et al. 2011), albeit only at certain axonal boutons. As such, it may be the case that expression of preNMDARs is synapse-specific, something which may have complicated their previous detection (Christie and Jahr 2009).

4.3.4. Aims of this chapter

In this chapter, the detailed expression pattern of preNMDARs in microcircuits of cortical L5 is elucidated, along with insight into the functional role of preNMDARs. Using 2PLSM imaging and the morphometric methods outlined in chapter 3 to identify the anatomical type of cells used for paired recordings in transgenic mice, it is found that postsynaptic cell-type determines preNMDAR expression, which may explain why these receptors had proved difficult to detect. Calcium imaging and neurotransmitter uncaging[4] confirms the axonal location of preNMDARs (Buchanan, Blackman et al. 2012). The specific expression pattern of preNMDARs in L5 affects target-cell-specific short-term plasticity, and in turn information flow during high-frequency firing, particularly the spatio-temporal remapping of inhibition across the somato-dendritic axis of L5 PCs. Finally, a novel parvalbumin-expressing interneuron mediating ascending inhibition is described.

4.4. Results

4.4.1. APV selectively suppresses neurotransmission at PC-PC but not PC-IN synapses

In many of the studies discussed in 4.3, the NMDAR antagonist APV supresses excitatory neurotransmission at, for example, L4-L2/3 (Bender, Bender et al. 2006) or L5 PC-PC (Sjostrom, Turrigiano et al. 2003) synapses, with an apparently presynaptic locus of effect. Furthermore, these effects appear to be pathway or synapse-specific, with L4-L4 or L2/3-L2/3 connections appearing resistant to APV application (Brasier and Feldman 2008). The existence of pathway-specific differences in preNMDAR expression suggests the possibility of similar target-cell-specific differences at connections onto different cell types. To investigate this possibility, initial experiments examined the effect of bath application of APV on monosynaptic

[4] These experiments were performed by other researchers, as detailed in 4.2

evoked responses at L5 PC-PC and PC-IN connections (IN = unidentified interneuron, targeted by small round somata, see chapter 2).

Whilst, as expected based on previous studies (Sjostrom, Turrigiano et al. 2003), APV application supressed PC-PC EPSPs evoked during 30Hz firing, PC-IN connections were unaffected, including in triplet recordings where one PC was connected to a postsynaptic PC and IN (Figure 4-1). Where an APV-mediated suppression of neurotransmission was observed, the locus of this effect appeared presynaptic; analysis of paired-pulse facilitation (PPF) for PC-PC connections identified significant changes after APV application (ΔPPF; Figure 4-1), and analysis of changes coefficient of variation (CV; see 2.2.7) identified points below the diagonal, indicating a presynaptic effect if common assumptions are correct (Faber and Korn 1991, Sjostrom, Turrigiano et al. 2007). In contrast, no APV-mediated changes in PPF or CV were observed at PC-IN connections.

Location of putative synapses and preNMDARs

The experiments described above replicate previous studies in L5 (Sjostrom, Turrigiano et al. 2003) and expand upon those describing pathway-specific expression of preNMDARs (Brasier and Feldman 2008) by identifying synapse- and target-cell-specific differences in putative preNMDAR expression at L5 PC-PC and PC-IN synapses, even when the postsynaptic PC and IN share a common presynaptic PC. The existence of differences in APV effect at PC-PC and PC-IN connections in such triplets suggests this is not solely due to presynaptic cell type. Investigation of the location of putative synapses in anatomically reconstructed cell pairs (Figure 4-1) did not identify a proximal-distal gradient of synapses onto PCs or INs in such triplets, arguing against a propagation of effect from dendritic NMDAR activation in the presynaptic cell (Christie and Jahr 2008, Christie and Jahr 2009). A more parsimonious explanation for these results would be that NMDARs mediating the synapse-specific effects described are located near PC-PC, but not PC-IN synapses.

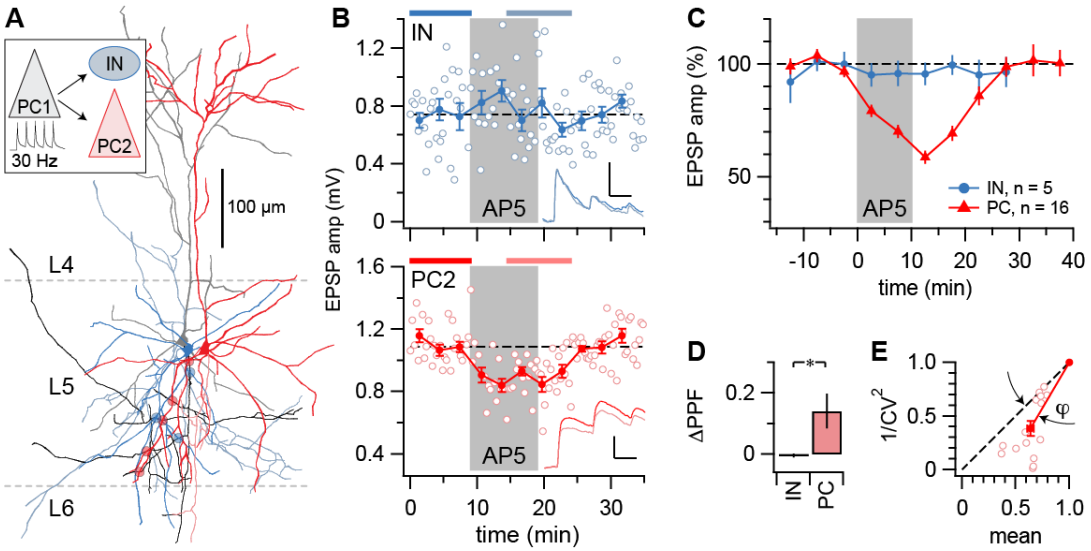

Figure 4-1: APV suppresses PC-PC but not PC-IN EPSPs

A: Representative triplet recording with a presynaptic PC (grey; "PC1") connected to both a postsynaptic PC (red; "PC2) and IN (blue; "IN"). Circles indicate putative synaptic contacts (see 2.6.4). Dashed lines indicate cortical layer boundaries (see 2.6.1). For clarity, PC2 and IN axon is shown in a lighter colour than dendrite, whilst for PC1 the opposite is true. B: APV wash-in failed to suppress PC1-IN EPSP amplitude during 30Hz firing (top; 0.74 mV ± 0.04 mV vs. 0.72 mV ± 0.04 mV, p=0.722), however PC1-PC2 EPSPs were reversibly suppressed by APV (bottom; 1.1 mV ± 0.03 mV vs. 0.89 mV ± 0.02 mV, p<0.001). Bars at top of time panels indicate time periods (before and after) used for statistics and averages. Scale bar = 0.5 mV, 20 ms. C: Ensemble averages of PC-PC and PC-IN recordings revealed that PC-PC connections were consistently reversibly suppressed by APV (after/before = 63% ± 3%, n=15), whilst PC-IN connections were not (after/before = 95% ± 2%, n=6; p<0.001 vs. PC-PC). Averages were of same periods as in B. D: APV altered ΔPPF for PC-PC but not PC-IN connections (cf. traces in panel B), indicative of a presynaptic effect for PC-PC connections (p<0.05). E: CV analysis of PC-PC data identified points on or below the diagonal (angle φ = 14° ± 2°, p<0.001), indicative of a presynaptic effect of APV (Faber and Korn 1991, Sjostrom, Turrigiano et al. 2007), whilst CV was unaffected for PC-IN connections (angle φ = -48° ± 40°, p=0.25, data not shown). Error bars = mean ± SEM. Some data in this figure (paired recordings) were produced by KAB and DE as described in 4.2. Reproduced from Buchanan *et al.* (2012) with permission from Elsevier.

Identification of IN cell type

The neocortex contains a wide variety of interneuronal cell types, with varying physiological and functional properties (Markram, Toledo-Rodriguez et al. 2004). As synapse-specific differences in PC-PC and PC-IN putative preNMDAR expression were identified in 4.4.1, and these INs were patched 'blind' to type, the anatomical and physiological properties of these INs were investigated in order to gain insight into the cell type represented (Ascoli, Alonso-Nanclares et al. 2008), as it remains a possibility that other IN types may have differing putative preNMDAR expression.

'Blind' INs were examined using the FI morphometric techniques described in chapter 3, with additional quantification of the extent of morphology in

different neocortical layers. Inspection of individual morphologies, convex hulls and Sholl analysis revealed IN neurites ramified locally, with few long-range processes. Both axonal and dendritic morphology were largely confined to layer 5, and INs unsurprisingly had small rounded somata, the presence of which was used to visually target these cells for recording. Inspection of reconstructions and stacks did not identify the characteristic vertical axonal cartridges of chandelier cells (Somogyi 1977, Markram, Toledo-Rodriguez et al. 2004).

Alongside anatomy, electrophysiological properties can be a key indicator of IN type (Markram, Toledo-Rodriguez et al. 2004, Ascoli, Alonso-Nanclares et al. 2008, DeFelipe, Lopez-Cruz et al. 2013). As such, the electrophysiological properties of INs were investigated and compared to PCs to gain further insight into cell type. Rheobase spiking patterns appeared to be typically fast-spiking and non-accommodating (Figure 4-2, Table 4-1). Comparison of physiological properties to PCs (Figure 4-2, Table 4-1) revealed INs to have significantly smaller spike height ($p<0.01$), smaller spike half-width ($p<0.01$), less afterhyperpolarisation ($p<0.001$) and a smaller membrane time constant (τ_m; $p<0.001$).

Taken together, the localised morphology and high-frequency narrow half-width spiking observed in INs appears typical of neocortical basket cells, perhaps small basket cells (Markram, Toledo-Rodriguez et al. 2004, Ascoli, Alonso-Nanclares et al. 2008, DeFelipe, Lopez-Cruz et al. 2013). As INs appeared consistent in representing a basket cell type, this both suggests that L5 PC-BC connections may lack preNMDARs, and highlights the possibility that PC connections to other IN types may exhibit different synaptic properties and ion channel expression (Blackman, Abrahamsson et al. 2013).

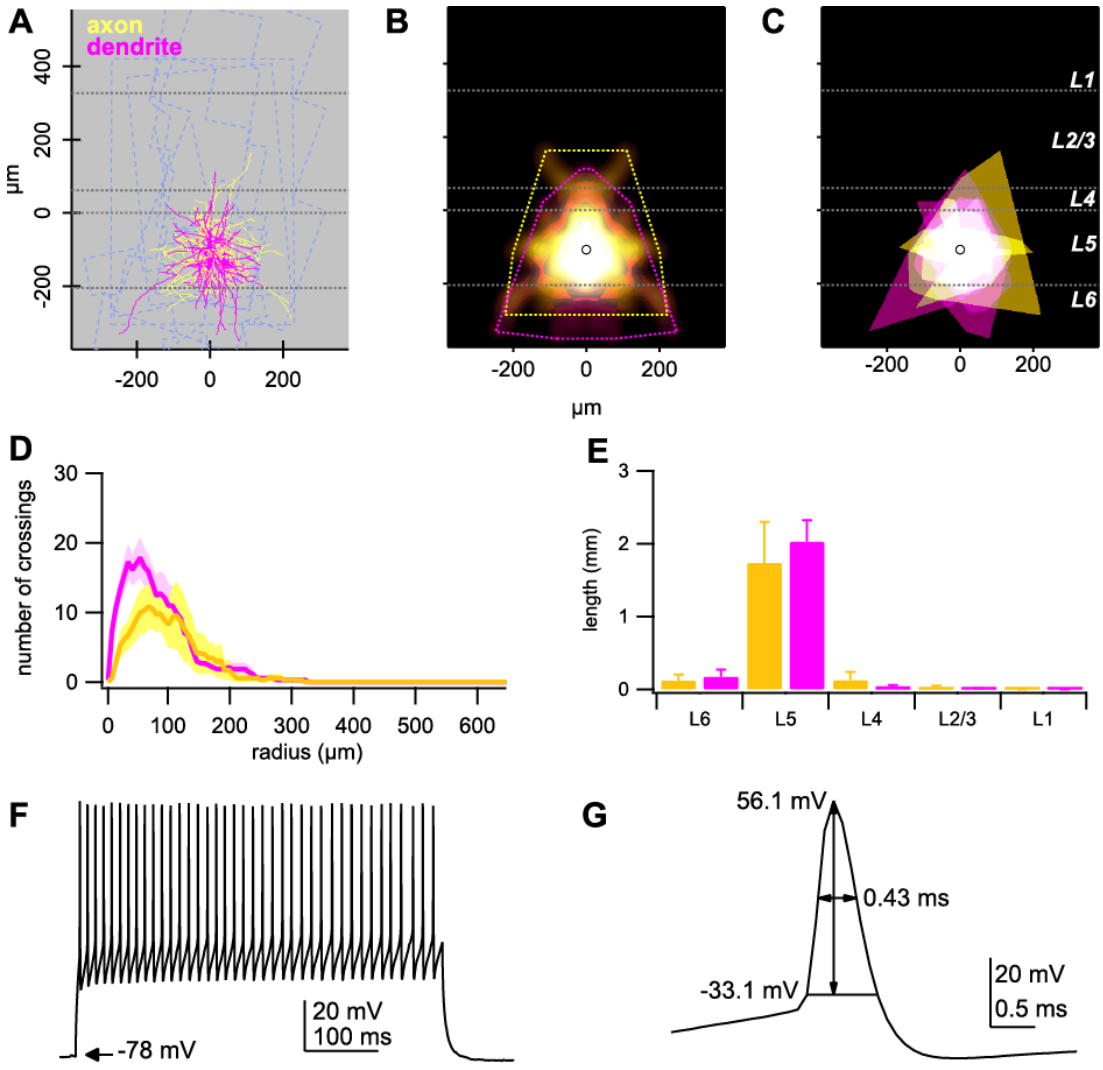

Figure 4-2: IN characteristics suggest a basket cell identity

A: Seven overlaid IN reconstructions (from Figure 4-1). Blue dashed lines indicate extent of 2PLSM FI. Axon = yellow, dendrite = magenta. B: Density map (yellow/magenta; see 2.6.1) and convex hull (dotted yellow/magenta lines) of reconstructions in (A), indicating density and extent of compartments and arborisation. White dotted lines indicate neocortical layers. Open circle indicates soma position. C: Overlay of all convex hulls of reconstructions in (A), indicating individual cell's arborisation extent. D: Ensemble Sholl diagram showing number of axonal (yellow) or dendritic (magenta) processes crossing a given radial distance from the soma (see 2.6.1). E: Histogram of total length of axonal (yellow) and dendritic (magenta) arborisation in different neocortical layers. The majority of both axonal and dendritic arborisation remained confined to layer 5. F: Representative example rheobase spiking pattern of IN. Note fast, regular spiking, indicative of BC identity. G: Illustration of first spike in (F), indicating threshold, half-width and spike height. Note narrow spike half-width, indicative of BC type. See (Table 4-1) for further measures of these cells. Reproduced from Buchanan *et al.* (2012) with permission from Elsevier.

	IN	n	PC	n
Spike threshold (mV)	-42.04 ± 1.89	9	-45.11 ± 2.19	19
Spike height (mV)	43.42 ± 3.99	9	62.64 ± 2.63	19
Spike half-width (ms)	0.82 ± 0.21	9	1.81 ± 0.22	19
Spike afterhyperpolarization (mV)	-13.46 ± 3.16	9	6.64 ± 1.75	19
Rheobase (nA)	0.31 ± 0.11	9	0.15 ± 0.02	19
Frequency (Hz)	25.17 ± 8.57	9	9.17 ± 1.58	19
Accommodation (%)	33.2 ± 7.52	9	384.92 ± 147.14	18
CV (%)	11.97 ± 3.89	9	17.13 ± 3.22	19
V_m (mV)	-68.81 ± 3.69	9	-70.45 ± 2.17	19
R_{in} (MΩ)	153.35 ± 25.04	9	223.34 ± 26.88	19
τ_m (ms)	13.3 ± 2.9	9	29.43 ± 2.9	19
EPSP amplitude (mV)	2.37 ± 0.85	10	0.55 ± 0.11	11
EPSP PPF	-0.16 ± 0.2	10	-0.39 ± 0.11	11
IPSP amplitude (mV)	-0.85 ± 0.5	3		
IPSP PPF	-0.12 ± 0.24	3		

Table 4-1: Electrophysiological properties of INs in comparison to a subset of PCs

Numbers are mean ± SEM. All comparisons are indistinguishable, except spike height ($p<0.01$), spike half-width ($p<0.05$), spike afterhyperpolarisation ($p<0.001$) and τ_m ($p<0.001$).

4.4.2. PreNMDAR expression is specific to postsynaptic IN type[5]

The results described in 4.4.1 indicate that putative preNMDARs may be present at L5 PC-PC connections, but not at connections from PCs to basket-like INs. As such, it remains possible that further differences in preNMDAR expression may be apparent at different PC-IN synapses; as many synaptic properties are cell-type-specific, proper identification of cell type is required to fully elicit such differences (Ascoli, Alonso-Nanclares et al. 2008, Blackman, Abrahamsson et al. 2013). Whilst anatomical and physiological properties are useful markers of cell type, a further approach is to use genetic markers; expression of calcium-binding proteins or neuropeptides may be a useful indicator of cortical IN type (Toledo-Rodriguez, Goodman et al. 2005). For the above reasons, and as all INs investigated appeared to be basket cells, transgenic mice which genetically

[5] The results described in 4.4.2 represent pooled data produced by both myself (extracellular stimulation experiments) and others (paired recordings), as mentioned in 4.2

labelled IN classes were employed to further explore preNMDAR expression at connections to different IN types.

PreNMDAR antagonism suppresses PC-SOM IN transmission

Evidence suggests that somatostatin (SOM) is one of the most specific available genetic markers for cortical IN type (Toledo-Rodriguez, Goodman et al. 2005), labelling Martinotti cells (MCs) relatively consistently (Silberberg and Markram 2007); as such, SOM+ L5 INs were investigated first, taking advantage of transgenic mice these cells are labelled with GFP (Oliva, Jiang et al. 2000) to perform targeted recordings (Buchanan, Blackman et al. 2012) with 2PLSM.

Recorded SOM INs exhibited low-threshold accommodating spiking (Table 4-2) and received facilitating excitatory inputs (Table 4-2), consistent with a MC identity (Fino and Yuste 2011). Despite reports of this transgenic mouse line labelling distinct SOM IN subtypes (McGarry, Packer et al. 2010), quantitative morphometry revealed all cells had typical MC morphology (Figure 4-4), including distinctive ascending axon (Buchanan, Blackman et al. 2012). Therefore, these SOM INs are referred to here as MCs.

As PC-MC connections exhibit striking short-term facilitation, with low initial probability of release (Silberberg and Markram 2007), and as preNMDAR blockade (Figure 4-1) has been shown to lower release probability (Sjostrom, Turrigiano et al. 2003), it might be expected that PC-MC connections do not express preNMDARs. Surprisingly, 30Hz trains of EPSPs were consistently and reversibly supressed by APV application at PC-MC synapses (Buchanan, Blackman et al. 2012) as compared to controls (56% ± 7%, n=9 vs. 102% ± 2%, n=4; $p<0.001$). As with PC-PC connections (Sjostrom, Turrigiano et al. 2003, Buchanan, Blackman et al. 2012), PRR and CV analysis (Sjostrom, Turrigiano et al. 2007) indicated a presynaptic locus of effect (Buchanan, Blackman et al. 2012).

Excitatory connections to a subset of PV INs are supressed by preNMDAR blockade

In contrast to 'blind' INs, PC-MC connections appeared to express preNMDARs (Buchanan, Blackman et al. 2012), providing further indication that preNMDAR expression may be pathway and target-cell-specific (Brasier and Feldman 2008, Blackman, Abrahamsson et al. 2013), and as such may serve a specific functional role where they are present. To investigate preNMDAR expression at connections to other L5 cortical INs, and in an attempt to further identify the IN subtype (Figure 4-1) without preNMDARs at PC-IN connections, a transgenic mouse line expressing GFP in parvalbumin (PV) positive INs was employed (Chattopadhyaya, Di Cristo et al. 2004). After SOM, PV appears the next most specific genetic marker for cortical IN types (Toledo-Rodriguez, Goodman et al. 2005), labelling mainly BCs and axo-axonic chandelier cells (Markram, Toledo-Rodriguez et al. 2004, Wang, Toledo-Rodriguez et al. 2004, Ascoli, Alonso-Nanclares et al. 2008, Woodruff, Xu et al. 2009). As INs (Figure 4-2) appeared to have a BC identity, this marker appeared useful as a way to confirm this. As with SOM INs, targeted recordings of GFP expressing PV INs were performed using this mouse line (Chattopadhyaya, Di Cristo et al. 2004).

Similarly to 'blind' INs, targeted PV INs (Table 4-2) exhibited nonaccommodating high-threshold and narrow half-width spiking patterns (Buchanan, Blackman et al. 2012), consistent with descriptions of basket cells (Chattopadhyaya, Di Cristo et al. 2004, Markram, Toledo-Rodriguez et al. 2004). PV INs also received short-term depressing inputs (Table 4-2), in agreement with this (Wang, Gupta et al. 2002, Markram, Toledo-Rodriguez et al. 2004, Wang, Toledo-Rodriguez et al. 2004).

Surprisingly, given the similarity of electrophysiological properties between PV INs and 'blind' INs – suggesting both represented BCs – PV INs exhibited heterogeneity in the effect of APV at excitatory inputs, in contrast to PC-IN connections which all appeared to lack preNMDARs. Hierarchical clustering independently grouped PV INs into two classes based on suppression of

EPSPs in response to APV wash-in (Buchanan, Blackman et al. 2012). These classes are termed type-1 and type-2 PV INs, where PC connections to type-1 PV INs are supressed by APV (EPSP suppression; type-1, 61% ± 3%, n=9, $p<0.001$ vs. controls or type-2; type-2, 91% ± 2%, n=7 vs. controls, 95% ± 3%, n=6, $p=0.25$). For type-1 PV INs, changes in PPF (type-1, 0.13 ± 0.03, n=9 vs. controls, -0.033 ± 0.06, n=6, $p<0.05$) and CV (type-1, $\varphi = 15° \pm 3°$, $p<0.001$) indicated a presynaptic locus of effect. The same measures failed to identify consistent localisation for type-2 PV INs (Buchanan, Blackman et al. 2012).

The heterogeneity of APV's effect at inputs onto PV INs here is in some ways surprising and counter-intuitive, as inputs to 'blind' INs all appeared to lack preNMDARs, and both PV and 'blind' INs appeared to exhibit the physiological properties of BCs (Markram, Toledo-Rodriguez et al. 2004, Toledo-Rodriguez, Goodman et al. 2005), whilst PV INs might be expected to provide more accurate genetic targeting of BCs (Chattopadhyaya, Di Cristo et al. 2004, Toledo-Rodriguez, Goodman et al. 2005). However, it remains possible that the use of PV-GFP mice resulted in targeting of a different subset of INs than targeting based on soma shape – a fact that warrants the use of further and more detailed methods to explore and classify cell-type.

4.4.3. Postsynaptic morphology predicts functional preNMDAR expression

Whilst the use of transgenic mice to target SOM INs revealed that PC connections to these cells expressed preNMDARs, it was surprising that the use of PV-GFP transgenic mice revealed a heterogeneity in putative preNMDAR expression compared to 'blind' INs (see 4.4.2), as these mice were used in an attempt to increase specificity. Furthermore, the electrophysiological properties of both type-1 and type-2 PV INs matched those of basket cells (Chattopadhyaya, Di Cristo et al. 2004), similarly to 'blind' INs, where PC-IN connections were consistently unaffected by APV (Figure 4-1).

As it has been noted that the one of the best indicators of cortical IN cell type is axonal morphology (Markram, Toledo-Rodriguez et al. 2004, Ascoli, Alonso-Nanclares et al. 2008, DeFelipe, Lopez-Cruz et al. 2013), and that a single genetic marker may not be enough to completely determine anatomical type (Toledo-Rodriguez, Goodman et al. 2005), the morphological characteristics of recorded postsynaptic cells were investigated (PCs, PV and SOM INs), using the 2PLSM FI methods outlined in Chapter 3 (Figure 4-3).

Morphometric analysis (Figure 4-3) revealed PCs characteristic apical dendrite branching in the upper layers, alongside an axon mostly confined to L5, with some cells exhibiting ascending axonal collaterals to L1 (Markram, Lubke et al. 1997). As described in 4.4.2, SOM+ MCs consistently exhibited a morphology comparable to an 'inverted' PC, with an axon ascending and branching in L1 and dendrites curved downwards towards lower layers but remaining in L5, typical of descriptions of Martinotti cells (Wang, Toledo-Rodriguez et al. 2004, Silberberg and Markram 2007).

PV INs were reconstructed from 2PLSM FI imaging blind to electrophysiological type (type-1 or type-2 as determined by clustering of response to APV). When the data were unblinded, a clear difference in axonal morphology between the two PV IN types was apparent; type-1 PV INs exhibited an ascending axon branching in L2/3, whilst type-2 PV INs axonal arborisation remained chiefly within L5, similar to 'blind' INs (Figure 4-2, Figure 4-3). Indeed, clustering independently segregated PV INs into two types based on the total length of axonal arborisation in supragranular layers (L2/3 and L1) (Figure 4-3). In contrast, no significant differences were seen in dendritic morphology, in line with previous evidence suggesting axonal but not dendritic morphology is important for classifying IN type (Markram, Toledo-Rodriguez et al. 2004, Ascoli, Alonso-Nanclares et al. 2008, DeFelipe, Lopez-Cruz et al. 2013).

As discussed in Chapter 3, FI imaging is limited by the extent of the acquired stacks; as such, it was a concern that the layer-specific differences in axonal arborisation for PV IN types were a result of a 2PLSM imaging bias. However, comparison of the area imaged (Figure 4-4) between types found this to be indistinguishable, as was soma position within L5. Combined with the fact that reconstructions were performed blind to type, this suggests that the morphological differences identified represent two separate PV cell types. Interestingly, Sholl analysis appeared relatively poor at separating these cell types (Figure 4-4), perhaps as this method is soma-centric and may ignore the importance of layer-specific morphometry (Figure 4-3).

Importantly, clustering based on either the effect of APV on PC-PV connections or supragranular axon extent resulted in two groups containing the exact same cells (Figure 4-3). The fact that postsynaptic cell morphology thus consistently predicted the presence of preNMDARs at PC inputs onto individual PV cells suggests that postsynaptic cell type may in part determine presynaptic molecular identity – cf. (Buchanan, Blackman et al. 2012, Sylwestrak and Ghosh 2012, Blackman, Abrahamsson et al. 2013).

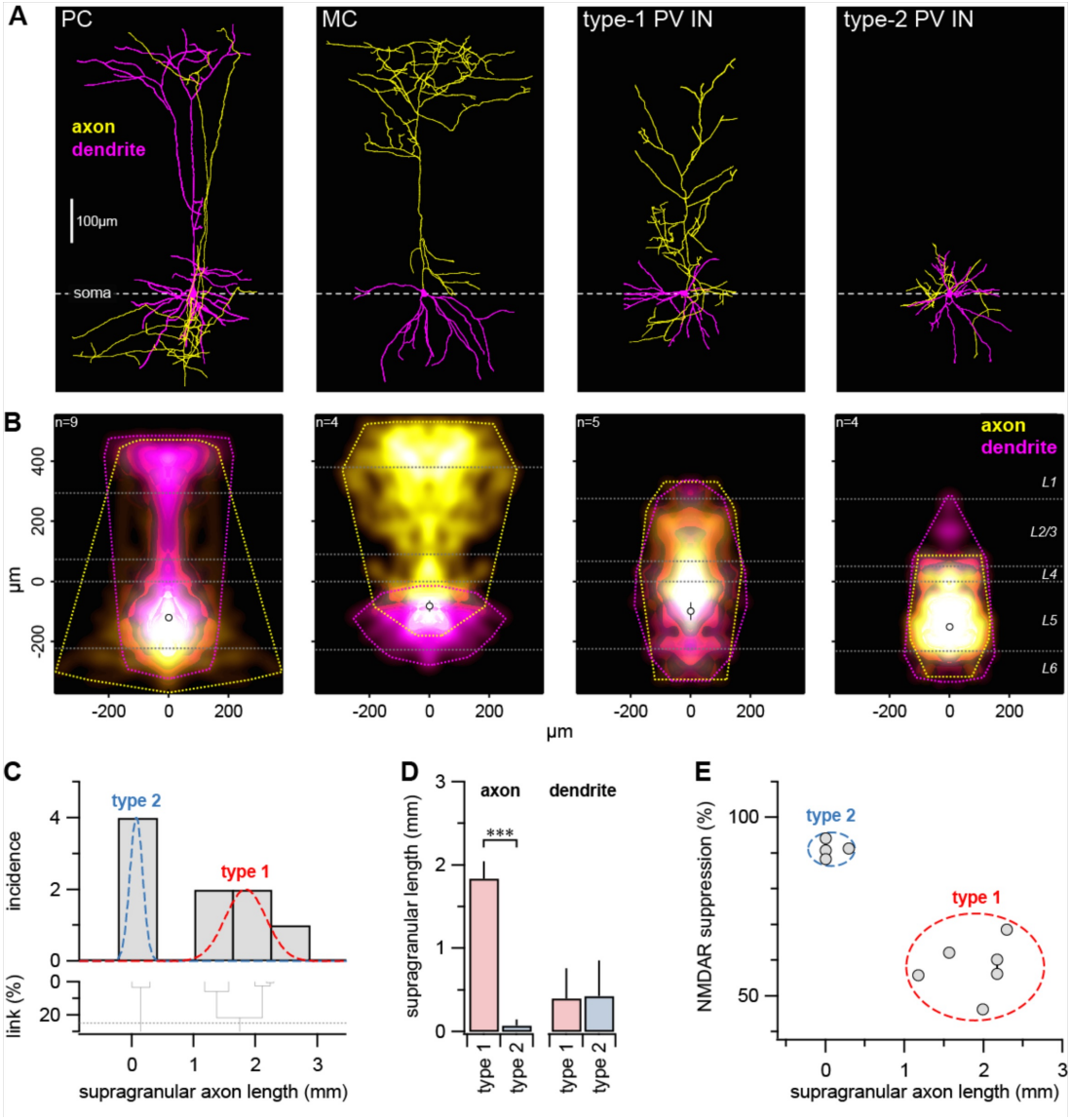

Figure 4-3: Postsynaptic axonal morphology predicts preNMDAR expression

A: Representative reconstructions of PC, MC, type-1 and type-2 PV INs, aligned on somata (dashed line). B: Density maps (axon = yellow, dendrite = magenta) and convex hulls (dotted lines; see 2.6.1) indicate average and maximum extent of arborisation, respectively. White dotted lines indicate neocortical layers. Open circles indicate somata (soma position n.s. for all comparisons). C: Clustering of PV morphologies based on supragranular axon length independently identified two types (25% cut, see 2.11.2). D: For PV INs, supragranular axonal length was significantly different between types (type-1 vs. type-2; 1.8 ± 0.2 mm vs. 0.073 ± 0.070 mm, $p<0.001$), whilst supragranular dendritic length was indistinguishable (type-1 vs. type-2; 0.36 ± 0.4 mm vs. 0.43 ± 0.4 mm, $p=0.96$). E: Postsynaptic axonal morphology predicts functional preNMDAR expression for PV INs where both electrophysiological and morphological data were obtained. Dashed ovals = mean ± 2SD. Connected data points represent one PV IN with two presynaptic PCs. Error bars = mean ± SEM. Reproduced from Buchanan *et al.* (2012) with permission from Elsevier.

Identity of PCs, SOM, type-1 PV and type-2 PV INs

Although the PV-GFP mouse line used (Chattopadhyaya, Di Cristo et al. 2004) was intended to improve specificity as compared to 'blind' IN recordings, somewhat counterintuitively this resulted in the identification of

two IN types rather than one (Figure 4-3, Figure 4-4). The key difference between the PV types identified appeared to be axonal morphology – whilst type-2 PV INs exhibited classical BC morphology, type-1 PV INs had an ascending axon ramifying in L2/3 that does not appear to have been described prior to the present study (Buchanan, Blackman et al. 2012) – cf. (Markram, Toledo-Rodriguez et al. 2004, Katzel, Zemelman et al. 2011, Bortone, Olsen et al. 2014). Comparison of PV INs to 'blind' INs recorded in Figure 4-1 revealed that type-2 PV INs were indistinguishable from 'blind' INs both morphologically (Figure 4-4) and electrophysiologically (Table 4-2), supporting the BC identity of both these cell types.

As chandelier cells (Woodruff, Xu et al. 2009) may express PV, the possibility that the PV INs described here had a chandelier identity was explored by identification of putative synaptic contacts onto PCs that possessed functional connections from PV INs (Figure 4-5); as chandelier cells are axo-axonic, putative contacts should be found on the axon or axon hillock of PCs. Using this approach, putative contacts from both type-1 and type-2 PV INs onto PCs were found to be perisomatically located on dendrites, arguing against a chandelier identity for these cells. Importantly, whilst identification of putative synaptic contacts using this method (see 2.6.4) may result in false positives, false negatives should be far less of a problem, and no synapses onto axons were identified.

A further possibility is that type-1 and type-2 PV INs may represent cells from different ages. However, the age of type-1 and type-2 cells at recording was indistinguishable (type-1 vs. type-2; postnatal day [P] 13.6 ± 0.9 vs. 13.5 ± 1.5, p=0.96). Type-1 and type-2 PV INs were sometimes even found in the same acute slice, arguing against them representing different developmental stages.

A final exploration of PV IN identity was performed by immunolabelling for PV and GFP in the PV-GFP mouse line (Chattopadhyaya, Di Cristo et al. 2004). As previously described (Chattopadhyaya, Di Cristo et al. 2004), GFP-expressing cells had almost complete colocalisation with PV in mature

animals (Figure 4-6). However, at P14, a subset of GFP-positive cells did not appear to express PV (Figure 4-6). This suggests that, for example, type-1 PV INs may be immature at the ages recorded (P12-20) and may not yet have developed PV expression. As immature PV-negative GFP+ INs are still genetically defined by this mouse line and may mature to PV expression during development, they are referred to here as PV INs for simplicity.

	Type-1 PV IN	*n*	*Type-2 PV IN*	*n*	*SOM IN*	*n*
Spike threshold (mV)	-37.96 ± 2.31	13	-36.32 ± 1.25	14	-41.81 ± 1.26	13
Spike height (mV)	40.71 ± 3.27	13	44.84 ± 2.84	14	34.45 ± 3.39	13
Spike half-width (ms)	0.67 ± 0.07	13	0.79 ± 0.07	14	1.57 ± 0.22	13
Spike afterhyp (mV)	-15.33 ± 1.63	13	-16.5 ± 1.62	14	-1.54 ± 1.67	13
Rheobase (nA)	0.4 ± 0.06	13	0.23 ± 0.04	14	0.17 ± 0.02	13
Frequency (Hz)	17.23 ± 2.08	13	16.14 ± 3.4	14	6.67 ± 1.01	13
Accommodation (%)	-21.14 ± 10.6	13	25.01 ± 9.64	14	119.73 ± 37.09	13
CV (%)	13.77 ± 5.08	13	5.82 ± 1.08	14	11.56 ± 4.24	13
V_m (mV)	-68.42 ± 2.9	13	-61.38 ± 2.86	14	-60.7 ± 1.99	13
R_{in} (MΩ)	109.59 ± 14.48	13	144.19 ± 14.48	14	171.53 ± 22.81	13
τ_m (ms)	16.33 ± 2.37	13	14.19 ± 1.55	14	24.34 ± 3.66	13
EPSP amp (mV)	1.77 ± 0.62	5	3.34 ± 1.27	5	0.19	1
EPSP PPF	-0.56 ± 0.05	5	-0.63 ± 0.03	5	1.11	1
IPSP amp (mV)	-0.41 ± 0.3	5	-0.31 ± 0.13	5	-0.09	1
IPSP PPF	-0.37 ± 0.07	5	-0.37 ± 0.13	5	-0.1	1
mEPSC amp (pA)	-17 ± 3	4	-15 ± 1	8	-12 ± 1	9
mEPSC freq (Hz)	7.3 ± 2	4	8.0 ± 0.9	8	3.4 ± 1	9

Table 4-2: Electrophysiological properties of INs show similarity of PV and 'blind' INs, whilst SOM INs are distinct

Only one significant difference was identified between type-1 and type-2 PV INs (accommodation, $p<0.05$), indicating their general similarity. 'Blind' INs (Figure 4-2) were indistinguishable from both type-1 and type-2 PV INs in all measures. As such, all three of these IN groups appear similar to BCs when regarding electrophysiological properties. This said, type-1 PV INs exhibit an ascending morphology uncharacteristic of BCs. Therefore, these three IN groups may actually represent two distinct cell types.

In contrast to this, SOM INs exhibited many significant differences compared to pooled PV IN types. These included spike threshold ($p<0.05$), spike height ($p<0.001$), spike half-width ($p<0.05$), afterhyperpolarisation ($p<0.001$), and V_m ($p<0.01$). Comparing SOM INs separately to type-1 and type-2 PV INs identified similar differences. Values were obtained as in Figure 4-2. Numbers are mean ± SEM. Bonferroni-Dunn *post-hoc* correction for multiple comparisons was applied.

4.4.4. Target-specific expression of preNMDARs in L5 of developing mouse visual cortex

Taken together, the results described above justify the classification of type-2 PV INs and 'blind' INs as BCs, and SOM INs as MCs. However, the type-1 PVs identified – with ascending axon mediating cross-layer inhibition – appear to require further study to be classified, as these cells have not been previously described and their postsynaptic target in L2/3 is unknown. This said, the clear clustering of PV INs into two types based on supragranular axon length or APV-mediated EPSP suppression lends support to the idea

that synaptic markers may help classify cells (Nissen, Szabo et al. 2010) and that postsynaptic cells may signal to their presynaptic partners in a way that affects synaptic properties (Sylwestrak and Ghosh 2012). Similarly, along with previous studies (Brasier and Feldman 2008), the results here suggest that preNMDAR expression is specific to certain pathways and postsynaptic cell classes (Buchanan, Blackman et al. 2012). As such, preNMDARs may serve a specific functional role at these synapses; for example they may be involved in controlling the timing of inhibition mediated by Martinotti cells (Silberberg and Markram 2007, Buchanan, Blackman et al. 2012, Blackman, Abrahamsson et al. 2013). Due to this possibility suggesting preNMDARs as a feature rather than a bug in cortical function during development, it appears that the expression and function of preNMDARs warrants further study.

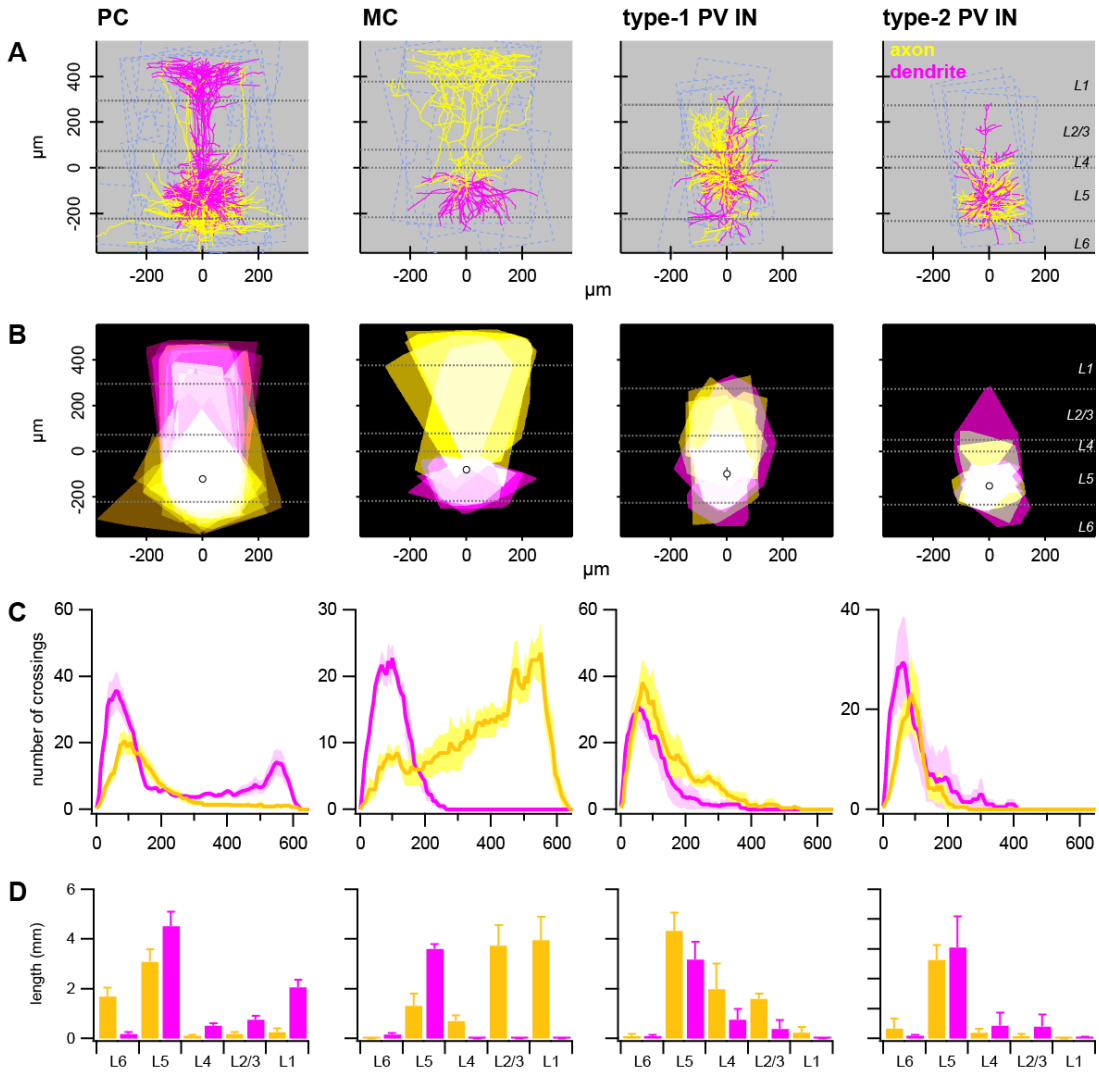

Figure 4-4: Morphometric analysis of PCs, MCs and PV INs

A: All reconstructed morphologies of each cell type overlaid and aligned to show arborisation (axon = yellow, dendrite = magenta) and the extent of 2PLSM imaging acquired (dashed blue lines). Whilst type-1 and type-2 PV INs had strikingly different axonal arbours, the extent of imaging acquired was indistinguishable (y-axis extent, type-1 vs. type-2; 720 ± 50 µm vs. 680 ± 30 µm, p=0.57), arguing against the difference being due to an imaging bias. B: Overlay of individual convex hulls for each reconstruction to indicate homogeneity of axonal (yellow) and dendritic (magenta) arbour extent within cell classes. As indicated in text, supragranular axon hull area was significantly different between PV IN types (type-1 vs. type-2; 55000 ± 5000 µm^2 vs. 4700 ± 3000 µm^2, p<0.001), whilst supragranular dendritic length was indistinguishable (type-1 vs. type-2; 18000 ± 10000 µm^2 vs. 11000 ± 10000 µm^2, p=0.67). C: Ensemble average Sholl diagrams for each cell type (axon = yellow, dendrite = magenta). Whilst type-1 and type-2 PV INs had slightly different Sholl profiles, this was not useful in distinguishing PV IN types, perhaps due to the soma-centric nature of analysis (see text). D: Total arbour length in each neocortical layer (axon = yellow, dendrite = magenta), as used to classify PV IN types by axonal arbour length in supragranular layers (see text). Reproduced from Buchanan *et al.* (2012) with permission from Elsevier.

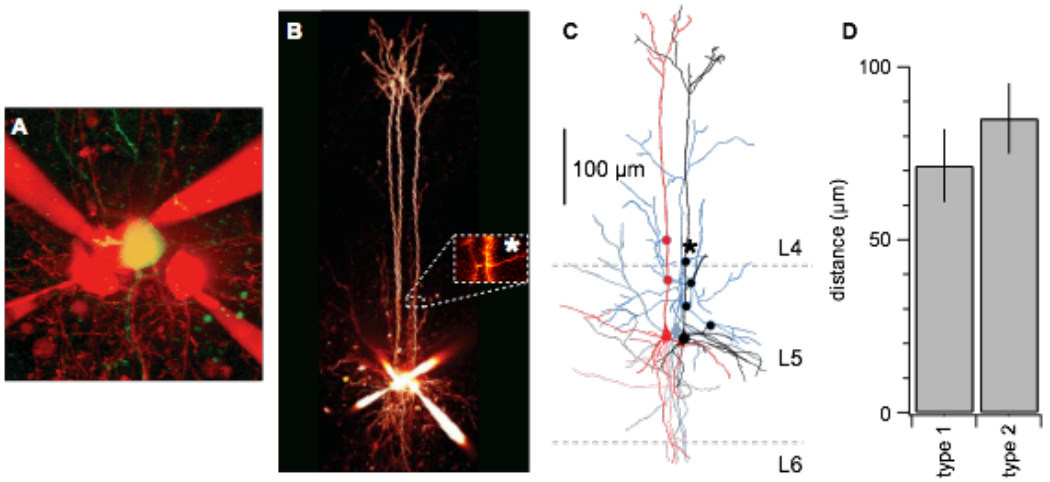

Figure 4-5: Synapses from PV INs to PCs have a perisomatic / dendritic location

A: Maximum intensity projection of 2PLSM stack with three recorded PCs and one type-1 PV IN (Alexa 594 = red, GFP = green). B: Flattened projection of the same four cells. Inset = putative synaptic contact (see 2.6.4). C: Reconstruction of the three connected cells from the recording in A/B, omitting the unconnected PC for clarity. Circles = putative synaptic contacts from the type-1 PV IN (blue) onto PCs (black / red). Asterisk = contact shown in B. D: The mean distance of synaptic contacts from target cell soma was indistinguishable regardless of if these contacts originated from type-1 or type-2 PV INs (type-1 vs. type 2; 72 ± 11 µm, n=4 cells, n=3 connections, n=8 contacts vs. 85 ± 10 µm, n=4 cells, n=2 connections, n=7 contacts, p=0.258). No synaptic contacts were found on or near the axon hillock of PCs, instead being located perisomatically or on dendrites (see text). Reproduced from Buchanan *et al.* (2012) with permission from Elsevier.

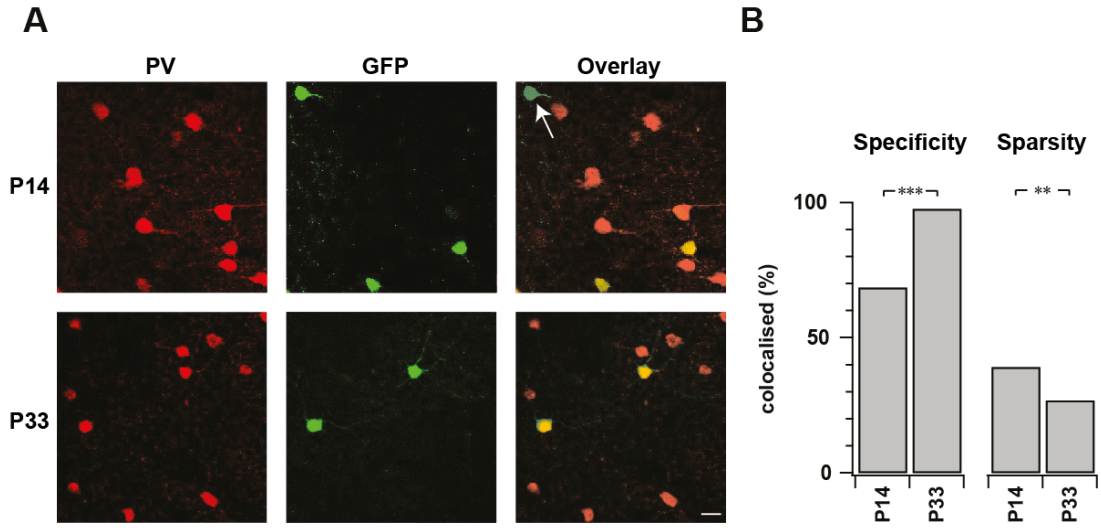

Figure 4-6: A subset of immature PV INs in PV-GFP animals are not positive for PV

A: To verify the specificity of PV-GFP mice, immunolabelling was carried out for PV. In mature animals, nearly all GFP-expressing cells exhibited PV labelling; however, in immature visual cortex (P14), some putative PV INs did not appear PV positive (white arrow, top left). Scale bar = 20 µm. B: Upon quantification of results, it was revealed that the PV specificity of this mouse line (see 2.3) matured with age. At P14, 70% of GFP-expressing cells were labelled with PV, whilst almost all were at P33 (specificity; $p<0.001$). In mature cortex, the percentage of PV-positive cells expressing GFP also became sparser (sparsity; $p<0.01$). At P14 the ratio of double-labelled to all GFP+ cells was r_{GFP} = 90/131, and for PV+ cells r_{PV} = 90/229; n=3 animals. At P33, r_{GFP} = 87/89, r_{PV} = 87/324; n=3 animals. Significance was determined using an χ^2 test. Reproduced from Buchanan *et al.* (2012) with permission from Elsevier.

4.5. Discussion

In this chapter, the specific expression pattern of preNMDARs between PCs and 3 different IN types in developing L5 of mouse visual cortex has been elucidated, by the combination of electrophysiological evidence and morphological and genetic classification of cell types. The methods for cell classification defined and validated in Chapter 3 were used as the key indication and classifier of cell type, further supporting the importance of 2PLSM FI combined with electrophysiological approaches when investigating cell-type specific properties of neural circuits. The results presented in this chapter support and expand on the idea that a presynaptic cell may exhibit greatly different synaptic properties depending on the postsynaptic partner (Galarreta and Hestrin 1998, Markram, Wang et al. 1998), including the possibility that postsynaptic cell type determines presynaptic molecular identity (Sylwestrak and Ghosh 2012, Blackman, Abrahamsson et al. 2013), potentially affecting e.g. MC-mediated inhibition (Silberberg and Markram 2007). Finally, a novel, putative PV-expressing IN type is described which presumably mediates cross-laminar ascending inhibition from L5 to L2/3 – cf. (Katzel, Zemelman et al. 2011, Bortone, Olsen et al. 2014).

4.5.1. The precise location of preNMDARs

Whilst there is a growing body of electrophysiological evidence for the presence of preNMDARs in cortex (Fink, Bonisch et al. 1990, Aoki, Venkatesan et al. 1994, Woodhall, Evans et al. 2001, Sjostrom, Turrigiano et al. 2003, Brasier and Feldman 2008, Corlew, Brasier et al. 2008, Duguid and Smart 2009), cerebellum (Glitsch and Marty 1999, Duguid and Smart 2004) and elsewhere (Duguid and Sjostrom 2006, Corlew, Brasier et al. 2008, Duguid and Smart 2009), their localisation to presynaptic axonal terminals remains controversial, with studies reporting conflicting results (Duguid 2013). For example, in cerebellum, electrophysiological evidence suggests the presence of preNMDARs at parallel fiber – Purkinje cell synapses (Casado, Dieudonne et al. 2000, Casado, Isope et al. 2002); however,

imaging of parallel fibers did not identify preNMDAR-mediated calcium signals, whilst imaging of stellate interneuron terminals did (Shin and Linden 2005). Interestingly, this result was further challenged by the suggestion that calcium transients in stellate interneuron terminals were in fact mediated by presynaptic dendritic NMDA receptors, which indirectly activate axonal calcium channels (Christie and Jahr 2008). Such conflicting results have led to an increased drive to clearly define criteria for identifying presynaptic receptors, such as the combination of EM, electrophysiological, and imaging techniques (Duguid 2013).

Similarly to in cerebellum, Christie and Jahr reported that calcium transients could not be imaged in L5 PC axons, arguing against the presence of preNMDARs here (Christie and Jahr 2009). At other neocortical synapses between L4 and L2/3, however, strong evidence for presynaptically located NMDARs in axon has been provided by both the use of presynaptic MK801 loading (Rodriguez-Moreno and Paulsen 2008) and compartment-specific photorelease of a novel caged form of MK801 (Rodriguez-Moreno, Kohl et al. 2011). Interestingly, electrophysiological evidence for preNMDARs in neocortex suggests their expression may be specific to particular synapses and stages of development, perhaps complicating their detection (Corlew, Wang et al. 2007, Brasier and Feldman 2008).

In this chapter, 2PLSM imaging, neural reconstructions and morphometry have been combined with electrophysiological evidence to indicate that in neocortical L5, preNMDAR expression may be specific to synapses contacting particular cell types. For example, PC-PC synapses appear to express functional preNMDARs, whilst PC-BC synapses do not. Synapses onto these cell types were interspersed along the axon, arguing against the differential propagation of dendritic NMDAR-dependent depolarisation to particular synapses; indeed, Christie and Jahr found that subthreshold somatic depolarisation did not activate axonal Ca^{2+} channels (Christie and Jahr 2009).

Although synapse-specific expression of preNMDARs introduces heterogeneity and thus may complicate detection of these receptors, it remains possible that putative preNMDARs are expressed on e.g. nearby glial cells to these particular synapses. This issue was addressed in a study combining the results presented in this chapter with further pharmacological, electrophysiological and imaging techniques (Buchanan, Blackman et al. 2012). Firstly, presynaptic, but not postsynaptic MK801 loading supressed PC-PC EPSPs, consistent with a localisation of preNMDARs to the presynaptic PC. Neither pre- or postsynaptic MK801 supressed PC-IN EPSPs, however, providing further evidence that the function of preNMDARs is target-cell-specific (Buchanan, Blackman et al. 2012). In a subset of axonal boutons, uncaging of NMDA paired with action potentials resulted in supralinear Ca^{2+} signals; APV puff similarly reduced action potential mediated Ca^{2+} signals in a subset of boutons. Such differences in Ca^{2+} imaging were seen even in boutons in close proximity along the same axon, arguing against the existence of two types of PCs with or without preNMDARs. Similarly, an APV-mediated reduction in mEPSC frequency was observed onto the cell types where PC connections expressed preNMDARs, providing a relatively global sampling of PC inputs (Buchanan, Blackman et al. 2012). Triplet recordings where one PC was connected to two cell types differentially affected by APV (Figure 4-1) also imply that preNMDAR expression is specific to the target-cell, and not presynaptic cell type.

The most parsimonious explanation for these results seems to be the expression of NMDA receptors at a subset of axonal compartments – this is consistent with the target-specific expression patterns described in this chapter (Buchanan, Blackman et al. 2012). Why Christie and Jahr (Christie and Jahr 2009) were unable to identify preNMDARs in L5 axons remains unclear, however the heterogeneous and target-specific expression of preNMDARs described here is likely to have contributed.

4.5.2. Target-specific expression of preNMDARs

Whilst the functional role of preNMDARs may appear puzzling and is at present somewhat unclear (see 4.5.4), the existence of a non-random expression pattern of preNMDARs during development may imply a dedicated function in circuit development.

Initial evidence for non-random preNMDAR expression in neocortex suggested that preNMDARs were expressed at L4-L2/3, but not L4-L4 or L2/3-L2/3 synapses (Brasier and Feldman 2008). In this chapter, these findings are extended to intralayer specificity by showing that connections from PCs in L5 exhibit specific preNMDAR expression dependent on the postsynaptic cell type (see 4.4). A combination of electrophysiology, morphometry and imaging reveals the precise cell-types that receive inputs from L5 PCs with or without preNMDAR expression (Buchanan, Blackman et al. 2012). In developing mouse visual cortex, L5 PC connections to other PCs, MCs and type-1 PV INs express preNMDARs, whilst connections to BCs do not (see 4.4). Triplet recordings (Figure 4-1) and changes in spontaneous release (Buchanan, Blackman et al. 2012) argue against the existence of two presynaptic PC types with and without preNMDARs, instead favouring preNMDAR expression specific to presynaptic terminals contacting a particular postsynaptic cell type. Together with the findings of (Brasier and Feldman 2008), the target-specific preNMDAR expression pattern described in this chapter supports the idea that preNMDARs may be dedicated to a particular function during the development of neocortical circuits.

4.5.3. The classification of interneurons

In addition to increasing the understanding of preNMDARs in cortical function and development, the results presented in this chapter give further validation to the importance of properly defining cell-type when investigating circuit properties. Typically, INs are classified using a variety of genetic, physiological and anatomical measures (Markram, Toledo-Rodriguez et al. 2004, Toledo-Rodriguez, Goodman et al. 2005, Ascoli, Alonso-Nanclares et

al. 2008), with an increasing focus on axonal branching (Ascoli, Alonso-Nanclares et al. 2008, DeFelipe, Lopez-Cruz et al. 2013).

In this chapter, it was found that presumably PV-expressing, fast-spiking interneurons targeted by the use of a transgenic mouse line clustered into two groups based on the presence or absence of an ascending axon branching in L2/3. Clustering based on preNMDAR expression at inputs to these cells also resulted in the same two groups, providing further evidence that these indeed represented two distinct cell types, and that postsynaptic identity may determine presynaptic receptor expression. These results were surprising, as the use of a PV-GFP mouse line was intended to increase specificity when targeting INs (Chattopadhyaya, Di Cristo et al. 2004). Immunolabelling of these cells revealed that a subset may not express PV at a young age, which may be a contributing factor to the identification of two groups. Nevertheless, it appears that despite exhibiting indistinguishable electrophysiological properties, these PV INs do represent two distinct cell classes. As such, this lends further support to the idea that axonal morphology may be the key indicator of cortical IN class (Ascoli, Alonso-Nanclares et al. 2008, DeFelipe, Lopez-Cruz et al. 2013). Similarly, the results presented here suggest that synaptic markers such as the presence of preNMDARs may be useful in defining cell type – whilst this is less common, such approaches have been useful in for example identifying IN type by the presence or absence of Ca^{2+} permeable AMPA receptors, CB1 receptors and certain types of plasticity (Nissen, Szabo et al. 2010).

Type-1 PV INs: a novel interneuron type?

To the knowledge of the author, the type-1 PV IN with interlayer ascending axon described in this chapter is a novel interneuron type. Whilst this IN may or may not express PV at an immature stage, it appears to differ from other interneurons with ascending axons. For example, MCs exhibit an axon corresponding to an ‘inverted’ PC dendrite, branching heavily in L1 and targeting PC apical dendrites. Type-1 PV INs here instead branch more consistently in L2/3, not reaching L1. This said, a ‘basket cell’ with an

ascending interlaminar axon has been described in cat (Kisvarday, Martin et al. 1987), which bears some similarity to the type-1 PV INs described here. However, the cell described in (Kisvarday, Martin et al. 1987) exhibited a greater horizontal axonal arborisation and less branching in L4 than PV type-1 INs. As electrophysiological and genetic properties are unclear for the cell described in (Kisvarday, Martin et al. 1987), it is uncertain if this cell is analogous to a type-1 PV IN, or, for example, an MC-like IN branching in L2/3 instead of L1. More recent studies have described a similar cell to that described here in L6 (Bortone, Olsen et al. 2014).

The precise function and postsynaptic target of type-1 PV INs remains to be elucidated, however some studies have reported inhibition that may involve such cell types. For example, type-1 PV INs may be involved in the ascending L5 – L2/3 inhibition reported in (Katzel, Zemelman et al. 2011). If so, it may be the case that these INs have a perisomatic target in L2/3, in contrast to MCs. A potentially similar fast-spiking L6 IN has recently been described, which mediates ascending inhibition with similar axonal branching to the type-1 PV INs here (Bortone, Olsen et al. 2014). Such interneurons have the potential to regulate cortical activity across many layers.

4.5.4. Functional role of preNMDARs

In addition to being a controversial topic, the presence of preNMDARs raises questions as to their functional role; it is perhaps puzzling that preNMDARs exist, as the canonical function of NMDARs is as a postsynaptic coincidence detector (Ascher and Nowak 1988, Duguid and Sjostrom 2006). As such, the function of presynaptic NMDARs is unclear, although several possibilities have been proposed.

Long-term plasticity and preNMDARs

It has been suggested that preNMDARs may be involved in the induction of LTD in neocortex and cerebellum (Casado, Isope et al. 2002, Sjostrom, Turrigiano et al. 2003), as well as LTP in amygdala (Humeau, Shaban et al. 2003). However, if preNMDARs are to act as coincidence detectors in these

situations, this must rely on a different mechanism than classical pairing of postsynaptic glutamate binding and depolarisation allowing Ca^{2+} flux. It has been suggested that a novel form of tLTD between L5 PCs may require coincident activation of preNMDARs and CB1 receptors (Sjostrom, Turrigiano et al. 2003, Corlew, Brasier et al. 2008), which may in fact be located on astrocytes at similar L4-L2/3 synapses (Min and Nevian 2012). As such, the target-specific expression of preNMDARs described in this chapter may imply that at, for example, PC-BC synapses this form of plasticity is not present, or relies on a different mechanism; this may have implications for circuit refinement during development. In line with this, a recent study suggests preNMDARs specifically control tLTD at L4-L2/3 synapses during development, and that sensory deprivation can restore this during adulthood (Larsen, Smith et al. 2014). As L2/3-L2/3 synapses express a different form of tLTD mediated by postsynaptic NMDARs which is not developmentally downregulated, preNMDARs may provide an alternative pathway for synapse-specific plasticity which is differentially affected by development and experience (Larsen, Smith et al. 2014).

PreNMDAR regulation of neurotransmitter release

Many studies have also implicated preNMDARs in modulation of evoked and spontaneous neurotransmitter release (Sjostrom, Turrigiano et al. 2003, Duguid and Smart 2004, Corlew, Brasier et al. 2008). During high-frequency firing, preNMDARs may enhance neurotransmission with the properties of a high-pass filter (Sjostrom, Turrigiano et al. 2003, Bidoret, Ayon et al. 2009). The target-specific expression of preNMDARs described here may allow this to facilitate particular functions; for example, MC-mediated frequency-dependent disynaptic inhibition (FDDI) between PCs (Silberberg and Markram 2007) appears to require preNMDAR activation during high-frequency firing, whilst BC-mediated frequency-independent inhibition is unaffected by preNMDARs (Buchanan, Blackman et al. 2012). As such, the presence of preNMDARs may aid the spatio-temporal remapping of inhibition across the somato-dendritic axis, a phenomenon identified in multiple brain areas (Blackman, Abrahamsson et al. 2013).

Whilst the target-specific expression of preNMDARs facilitating neurotransmitter release appears to be related to and in some ways mirror the large differences in synaptic dynamics observed at connections from PCs onto different cell types – cf. (Galarreta and Hestrin 1998, Markram, Wang et al. 1998, Buchanan, Blackman et al. 2012, Blackman, Abrahamsson et al. 2013) – the expression of preNMDARs was not found to be linked to the type of short-term plasticity at a given synapse. For example, PC-PC and PC-MC synapses exhibit strikingly different depressing and facilitating dynamics respectively, however both appear to possess preNMDARs (Buchanan, Blackman et al. 2012). The ability of preNMDARs to modulate transmitter release also does not seem to depend on initial release probability at a given synapse (Buchanan, Blackman et al. 2012). This said, both phenomena provide evidence that postsynaptic cell type may determine presynaptic terminal properties, something that may have specific functional impact at different synapses.

Alongside modulation of evoked release, preNMDARs appear to play a role in maintaining a certain level of spontaneous release (Sjostrom, Turrigiano et al. 2003, Brasier and Feldman 2008, Corlew, Brasier et al. 2008). How spontaneous release is affected by preNMDARs is perhaps unclear; it has been suggested that there may be sufficient ambient glutamate for preNMDARs to flicker open at resting potentials (Sjostrom, Turrigiano et al. 2003), that the presence of the GluN3A subunit confers a resistance to Mg^{2+} block (Larsen, Corlew et al. 2011), and that preNMDAR-mediated enhancement of spontaneous release is Ca^{2+} independent but relies on Na^{2+} and protein kinase C activity (Kunz, Roberts et al. 2013). Similar Ca^{2+} independent mechanisms could potentially also account for the observation that the first EPSP in a train is affected by APV in this chapter, a phenomenon that is counter-intuitive considering NMDA receptors are blocked by Mg^{2+} at normal resting potentials - but see (Larsen, Corlew et al. 2011). Alternatively, such an effect observed on the first EPSP could be a consequence of a longer-acting Ca^{2+} induced mechanism that has been blocked by APV by the time used for averaging here.

Regardless, for the synapses described in this chapter, the presence of preNMDARs appears to regulate spontaneous release (Buchanan, Blackman et al. 2012). It may be interesting to note that the preNMDARs in this chapter appear to express the GluN2B subunit (Buchanan, Blackman et al. 2012); whether these are triheteromeric receptors expressing GluN2B and GluN3A remains to be explored, along with the possibility that a mixture of receptors with different subunit identities are expressed.

PreNMDARs and development

In addition to pathway and target-specific differences in preNMDAR expression, a further factor both implying a dedicated function for, and complicating the detection of preNMDARs is developmental regulation. In many brain areas, preNMDAR function attenuates with development, albeit with differing rates and timings in different areas (Corlew, Brasier et al. 2008). For example, in hippocampal CA1, neurosteroid-induced, preNMDAR-mediated modulation of neurotransmission occurs only before P5 (Mameli, Carta et al. 2005), implying a loss of at least some preNMDAR function beyond this age.

In cortex, a similar loss in preNMDAR function is observed, although this occurs later in development (Corlew, Brasier et al. 2008). For example, preNMDAR-mediated increases in spontaneous EPSC frequency are observed in entorhinal cortex at five weeks of age, but not at five months (Yang, Woodhall et al. 2006). In primary visual cortex, including presumably at the synapses described in this chapter, preNMDAR-mediated enhancement of spontaneous release is lost by three weeks (Corlew, Wang et al. 2007, Corlew, Brasier et al. 2008). Interestingly, the loss of such preNMDAR function often coincides with a developmental shift in short-term plasticity from depressing to facilitating responses (Corlew, Wang et al. 2007, Corlew, Brasier et al. 2008, Blackman, Abrahamsson et al. 2013), which may be a function of circuit development and stability.

Although preNMDAR function appears to decrease with development, the studies mentioned above do not preclude entirely some preNMDAR function at maturity. The majority of studies of preNMDAR regulation during development have focused on modulation of spontaneous release, as such leaving preNMDAR-mediated modulation of evoked release unexplored. At synapses onto L2/3 PCs in visual cortex, it has been suggested that a developmental switch in subunit composition of preNMDARs occurs, with a loss of the GluN3A subunit resulting in increased sensitivity to Mg^{2+} block (Larsen, Corlew et al. 2011). Whilst the precise subunit composition of the preNMDARs at cortical L5 synapses is unclear, it may be the case that despite the loss of tonic function (Corlew, Wang et al. 2007), effects on evoked release, such as high-pass filtering, remain into adulthood (Buchanan, Blackman et al. 2012) – a concept perhaps supported by the continuing, yet reduced presence of GluN1 at P27 in layer 2/3 (Corlew, Wang et al. 2007).

Potential involvement of preNMDARs in disease and dysfunction

The potential for preNMDARs to control transmitter release, synaptic plasticity and recruitment of specific inhibitory circuits shows that they may exert a powerful control over cortical circuits. For example, FDDI, which is up-regulated by preNMDARs, may be able to silence cortical columns when triggered by as few as four PCs (Berger, Silberberg et al. 2010). Despite such potentially important roles for preNMDARs in circuit function, the role of preNMDARs in disease has not yet been investigated in detail. One potential involvement of preNMDARs in disease suggested by the results in this chapter may be in schizophrenia, which has been proposed to involve both NMDAR and interneuron hypofunction (Lisman, Coyle et al. 2008, Lewis 2014). Whilst most research to date has focused on postsynaptic NMDARs, the links between preNMDARs and certain interneuron types revealed in this chapter imply a potentially interesting relationship in disease and circuit dysfunction, and offers a new perspective for future research.

5. Cell-type classification directly from bitmap images

5.1. Overview

This chapter is based on a manuscript recently published in *Nature Methods* (Ferreira, Blackman et al. 2014) of which I am second author. It describes open-source software to be used with *ImageJ* which allows for the important morphometric technique of Sholl analysis (Sholl 1953) to be performed directly on bitmap images (of any type), without the need for manual reconstruction. This software is validated by comparison with manual techniques and cell classification results, similar to those described in Chapters 3 and 4. Whilst other authors performed all programming and software development (see 5.2), I made an important intellectual contribution by providing imaging data, reconstructions and benchmark cell classification results, without which the project would not be possible. The development of such software provides an extremely efficient, novel and timesaving approach to cell classification based on the Sholl technique, which enables rapid measurement for large datasets.

5.2. Authorship

All software was developed and data analysed by Tiago A. Ferreira. I provided and performed imaging, reconstructions and benchmark cell classification of neocortical cells. Further reconstructions and imaging were provided by Julia Oyrer, Andrew J. Chung and Sriram Jayabal. Brainbow images of Purkinje cells were provided by Alanna J. Watt and reconstructed by Sriram Jayabal. Guidance was provided by P. Jesper Sjöström and Donald J. van Meyel.

5.3. Introduction

5.3.1. Scope for improvements to morphometric techniques

Morphological measurements, as discussed in Chapters 3 and 4, are a crucial tool in the understanding of neural circuits. Quantification of morphology is vital for studies of neural structure and function; at present, this typically requires reconstruction of neurons, requiring manual or semi-automated tracing of neurites (Senft 2011, Svoboda 2011, Halavi, Hamilton et al. 2012). Whilst for some applications such as computer modelling, accurate 3D reconstructions of neurons are necessary, for many other purposes – including cell-type classification in studies of neural circuits such as that in Chapter 4 – this level of detail may not be required. For functions such as these, the development of approaches to bypass time-consuming steps such as manual reconstruction of cells would be of great benefit.

5.3.2. Sholl analysis

Sholl analysis (Sholl 1953), as discussed in prior chapters, is a well-known and classical technique to quantify morphology. To re-iterate, Sholl analysis is performed by counting the number of e.g. dendritic intersections over usually soma-centred circles of increasing radius, which results in an integrated and relatively global morphological metric. In this way, many differences between cell types can be shown, for example as cortical pyramidal cells exhibit an increase in intersections due to apical dendrite branching at a distance where stellate cells do not (Sholl 1953).

Whilst Sholl analysis suffers from some limitations, such as ignoring layer-specific morphology (see 4.4) or failing to fully describe e.g. dendritic length and tortuosity (Meijering 2010), its enduring use – cf. (Ascoli, Alonso-Nanclares et al. 2008, Bloodgood, Sharma et al. 2013, Inan, Blazquez-Llorca et al. 2013) – is testament to its broad application, utility and importance. Indeed, Sholl analysis is applicable in many fields outside of neuroscience,

such as studies of vasculature and angiogenesis – cf. (Pan, Chanthery et al. 2007, Strasser, Kaminker et al. 2010). The broad usage and popularity of Sholl analysis thus render it an attractive candidate for automation and improvement, as this may benefit a larger number of researchers across more disciplines than more specific and detailed morphological measures.

In this chapter, an automated method to retrieve Sholl metrics directly from fluorescence imaging stacks is described (developed by Tiago Ferreira, see 5.2). This method was developed and its accuracy measured with reference to manual reconstructions and cell-type classification of two groups of cortical interneurons with a high degree of similarity. The ability to bypass manual or semi-manual reconstruction entirely for some purposes using this method should offer a preferable and timesaving alternative for a wide range of applications utilising cell-level morphology, and may enable such metrics to be obtained in e.g. studies using large datasets where previously this would have been unfeasible.

5.4. Results

Sholl Analysis is an open-source plugin for ImageJ, included in Fiji, an image-analysis-focused distribution of ImageJ (see http://fiji.sc/Sholl_Analysis for full details and functionality), and developed by Tiago Ferreira. It performs the Sholl technique directly on 2D or 3D images of fluorescently labelled cells, as well as data obtained from software such as *Simple Neurite Tracer* (Longair, Baker et al. 2011) and is compatible with many image formats. It requires only that neurons be resolved in spectral or spatial isolation, and outputs linear, log-log and semi-log Sholl plots, as well as metrics such as critical value, critical radius and Shoenen ramification index (ratio between the maximum and number of primary root branches), amongst others. Segmentation of image stacks to identify the neural arbour prior to analysis can be performed with a suite of manual and automated tools included in the Fiji package (for example using global thresholding or more advanced processes).

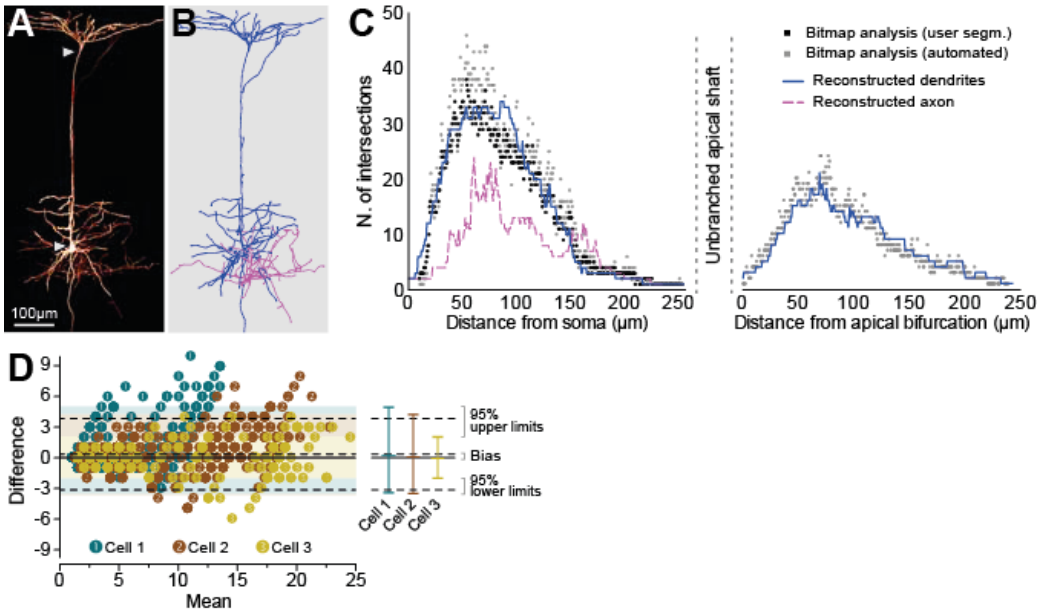

Figure 5-1: Accuracy of bitmap based Sholl analysis

A: Representative maximum intensity projection of L5 PC filled with Alexa 594. Arrowheads = apical tuft (top) and soma (bottom), as used for centres of analysis. B: Manual reconstruction of neuron in A. Dendrites = blue; axon = magenta. C: Linear Sholl plots obtained from bitmap images after either manual ("user segm.") or automated segmentation of the image stacks, using either soma or apical branch point as centre of analysis. Results from manual reconstructions are shown for comparison (dashed line = axon; solid line = dendrite). As noted in text, thresholding to remove axonal segments results in a bitmap Sholl profile matching that of reconstructed dendrites alone (left panel). D: Bland-Altman or Tukey mean-difference plot to show level of agreement between Sholl analysis of bitmap images or reconstructed cells for 3 separate PCs. Each point represents the count of intersections at a given distance (from the apical branch point) for a given cell; the difference between methods for each point is plotted against the mean value. 95% limits of agreement and averages for each cell are shown to the right along with average bias and average 95% limits of agreement (dotted lines). Figure adapted from (Ferreira, Blackman et al. 2014).

5.4.1. Verification of *Sholl Analysis'* accuracy and performance

In order to assess the accuracy of *Sholl Analysis* for 3D images, Sholl plots for neocortical L5 PCs were compared from results obtained both through the software and traditional manual reconstruction and analysis (Figure 5-1). Using this approach, a general similarity of both methods was demonstrated in both Sholl plots and Bland-Altman (or Tukey mean-difference) analysis. It should be noted that *Sholl Analysis* cannot discriminate axonal and dendritic segments in the same image, however, elimination of axonal segments is possible as axons typically exhibit weaker fluorescence; by limiting analysis to pixels above a certain threshold (identified manually with visual inspection), Sholl profiles matched those of manual reconstructions of dendrites alone. In the apical region, the limits of agreement of Sholl analysis

from bitmap or manual images fell between -3.2 and +3.9 intersections (Figure 5-1), with a bias (mean difference) for the bitmap approach of *Sholl Analysis* to oversample by 0.34 intersections (1.5%); this indicates a good level of agreement between bitmap based Sholl analysis and results from traditional manual reconstructions.

In addition to neocortical PCs, accuracy was assessed in cerebellar Purkinje cells labelled with Brainbow 2.1 (Livet, Weissman et al. 2007), which have particularly complex arbours and are slow to reconstruct[6]. Here, comparison of ten metrics from manual reconstructions or *Sholl Analysis* indicated the two approaches were indistinguishable (recons. vs. bitmap; n=7 cells; sum of intersections, 3230 ± 242 vs. 3326 ± 401, p=0.480; max intersections, 24.5 ± 2.5 vs. 21.6 ± 2.3, p=0.982; max intersections radius, 103.7 ± 4.9 vs. 98.8 ± 7.8, p=0.965; centroid intersections, 7.8 ± 0.6 vs. 7.2 ± 0.9, p=0.996; centroid radius, 90.9 ± 1.7 vs. 85.0 ± 2.0, 0.959; enclosing radius, 148.7 ± 4.1 vs. 146.6 ± 3.0, p=0.987; critical value, 20.3 ± 2.1 vs. 19.0 ± 2.4, p=0.989; critical radius, 107.5 ± 3.9 vs. 100.3 ± 3.4, p=0.951, mean value, 9.8 ± 0.8 vs. 10.0 ± 1.4, p=0.998; Sholl regression coefficient, 2.33 ± 0.05 vs. 2.47 ± 0.03, p=0.999; see http://fiji.sc/Sholl_Analysis for full details of analyses).

Whilst *Sholl Analysis* thus appeared comparable to analysis of manual reconstructions for the Sholl approach, its utility in e.g. cell classification should also be validated to provide insight into the scope of its use for studies of neural structure and function. As a particularly difficult classification task, PV type-1 and type-2 (see Chapter 4) INs were chosen to be analysed with the software; as these cells have indistinguishable dendritic arbours (Buchanan, Blackman et al. 2012) and appear to differ only in supragranular axonal branching, their classification using *Sholl Analysis* is a demanding test. Using *Sholl Analysis,* all possible (18) metrics were retrieved directly from 3D image stacks of 12 PV INs previously classified as type-1 or type-2 from manual reconstructions and analysis with the method described

[6] Reconstructions of Purkinje cells provided by others, see 5.2; as such, example figures are not shown here, but are available in *Ferreira et al., 2014*

in Chapter 4; type-1 PV INs have an ascending axon ramifying in L2/3, whilst type-2 INs do not. Unsupervised hierarchical clustering (see 2.11.3) was then performed using the extracted metrics from *Sholl Analysis* to automatically classify these cells (Figure 5-2). Two groups were formed – one with five neurons and another with seven. All but two (one in each group) were correctly classified when compared to manual reconstructions, indicating an 80-86% classification success rate. Similarly, linear Sholl plots revealed more branching for type-1 PV INs at a distance of 225-300 μm from the soma (Figure 5-2). Whilst as discussed in Chapter 4 classifying these cell types using Sholl analysis is difficult, clustering based on multiple metrics extracted using *Sholl Analysis* may successfully classify these closely related INs in the majority of cases.

Taken together, the verification of *Sholl Analysis'* performance when compared to conventional manual reconstructions presented here indicate that it is accurate and may be used for a variety of cell types and purposes, including cell classification. As processing in *Sholl Analysis* requires only 10-15 minutes and may be automated for batch use, this software may provide a hugely timesaving and useful alternative to manual reconstruction taking up to multiple days per cell (see Chapter 3) for high-throughput studies utilising morphometry.

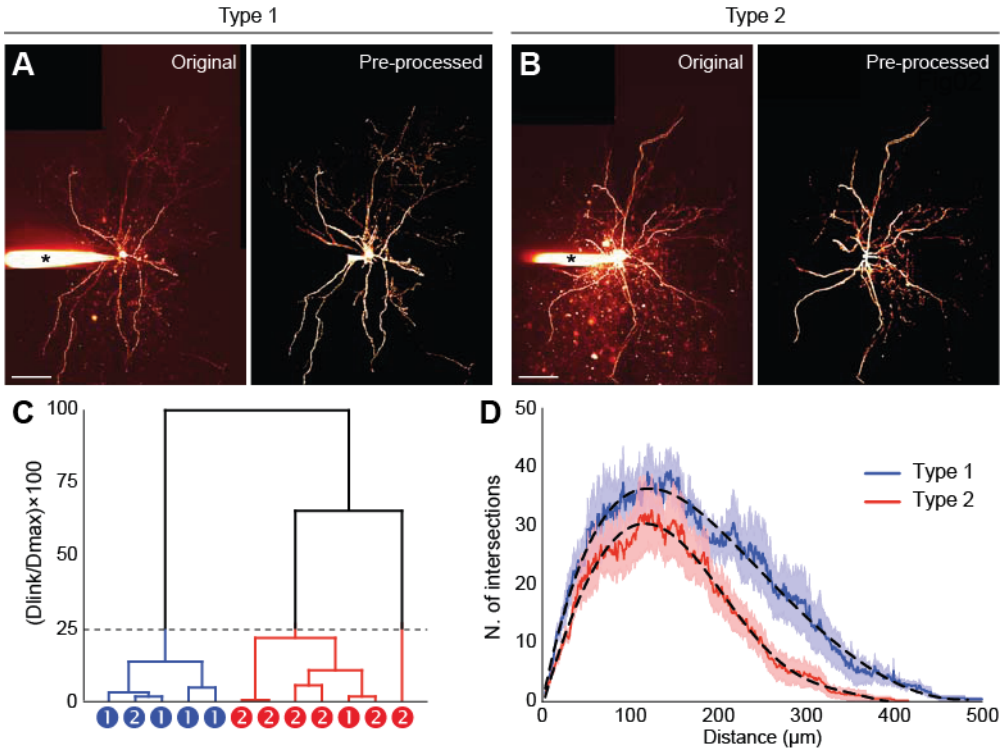

Figure 5-2: *Sholl Analysis* can classify cortical interneurons without manual reconstruction

A/B: Representative maximum intensity projections of image stacks of PV INs. Original stacks (left panels in A and B) were processed prior to extraction of metrics in *Sholl Analysis* (see (Ferreira, Blackman et al. 2014)) to remove pipette and reduce background. C: Dendrogram indicating classification performance using hierarchical clustering using metrics from *Sholl Analysis* (see text and 2.11.3). Linkage is normalised to furthest linkage distance. Dotted line indicates 25% best cut. Circles = PV IN type from manual reconstruction and analysis. D: Linear Sholl plots for type-1 (n=5) and type-2 (n=7) PV INs. Solid lines = mean; shaded regions = SEM; dashed lines = best-fit polynomials. Figure adapted from (Ferreira, Blackman et al. 2014).

5.5. Discussion

In this chapter, results have been presented from the development of a method to enable morphometry to be performed directly on bitmap images, without the need for time-consuming reconstruction of cells. The performance of this technique was verified by comparison with results from manual reconstructions and analysis, and its utility in cell classification was measured. Overall, *Sholl Analysis* produces comparable results to manual techniques, and can classify the majority of even closely related cortical interneuron types correctly. As such, it offers a preferable alternative to reconstruction and analysis in many experimental scenarios (for example the study presented in Chapter 4); *Sholl Analysis* may enable previously challenging high-throughput studies of morphometry with large datasets to be completed with ease.

5.5.1. Applicability of *Sholl Analysis* and the Sholl technique

Sholl analysis directly from images

Despite the age and relative simplicity of Sholl analysis (Sholl 1953), it has endured as one of the most popular methods to quantify morphology in cellular neuroscience. The bitmap approach described here extends this method by removing the requirement for tracing or reconstruction. The results presented in this chapter indicate that *Sholl Analysis* is comparable to traditional techniques for a variety of cell types and purposes, and preferable in regard to time demands. Clearly however this bitmap approach is not suitable for all purposes; consider for example the relationship between morphology and computational properties of cells – multicompartmental models exploring this are heavily affected by neurite diameters (see Chapter 3), and as such require detailed reconstructions.

The direct use of image stacks to extract Sholl metrics also introduces some requirements that should be noted. For example, care must be taken when thresholding images to segment the neuron from background that the dendritic / axonal tree is selected as opposed to the interstitial spaces. Similarly, as noted earlier (5.4.1), unless axonal and dendritic arbours are labelled separately, some difficulty may be encountered in separating them, although this is possible (see Figure 5-1), and classification of cells previously defined by axonal arborisation is achievable without this (Figure 5-2). This said, the potential importance of thresholding images should be made clear to any potential user. For example, whilst cell classification was possible even when including both axon and dendrite for type-1 and type-2 cells here, it remains possible that improper thresholding which removes important axonal arborisation could lead to erroneous results or failure to distinguish between cell classes. As axonal arborisation is perhaps a more useful morphological indicator of cell type than dendritic morphology (particularly for interneurons), this is an important consideration (Tsiola, Hamzei-Sichani et al. 2003, Toledo-Rodriguez, Goodman et al. 2005,

McGarry, Packer et al. 2010, DeFelipe, Lopez-Cruz et al. 2013, Sumbul, Song et al. 2014).

Whilst *Sholl Analysis* appears resistant to a wide range of noise (Ferreira, Blackman et al. 2014), image quality may affect results; a now out-dated version of *Sholl Analysis* has been reported to undercount intersections of dendrites labelled with diOlistics (Binley, Ng et al. 2014), highlighting the need for a certain image quality – discontinuous labelling of neurites or poor segmentation will negatively affect the accuracy of *Sholl Analysis*.

The Sholl technique for neural morphometry

Whilst Sholl analysis is an enduring, popular and useful technique to quantify morphology, there are many other metrics and methods available, and it is important to properly assess the strengths and weaknesses of each. For example, as noted in Chapter 4, Sholl analysis provides a relatively global and usually soma-centric description of morphology, and as such may pass over more subtle features of cells. As an example, it may be difficult to identify the axonal cartridges of chandelier cells with traditional Sholl metrics alone (Somogyi 1977). Earlier in this thesis (Chapter 4), it was found that comparison of Sholl metrics did not distinguish PV IN types as well as layer-specific differences in axonal branching (Buchanan, Blackman et al. 2012); despite this, a more complex approach using multiple Sholl metrics for hierarchical clustering was able to successfully group the same cell types in 80-86% of cases (5.4.1). Therefore, developments and enhancements to the Sholl technique may render it more useful and adaptable in future; further metrics based fundamentally on the Sholl technique may increase its capability to describe features of neuronal morphology (Garcia-Segura and Perez-Marquez 2014). Similarly, adaptation and further development of approaches based on this bitmap technique to enable morphometry including e.g. convex hull and density map analysis (see Chapters 3 and 4) directly from images may provide increased functionality in future.

Alternative approaches

Although morphometry from bitmap images as extracted by *Sholl Analysis* appears both accurate and sensitive, there are some situations where such an approach is not sufficient; for example, multicompartmental computer modelling requires full reconstruction (see Chapter 3). Whilst manual reconstruction may offer the greatest accuracy in such applications, there is also an increasing body of work dedicated to improving the quality of fully automatic reconstructions of neural morphology, which may enable rapid production of 3D reconstructions for more detailed analysis and simulations. Such developments are encouraged by initiatives such as the DIADEM (Digital Reconstruction of Axonal and Dendritic Morphology) challenge (Liu 2011), however automated reconstructions still often suffer from sensitivity to different cell types or imaging methods, and may require time-consuming manual error correction (Donohue and Ascoli 2011). As such, the reliable performance of *Sholl Analysis* identified here offers a complementary approach that has no requirement for the creation of reconstructions.

6. General Discussion

In this thesis, a combination of electrophysiology and imaging techniques have been employed and utilised to investigate cell-type-specific synaptic properties in neocortical layer 5 and their consequences for circuit function. Firstly, as morphology, and particularly axonal morphology, is a key indicator of neocortical interneuron type (Markram, Toledo-Rodriguez et al. 2004, Ascoli, Alonso-Nanclares et al. 2008, DeFelipe, Lopez-Cruz et al. 2013), and many neocortical circuit properties are cell-type-specific (Brown and Hestrin 2009a, Blackman, Abrahamsson et al. 2013), reconstructions of neurons from two-photon imaging were investigated as a timesaving method to identify cell type in electrophysiological studies. Whilst this method was found to produce useful results for this purpose with lower cost and time requirements than biocytin based reconstructions, multicompartmental modelling using these 2PLSM FI reconstructions suffered from errors, chiefly due to enlargement of process diameters, something that should influence the planning and design of future experiments (Blackman, Grabuschnig et al. 2014).

Using this validated FI cell-type identification method, the specific expression pattern of presynaptic NMDA receptors in neocortical layer 5 was elucidated; this was found to be target cell specific, with synapses from PCs onto PCs, MCs and a novel PV IN expressing preNMDARs, whilst synapses from PCs onto BCs lack preNMDARs. As preNMDARs upregulate high-frequency neurotransmission, they may act in concert with target-specific differences in STP to transform high frequency spike trains into sequential somatic and dendritic inhibition mediated by BCs and MCs, respectively (Buchanan, Blackman et al. 2012, Blackman, Abrahamsson et al. 2013). Further validation of the utility of axonal morphology in distinguishing cell-type comes from the identification of two distinct, putatively PV-expressing IN types with similar spiking properties, which are distinguished by their extent of supragranular axonal arborisation and differential expression of preNMDARs at PCs synapses contacting them (Buchanan, Blackman et al. 2012).

As discussed above, analysis of neuronal morphology may provide important insights into cell-type, even when other (e.g. genetic and physiological) properties appear similar. Morphometric analyses are becoming increasingly frequent throughout many fields of neuroscience and beyond (Ascoli 2006, Ascoli, Alonso-Nanclares et al. 2008, Halavi, Hamilton et al. 2012, DeFelipe, Lopez-Cruz et al. 2013). Despite this, neuronal imaging and reconstruction can be a very time-consuming process for the experimenter. In order to address this, an automated procedure to extract morphological metrics (*Sholl Analysis*) directly from imaging stacks was developed and verified with reference to the cell-types and 2PLSM FI reconstructions described previously in this thesis (Ferreira, Blackman et al. 2014). Using this method, closely related cell types could be discriminated with good accuracy, indicating that *Sholl Analysis* may be used to increase throughput in experiments where quantification of morphology provides important input into e.g. cell-type identification.

6.1. Cell-type-identity and neural circuit function

This thesis has focussed on the utility of robust cell-type identification in exploring neural circuit function. Building on a large body of previous work (Markram, Toledo-Rodriguez et al. 2004, Toledo-Rodriguez, Goodman et al. 2005, Ascoli, Alonso-Nanclares et al. 2008, Halavi, Hamilton et al. 2012, DeFelipe, Lopez-Cruz et al. 2013) – the focus of the present work has been on anatomical cell-type identification using 2PLSM. Application of this method was found to distinguish two closely related IN types in neocortex (see Chapter 4), which exhibited indistinguishable electrophysiological properties and were labelled by the same genetic marker (Buchanan, Blackman et al. 2012). The observation that preNMDARs were differentially expressed at inputs onto these two cell types validates their classification by morphological methods, indicating that type 1 and 2 PV INs are indeed separate classes, rather than an arbitrary subdivision of a single cell type or a continuum between two extremes (Buchanan, Blackman et al. 2012).

This said, it is important to note that whilst morphological classification methods can be useful in identifying cell-type in studies of neural circuits, care must be taken, as it can be unclear whether the resulting data represent distinct classes or subdivisions of a continuum. Complementary approaches such as analysis of the expression patterns of multiple genetic markers (Toledo-Rodriguez, Goodman et al. 2005) may provide additional evidence for the existence of particular classes. Particular interneuron classes may be determined by particular temporal and spatial origins, for example fast-spiking INs may originate in the medial ganglionic eminence whilst regular-spiking INs may be generated in the caudal ganglionic eminence (Butt, Fuccillo et al. 2005). This said, these classes may be refined and altered by activity and experience; as such it may be useful to define interneurons by function (Kepecs and Fishell 2014). Using a single genetic marker such as PV to classify cells may in fact label a number of distinct cell classes such as basket and chandelier cells, or the type-1 and type-2 PV INs identified in (Buchanan, Blackman et al. 2012), the function of which could potentially differ. Additionally, it should be noted that even superficially similar methods used in classifying cell type may produce different results; for example direct comparison of reconstructed cells from Neurolucida or 2-photon images may lead to erroneous classification – such factors must be taken into account when using data from multiple labs such as that hosted on NeuroMorpho.org (Ascoli, Donohue et al. 2007, Halavi, Hamilton et al. 2012, Blackman, Grabuschnig et al. 2014).

Despite the complicated nature of determining cell type, increasing evidence suggests that many features of neural circuits have cell-type-specific elements, and attempts to classify cell type correctly may aid elucidation of specific circuit properties. For example, in hippocampus, synapses from PCs onto O-LM INs are facilitating, whilst PC-PV IN synapses are depressing, a feature determined by postsynaptic expression of Elfn1 in O-LM INs (Sylwestrak and Ghosh 2012). Proper identification of pre- and postsynaptic cell type may thus reveal synapse specific physiological differences. Indeed, it is tempting to speculate that preNMDAR-mediated LTP induction and BDNF secretion recently identified at corticostriatal synapses may have

target-specific features similar to the expression patterns of preNMDARs described in Chapter 4 (Buchanan, Blackman et al. 2012, Park, Popescu et al. 2014).

Whilst the work in this thesis has chiefly utilised anatomical approaches to cell classification, in combination with genetic markers – cf. Chapter 4 and (Buchanan, Blackman et al. 2012) – this is not to imply that other approaches are not useful (see 6.2). For example, large-scale RNA sequencing may provide insight into the functional classification of sensory and other cells, including identification of markers for particular subtypes (Usoskin, Furlan et al. 2014). However, the anatomical approaches described in this thesis, particularly when utilising 2PLSM, offer a high level of ease and low cost (after the initial setup cost) whilst clearly facilitating the identification of cell-type-specific differences in, for example, electrophysiological studies of cortical circuit properties. The relative simplicity of this approach balanced against the increased level of insight it potentially provides are a testament to the utility of anatomical classification in studies of circuit function.

Elucidation of cell-type-specific phenomena may provide vital insight into disorders and diseases of the nervous system. For example, in schizophrenia, dysfunction of PV-expressing interneurons is widely observed (Lewis, Hashimoto et al. 2005, Nakazawa, Zsiros et al. 2012, Lewis 2014); here, differences may exist between BC-PC and Chandelier cell-PC synapses, with postsynaptic GABA-A receptor α1 mRNA decreasing and increased axonal GABA-A receptor α2 subunit expression at the former and latter synapses respectively (Lewis 2014). As PV-expressing INs may be comprised of further subgroups, for example potentially including the IN types described in Chapter 4 and (Buchanan, Blackman et al. 2012), more detailed investigation of cell-type-specific circuit properties in schizophrenia may reveal important information. For example, the translaminar fast-spiking INs described in (Buchanan, Blackman et al. 2012, Bortone, Olsen et al. 2014) could be affected by hypofunction of preNMDARs which are not present at synapses onto BCs; NMDAR hypofunction and NMDA anatognist

application is observed to cause schizophrenia-like symptoms (Nakazawa, Zsiros et al. 2012).

Similarly, cell-type specificity may confer more specific properties to cortical circuitry in healthy function, such as the preferential transmission of high frequency bursts by facilitating synapses. In the case of the expression pattern of preNMDARs discussed in this thesis, the presence or absence of preNMDARs at particular synapses may impact the transmission of high-frequency activity and in turn inhibition of particular cellular domains (Buchanan, Blackman et al. 2012). Additionally, as preNMDARs are implicated in timing-dependent LTD (Sjostrom, Turrigiano et al. 2003, Duguid and Smart 2004, Duguid and Sjostrom 2006, Sjostrom, Turrigiano et al. 2007, Rodriguez-Moreno and Paulsen 2008), this form of plasticity may be absent or may rely on different mechanisms at synapses lacking preNMDARs. Interestingly, the expression of preNMDARs and their involvement in synaptic plasticity may underlie experience-dependent refinement and remodelling of neural circuits. For example, visual deprivation is reported to increase expression of the GluN3A subunit at L4-L2/3 synapses and in turn restore preNMDAR-mediated tLTD (Larsen, Smith et al. 2014); this suggests that in normal experience, visual stimulation in adulthood supresses tLTD at specific synapses and that this may be part of a mechanism to decrease their propensity for synaptic modification, instead favouring information storage (Feldman 2012, Larsen, Smith et al. 2014). Likewise, in barrel cortex, single-row experience (selective whisker stimulation) during development increases both preNMDAR-mediated synaptic strength and depression, suggesting that sensory experience can influence the expression of preNMDARs and in turn neurotransmitter release probability and synaptic plasticity (Urban-Ciecko, Wen et al. 2014). The fact that these mechanisms may be selectively present at particular synapses to particular cell-types, as they rely on preNMDARs which are selectively expressed at particular locations (Brasier and Feldman 2008, Buchanan, Blackman et al. 2012, Blackman, Abrahamsson et al. 2013, Larsen, Smith et al. 2014), may provide insight into the importance of certain pathways and synapses in, for example, circuit formation and refinement. Importantly,

where preNMDARs are expressed at certain synapse types, they may serve specific functions; for example at corticostriatal synapses preNMDARs are reported to be involved in LTP by triggering BDNF release (Park, Popescu et al. 2014). This highlights the importance of differentiating between cell and synapse types to identify key mechanistic differences.

Whilst the discussion above focuses on the implications of the synapse-specific expression and function of preNMDARs, similar cell-, synapse- and pathway-specific properties could apply to many different circuits, receptors, cells and functions (Blackman, Abrahamsson et al. 2013). This underscores the utility and importance of investigating such differences and identifying cell type when investigating neural circuits. For example, the recently described cells that co-release GABA and glutamate (Shabel, Proulx et al. 2014) may do this in different ratios at different synapses, or synapse-specific differences in STP may alter the dynamics of such co-release. Similarly, one could imagine that recently described differences in myelination patterns between different pyramidal cells may exhibit further complexity depending on cell or synapse type, perhaps modulating transmission to particular synapses (Tomassy, Berger et al. 2014). The existence of such possibilities, coupled with increasing evidence for important cell- and synapse-specific synaptic properties in many circuits, provide a strong case for detailed examination of cell and synapse type in any investigation focussing on the contribution of cellular properties to circuit function.

6.2. Alternative methods of identifying cell types

Whilst the cell types in this thesis have been classified by anatomical means, the existence and merits of alternative methods should be discussed. As mentioned elsewhere in this thesis, cell types are often distinguished by physiology, such as the distinction between fast-spiking and low-threshold spiking cells (Gibson, Beierlein et al. 1999). Similarly, molecular markers such as SOM or PV are utilised to classify cells (Toledo-Rodriguez, Goodman et al. 2005). Any of these methods individually may pass over key differences between cells, for example the PV cell types described in this

thesis exhibit similar spiking properties (Buchanan, Blackman et al. 2012). For anatomical methods, it is possible that cells with similar morphology may exhibit differing molecular and physiological properties, so care must be taken when relying on morphological classification alone. A comprehensive classification strategy may be based on the combination of physiological, genetic and anatomical properties.

In addition to the methods described above, neuronal diversity also may be characterised by analysis of gene expression within individual cells and cell groups. Techniques such as single-cell RNA-seq may provide an unbiased approach for classifying cells based on their transcriptome, which in correlation with data on morphology and physiology may enable better understanding of cell types in future (Mortazavi, Williams et al. 2008, Usoskin, Furlan et al. 2014). Such approaches may also aid identification of transcription factors involved in generating neuronal subtypes, as discussed in 1.5 (Margolin, Wang et al. 2006).

The cell classification methods described above each offer different levels of description, practicality and completeness. However, for each one of them, an important and difficult question remains the point at which cell types are considered truly distinct. Whether cells are separated by morphology (Ascoli, Alonso-Nanclares et al. 2008, DeFelipe, Lopez-Cruz et al. 2013), function (Kepecs and Fishell 2014) or otherwise, the possibility that a particular class may contain distinct subclasses, or conversely be a continuum, is an important consideration.

6.3. Remapping of inhibition across the somato-dendritic axis

In Chapter 4 and (Buchanan, Blackman et al. 2012), in addition to the target-specific expression pattern of preNMDARs, target-specific differences in STP were observed (Figure 1-5); PC-BC connections exhibit short-term depressing synapses whilst PC-MC connections exhibit facilitating synapses, a phenomenon that may result in sequential somatic (BC-mediated) and

dendritic (MC-mediated) inhibition in neighbouring PCs during high-frequency PC firing (Silberberg and Markram 2007, Blackman, Abrahamsson et al. 2013).

As touched upon in 1.9, such differences in STP depending on postsynaptic target may be evident throughout a wide range of cell types and brain areas. Recent evidence indicates that in several different microcircuits, target-specific STP spatio-temporally remaps inhibition across the somato-dendritic axis (Blackman, Abrahamsson et al. 2013), as exemplified by the neocortical PC-BC-PC or PC-MC-PC disynaptic inhibitory motif described in this thesis.

In the cerebellum, parallel fiber (PF) connections between granule cells and Purkinje cells (PuCs) or basket / stellate INs exhibit target-specific STP; PF connections onto PuCs or stellate INs are facilitating, whilst PF-BC connections are depressing after initial paired-pulse facilitation (Bao, Reim et al. 2010). In a parallel to the neocortical L5 microcircuit, high-frequency PF firing thus recruits BCs before stellate INs; as BCs innervate PuCs perisomatically whilst stellate INs contact PuC dendrites, this may lead to sequential somatic followed by dendritic inhibition during high-frequency trains (Chadderton, Margrie et al. 2004).

In hippocampus, similar phenomena have been observed. In CA1, PCs connect to different interneuron types with target-specific dynamics. PCs form depressing connections to ‘onset-transient’ perisomatic-innervating BCs (Thomson 1997, Ali, Deuchars et al. 1998), and facilitating connections to apical dendrite-targeting ‘Martinotti-like’ cells (Pouille and Scanziani 2004, Blackman, Abrahamsson et al. 2013). As such, high-frequency firing leads to early-onset somatic followed by late-onset dendritic inhibition (Pouille and Scanziani 2004), similarly to in neocortex. However, further complicating factors are evident in these circuits. For example, even very similar basket cells distinguished by expression of CB1Rs may receive inputs with differing STP (Glickfeld and Scanziani 2006). Additionally, the early-onset INs may in turn inhibit the late-onset INs, which further accentuates the temporal differences in activation (Lovett-Barron, Turi et al. 2012).

Regardless, target-specific differences in STP from excitatory cells to differing IN types result in the spatio-temporal remapping of inhibition in many brain areas and circuits, with periosomatic inhibition occurring before inhibition of more distal dendrites. To the knowledge of the author, the functional purpose of this remains to be elucidated – although, for example, it has been shown that cortical late-onset inhibition is associated with wakefulness and with an attentive brain state (Haider, Hausser et al. 2013). However, the fact that target-cell-specific differences in synaptic properties share features in diverse brain areas, resulting in similar spatio-temporal modulation of circuit activity, suggests that these differences may serve a specific functional purpose and are not simply epiphenomena. This is a good example of the importance of carefully determining cell type in experimental studies of circuits to elucidate cell and synapse-specific properties such as specific differences in short-term plasticity.

6.4. Functional implications of proximal and distal inhibition

Although the behavioural and functional implications of the spatiotemporal remapping of inhibition described above may be unclear, research has shed some light on potential functional roles for distal and proximal targeting inhibitory axons. For example, one commonly discussed role for interneurons is in performing basic arithmetic operations. Here, a traditional view is that proximal inhibition may provide a divisive function whilst distal inhibition may be subtractive (Pouille, Watkinson et al. 2013); division by PV+ BCs may control gain in a divisive manner whilst SOM+ MCs may provide selectivity sharpening subtraction (Vu and Krasne 1992, Wilson, Runyan et al. 2012). Short-term depression may also influence the inhibitory effect on input-output functions (Rothman, Cathala et al. 2009). Whether the novel IN described in this thesis targets perisomatic or distal regions remains to be shown, along with similar cells described in L6 (Bortone, Olsen et al. 2014), however they may be well placed to provide inhibition across many layers.

Many classic studies have focussed on the effect of particular dendritic locations for inhibition, for example indicating that “on-path” inhibition is more effective than “off-path” inhibition, or that inhibitory conductance change is largest at the site of inhibition (Jack, Noble et al. 1975, Koch, Poggio et al. 1983). As such, inhibition at the soma may be well placed to globally regulate synaptic input whilst more distal inhibition may impart selectivity. Interestingly, however, it has been suggested that the shunting inhibition produced by Martinotti cells may in fact be highest away from its synapses on the apical dendrite, an effect which could enable effective decoupling of dendritic Ca^{2+} spikes and somatic spikes (Gidon and Segev 2012). The distal targeting MC-mediated inhibition described in this thesis may thus be ideally placed to prevent the initiation of dendritic Ca^{2+} spikes and integration of top-down cortical input forming synapses on distal dendrites of L5 PCs, during high-frequency local activity (Larkum, Zhu et al. 1999, Silberberg and Markram 2007). Once dendritic spikes are triggered, however, on-path inhibition in the classical form may be best placed to attenuate these (Jack, Noble et al. 1975). Branch-specific dendritic inhibition may modulate local regenerative and nonlinear events and in turn be well located to influence local synaptic plasticity (Sjostrom, Rancz et al. 2008). Similarly, whilst somatic inhibition may be ideal to veto somatically generated APs and edit AP timing (Cobb, Buhl et al. 1995), more distally located inhibition may be required to veto dendritically generated spikes (Schiller, Major et al. 2000, Larkum, Nevian et al. 2009, Lovett-Barron, Turi et al. 2012).

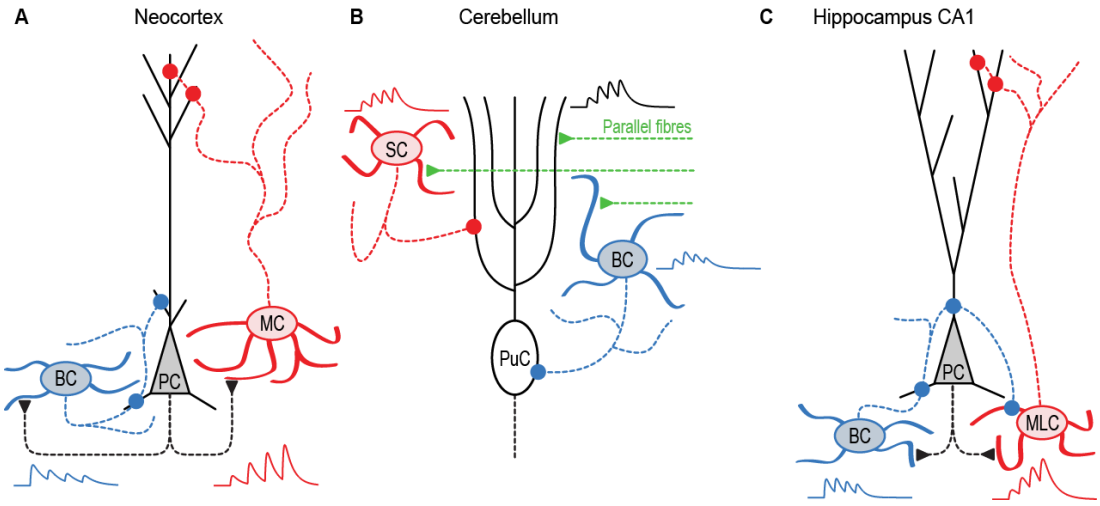

Figure 6-1: Target-cell-specific properties lead to remapping of inhibition across the somato-dendritic axis

A: In neocortex (see Chapter 4), PCs connect to BCs with depressing synapses, and MCs with facilitating synapses. As such, BCs are activated before MCs during a presynaptic spike train, and in turn BC-mediated perisomatic inhibition occurs before MC-mediated dendritic inhibition. B: In cerebellum, parallel fibres connect to Purkinje cells and stellate INs with facilitating synapses, and to basket INs with synapses that depress after initial facilitation. Soma-targeting BCs are thus recruited before dendrite-targeting SCs. C: In hippocampus, as in neocortex, PCs connect to BCs with depressing synapses, and to Martinotti-like cells (see text) with facilitating synapses. As in the other circuits discussed, this leads to sequential somatic followed by dendritic inhibition. Thick lines = dendrite; dotted lines = axon. Filled triangles = excitatory synapses; filled circles = inhibitory synapses. All traces are for illustrative purposes only and are simulated based on literature referred to in the text and discussed in (Blackman, Abrahamsson et al. 2013).

6.5. Conclusions and future directions

This thesis presents evidence for the utility of anatomical cell-type classification from 2PLSM imaging and applies this to a biological question in the investigation of the expression pattern of presynaptic NMDA receptors in layer 5 of neocortex. The results identified here are then used to validate a timesaving method of cell-type classification based on Sholl analysis from bitmap images without the need for reconstruction.

In order to further validate and explore the utility of 2PLSM FI and other reconstruction methods, one could compare neurons imaged with electron microscopy (as the closest to a 'ground truth') and other more recent techniques such as super-resolution two-photon imaging to gain a broader understanding of the effect of method choice on imaging and computer modelling, and the strengths and limitations of various methods. It may be the case, for example, that confocal and / or super-resolution techniques

result in more accurate reconstructions that are suitable for multicompartmental modelling.

Importantly, differences in peak depolarisation were identified in simulated EPSPs using reconstructions of the exact same cells using the exact same models (Stuart and Hausser 2001). Here, this shows that reconstruction method choice and process alone can significantly affect the results of modelling studies. This should influence the design of future experiments; consider, for example, a large-scale simulation using many realistic morphologies sourced from a database such as NeuroMorpho.org. Results in such a simulation could be unintentionally affected by reconstruction method – with 2PLSM / FI reconstructions exhibiting smaller depolarisations simply due to their reconstruction method. Similarly, if a model created and fitted to physiological data from particular cells reconstructed using a single method (e.g. biocytin) is used in the same cell type reconstructed with a different method (e.g. 2PLSM FI), the results may not be as representative of the physiological 'truth'. As such, one should take care to avoid mixing reconstruction methods in a study, and also in utilising models created with one reconstruction method in another. This is of particular relevance in the light of large-scale simulation projects or the increased use of morphologies created in other labs (Ascoli 2006, Ascoli, Donohue et al. 2007, Ascoli, Alonso-Nanclares et al. 2008, Halavi, Hamilton et al. 2012, DeFelipe, Lopez-Cruz et al. 2013, Markram 2013). Furthermore, the results described in this thesis should influence the choice of reconstruction method in anatomical or morphological studies. For accurate reconstruction of local morphology, despite exaggerating process diameters, 2PLSM FI reconstructions may be a superior choice due to their relative lack of distortions, compression or shrinkage. This said, if the experiment calls for long-range tracing, care must be taken in utilising FI as more distal collaterals may not be evident with this method.

The target-specific expression of preNMDARs, coupled with differing synapse-specific STP, contributes to spatiotemporal remapping of inhibition during high-frequency firing. As preNMDAR expression and STP may

change with development (Blackman, Abrahamsson et al. 2013, Gill, Droubi et al. 2014), it would be interesting to investigate both how the expression and function of preNMDARs and STP potentially changes at particular synapses in layer 5, and if this is similarly modulated by sensory experience as in L4 / L2/3 synapses (Corlew, Wang et al. 2007, Cheetham and Fox 2010, Larsen, Smith et al. 2014, Urban-Ciecko, Wen et al. 2014). Additionally, the putatively PV-expressing L5 INs with ascending translaminar axonal arbours identified in Chapter 4 may have similarities to recently described layer 6 INs which suppress cells across many cortical layers (Bortone, Olsen et al. 2014); future research could thus examine the postsynaptic target of these cells in superficial layers and the dynamics of inhibition recruited by L5 PC activity, including the contribution of preNMDARs to this.

Finally, it would potentially be useful to expand the functionality and apply the *Sholl Analysis* software to biological studies. For example, further validation could be performed in comparison with results from genetic, physiological or functional profiling (Butt, Fuccillo et al. 2005, Toledo-Rodriguez, Goodman et al. 2005, Ascoli, Alonso-Nanclares et al. 2008, McGarry, Packer et al. 2010, DeFelipe, Lopez-Cruz et al. 2013, Kepecs and Fishell 2014, Sumbul, Song et al. 2014, Usoskin, Furlan et al. 2014) and could be used to investigate cell-type specificity in connectivity, plasticity or other circuit properties.

7. References

Aarts, E., M. Verhage, J. V. Veenvliet, C. V. Dolan and S. van der Sluis (2014). "A solution to dependency: using multilevel analysis to accommodate nested data." Nature Neuroscience **17**(4): 491-496.

Abbott, L. F. and S. B. Nelson (2000). "Synaptic plasticity: taming the beast." Nature Neuroscience **3 Suppl**: 1178-1183.

Abbott, L. F., J. A. Varela, K. Sen and S. B. Nelson (1997). "Synaptic depression and cortical gain control." Science **275**(5297): 220-224.

Acker, C. D. and J. A. White (2007). "Roles of IA and morphology in action potential propagation in CA1 pyramidal cell dendrites." Journal of Computational Neuroscience **23**(2): 201-216.

Ali, A. B., J. Deuchars, H. Pawelzik and A. M. Thomson (1998). "CA1 pyramidal to basket and bistratified cell EPSPs: dual intracellular recordings in rat hippocampal slices." The Journal of Physiology **507 (Pt 1)**: 201-217.

Anderson, S. A., D. D. Eisenstat, L. Shi and J. L. Rubenstein (1997). "Interneuron migration from basal forebrain to neocortex: dependence on Dlx genes." Science **278**(5337): 474-476.

Aoki, C., C. Venkatesan, C. G. Go, J. A. Mong and T. M. Dawson (1994). "Cellular and subcellular localization of NMDA-R1 subunit immunoreactivity in the visual cortex of adult and neonatal rats." The Journal of Neuroscience **14**(9): 5202-5222.

Ascher, P. and L. Nowak (1988). "The role of divalent cations in the N-methyl-D-aspartate responses of mouse central neurones in culture." The Journal of Physiology **399**: 247-266.

Ascoli, G. A. (2006). "Mobilizing the base of neuroscience data: the case of neuronal morphologies." Nature Reviews Neuroscience **7**(4): 318-324.

Ascoli, G. A., L. Alonso-Nanclares, S. A. Anderson, G. Barrionuevo, R. Benavides-Piccione, A. Burkhalter, G. Buzsaki, B. Cauli, J. Defelipe, A. Fairen, D. Feldmeyer, G. Fishell, Y. Fregnac, T. F. Freund, D. Gardner, E. P. Gardner, J. H. Goldberg, M. Helmstaedter, S. Hestrin, F. Karube, Z. F. Kisvarday, B. Lambolez, D. A. Lewis, O. Marin, H. Markram, A. Munoz, A. Packer, C. C. Petersen, K. S. Rockland, J. Rossier, B. Rudy, P. Somogyi, J.

F. Staiger, G. Tamas, A. M. Thomson, M. Toledo-Rodriguez, Y. Wang, D. C. West and R. Yuste (2008). "Petilla terminology: nomenclature of features of GABAergic interneurons of the cerebral cortex." Nature Reviews Neuroscience **9**(7): 557-568.

Ascoli, G. A., D. E. Donohue and M. Halavi (2007). "NeuroMorpho.Org: a central resource for neuronal morphologies." The Journal of Neuroscience **27**(35): 9247-9251.

Atluri, P. P. and W. G. Regehr (1996). "Determinants of the time course of facilitation at the granule cell to Purkinje cell synapse." The Journal of Neuroscience **16**(18): 5661-5671.

Atwood, H. L. (1967). "Variation in physiological properties of crustacean motor synapses." Nature **215**(5096): 57-58.

Atwood, H. L. and G. D. Bittner (1971). "Matching of excitatory and inhibitory inputs to crustacean muscle fibers." Journal of Neurophysiology **34**(1): 157-170.

Azim, E., D. Jabaudon, R. M. Fame and J. D. Macklis (2009). "SOX6 controls dorsal progenitor identity and interneuron diversity during neocortical development." Nature Neuroscience **12**(10): 1238-1247.

Bao, J., K. Reim and T. Sakaba (2010). "Target-dependent feedforward inhibition mediated by short-term synaptic plasticity in the cerebellum." The Journal of Neuroscience **30**(24): 8171-8179.

Bargmann, C. I. and E. Marder (2013). "From the connectome to brain function." Nature Methods **10**(6): 483-490.

Barone, P., A. Batardiere, K. Knoblauch and H. Kennedy (2000). "Laminar distribution of neurons in extrastriate areas projecting to visual areas V1 and V4 correlates with the hierarchical rank and indicates the operation of a distance rule." The Journal of Neuroscience **20**(9): 3263-3281.

Bender, V. A., K. J. Bender, D. J. Brasier and D. E. Feldman (2006). "Two coincidence detectors for spike timing-dependent plasticity in somatosensory cortex." The Journal of Neuroscience **26**(16): 4166-4177.

Berger, T. K., G. Silberberg, R. Perin and H. Markram (2010). "Brief bursts self-inhibit and correlate the pyramidal network." PLoS Biology **8**(9).

Berretta, N. and R. S. Jones (1996). "Tonic facilitation of glutamate release by presynaptic N-methyl-D-aspartate autoreceptors in the entorhinal cortex." Neuroscience **75**(2): 339-344.
Bertram, R., A. Sherman and E. F. Stanley (1996). "Single-domain/bound calcium hypothesis of transmitter release and facilitation." Journal of Neurophysiology **75**(5): 1919-1931.
Bidoret, C., A. Ayon, B. Barbour and M. Casado (2009). "Presynaptic NR2A-containing NMDA receptors implement a high-pass filter synaptic plasticity rule." Proceedings of the National Academy of Sciences of the United States of America **106**(33): 14126-14131.
Binley, K. E., W. S. Ng, J. R. Tribble, B. Song and J. E. Morgan (2014). "Sholl analysis: a quantitative comparison of semi-automated methods." Journal of Neuroscience Methods **225**: 65-70.
Blackman, A. V., T. Abrahamsson, R. P. Costa, T. Lalanne and P. J. Sjostrom (2013). "Target-cell-specific short-term plasticity in local circuits." Frontiers in Synaptic Neuroscience **5**: 11.
Blackman, A. V., S. Grabuschnig, R. Legenstein and P. J. Sjostrom (2014). "A comparison of manual neuronal reconstruction from biocytin histology or 2-photon imaging: morphometry and computer modeling." Frontiers in Neuroanatomy **8**: 65.
Bland, J. M. and D. G. Altman (1986). "Statistical methods for assessing agreement between two methods of clinical measurement." Lancet **1**(8476): 307-310.
Bliss, T. V. and G. L. Collingridge (1993). "A synaptic model of memory: long-term potentiation in the hippocampus." Nature **361**(6407): 31-39.
Bliss, T. V. and T. Lomo (1970). "Plasticity in a monosynaptic cortical pathway." The Journal of Physiology **207**(2): 61P.
Bliss, T. V. and T. Lomo (1973). "Long-lasting potentiation of synaptic transmission in the dentate area of the anaesthetized rabbit following stimulation of the perforant path." The Journal of Physiology **232**(2): 331-356.
Bloodgood, B. L., N. Sharma, H. A. Browne, A. Z. Trepman and M. E. Greenberg (2013). "The activity-dependent transcription factor NPAS4 regulates domain-specific inhibition." Nature **503**(7474): 121-125.

Bortone, D. S., S. R. Olsen and M. Scanziani (2014). "Translaminar inhibitory cells recruited by layer 6 corticothalamic neurons suppress visual cortex." Neuron **82**(2): 474-485.
Bourque, C. W. (2008). "Central mechanisms of osmosensation and systemic osmoregulation." Nature Reviews Neuroscience **9**(7): 519-531.
Brasier, D. J. and D. E. Feldman (2008). "Synapse-specific expression of functional presynaptic NMDA receptors in rat somatosensory cortex." The Journal of Neuroscience **28**(9): 2199-2211.
Brette, R., M. Rudolph, T. Carnevale, M. Hines, D. Beeman, J. M. Bower, M. Diesmann, A. Morrison, P. H. Goodman, F. C. Harris, Jr., M. Zirpe, T. Natschlager, D. Pecevski, B. Ermentrout, M. Djurfeldt, A. Lansner, O. Rochel, T. Vieville, E. Muller, A. P. Davison, S. El Boustani and A. Destexhe (2007). "Simulation of networks of spiking neurons: a review of tools and strategies." Journal of Computational Neuroscience **23**(3): 349-398.
Brodmann, K. (1909). Vergleichende Lokalisationslehre der Großhirnrinde. Liepzig, Barth.
Brown, S. P. and S. Hestrin (2009a). "Cell-type identity: a key to unlocking the function of neocortical circuits." Current Opinion in Neurobiology **19**(4): 415-421.
Brown, S. P. and S. Hestrin (2009b). "Intracortical circuits of pyramidal neurons reflect their long-range axonal targets." Nature **457**(7233): 1133-1136.
Buchanan, K. A., A. V. Blackman, A. W. Moreau, D. Elgar, R. P. Costa, T. Lalanne, A. A. Tudor Jones, J. Oyrer and P. J. Sjostrom (2012). "Target-specific expression of presynaptic NMDA receptors in neocortical microcircuits." Neuron **75**(3): 451-466.
Bush, P. C. and T. J. Sejnowski (1993). "Reduced compartmental models of neocortical pyramidal cells." Journal of Neuroscience Methods **46**(2): 159-166.
Butt, S. J., M. Fuccillo, S. Nery, S. Noctor, A. Kriegstein, J. G. Corbin and G. Fishell (2005). "The temporal and spatial origins of cortical interneurons predict their physiological subtype." Neuron **48**(4): 591-604.
Cai, Y., Q. Zhang, C. Wang, Y. Zhang, T. Ma, X. Zhou, M. Tian, J. L. Rubenstein and Z. Yang (2013). "Nuclear receptor COUP-TFII-expressing

neocortical interneurons are derived from the medial and lateral/caudal ganglionic eminence and define specific subsets of mature interneurons." The Journal of Comparative Neurology **521**(2): 479-497.
Campbell, A. (1905). Histological studies on the localization of cerebral function. Cambridge, Cambridge University Press.
Cannon, R. C., H. V. Wheal and D. A. Turner (1999). "Dendrites of classes of hippocampal neurons differ in structural complexity and branching patterns." The Journal of Comparative Neurology **413**(4): 619-633.
Carnevale, N. T. and M. L. Hines (2006). The NEURON Book, Cambridge University Press.
Casado, M., S. Dieudonne and P. Ascher (2000). "Presynaptic N-methyl-D-aspartate receptors at the parallel fiber-Purkinje cell synapse." Proceedings of the National Academy of Sciences of the United States of America **97**(21): 11593-11597.
Casado, M., P. Isope and P. Ascher (2002). "Involvement of presynaptic N-methyl-D-aspartate receptors in cerebellar long-term depression." Neuron **33**(1): 123-130.
Caviness, V. S. (1975). "Architectonic map of neocortex of the normal mouse." The Journal of Comparative Neurology **164**(2): 247-263.
Chadderton, P., T. W. Margrie and M. Hausser (2004). "Integration of quanta in cerebellar granule cells during sensory processing." Nature **428**(6985): 856-860.
Chattopadhyaya, B., G. Di Cristo, H. Higashiyama, G. W. Knott, S. J. Kuhlman, E. Welker and Z. J. Huang (2004). "Experience and activity-dependent maturation of perisomatic GABAergic innervation in primary visual cortex during a postnatal critical period." The Journal of Neuroscience **24**(43): 9598-9611.
Cheetham, C. E. and K. Fox (2010). "Presynaptic development at L4 to l2/3 excitatory synapses follows different time courses in visual and somatosensory cortex." The Journal of Neuroscience **30**(38): 12566-12571.
Chen, W. X. and D. V. Buonomano (2012). "Developmental shift of short-term synaptic plasticity in cortical organotypic slices." Neuroscience **213**: 38-46.

Chittajallu, R., K. A. Pelkey and C. J. McBain (2013). "Neurogliaform cells dynamically regulate somatosensory integration via synapse-specific modulation." Nature Neuroscience **16**(1): 13-15.
Chittajallu, R., M. Vignes, K. K. Dev, J. M. Barnes, G. L. Collingridge and J. M. Henley (1996). "Regulation of glutamate release by presynaptic kainate receptors in the hippocampus." Nature **379**(6560): 78-81.
Choi, D. W., J. Y. Koh and S. Peters (1988). "Pharmacology of glutamate neurotoxicity in cortical cell culture: attenuation by NMDA antagonists." The Journal of Neuroscience **8**(1): 185-196.
Christie, J. M. and C. E. Jahr (2008). "Dendritic NMDA receptors activate axonal calcium channels." Neuron **60**(2): 298-307.
Christie, J. M. and C. E. Jahr (2009). "Selective expression of ligand-gated ion channels in L5 pyramidal cell axons." The Journal of Neuroscience **29**(37): 11441-11450.
Cobb, S. R., E. H. Buhl, K. Halasy, O. Paulsen and P. Somogyi (1995). "Synchronization of neuronal activity in hippocampus by individual GABAergic interneurons." Nature **378**(6552): 75-78.
Corbin, J. G., M. Rutlin, N. Gaiano and G. Fishell (2003). "Combinatorial function of the homeodomain proteins Nkx2.1 and Gsh2 in ventral telencephalic patterning." Development **130**(20): 4895-4906.
Corlew, R., D. J. Brasier, D. E. Feldman and B. D. Philpot (2008). "Presynaptic NMDA receptors: newly appreciated roles in cortical synaptic function and plasticity." The Neuroscientist **14**(6): 609-625.
Corlew, R., Y. Wang, H. Ghermazien, A. Erisir and B. D. Philpot (2007). "Developmental switch in the contribution of presynaptic and postsynaptic NMDA receptors to long-term depression." The Journal of Neuroscience **27**(37): 9835-9845.
Cull-Candy, S., S. Brickley and M. Farrant (2001). "NMDA receptor subunits: diversity, development and disease." Current Opinion in Neurobiology **11**(3): 327-335.
Dalva, M. B., A. C. McClelland and M. S. Kayser (2007). "Cell adhesion molecules: signalling functions at the synapse." Nature Reviews Neuroscience **8**(3): 206-220.

DeFelipe, J. (1997). "Types of neurons, synaptic connections and chemical characteristics of cells immunoreactive for calbindin-D28K, parvalbumin and calretinin in the neocortex." Journal of Chemical Neuroanatomy **14**(1): 1-19.
DeFelipe, J., S. H. Hendry and E. G. Jones (1989). "Visualization of chandelier cell axons by parvalbumin immunoreactivity in monkey cerebral cortex." Proceedings of the National Academy of Sciences of the United States of America **86**(6): 2093-2097.
DeFelipe, J., P. L. Lopez-Cruz, R. Benavides-Piccione, C. Bielza, P. Larranaga, S. Anderson, A. Burkhalter, B. Cauli, A. Fairen, D. Feldmeyer, G. Fishell, D. Fitzpatrick, T. F. Freund, G. Gonzalez-Burgos, S. Hestrin, S. Hill, P. R. Hof, J. Huang, E. G. Jones, Y. Kawaguchi, Z. Kisvarday, Y. Kubota, D. A. Lewis, O. Marin, H. Markram, C. J. McBain, H. S. Meyer, H. Monyer, S. B. Nelson, K. Rockland, J. Rossier, J. L. Rubenstein, B. Rudy, M. Scanziani, G. M. Shepherd, C. C. Sherwood, J. F. Staiger, G. Tamas, A. Thomson, Y. Wang, R. Yuste and G. A. Ascoli (2013). "New insights into the classification and nomenclature of cortical GABAergic interneurons." Nature Reviews Neuroscience **14**(3): 202-216.
Del Castillo, J. and B. Katz (1954). "Quantal components of the end-plate potential." The Journal of Physiology **124**(3): 560-573.
Delaney, A. J. and C. E. Jahr (2002). "Kainate receptors differentially regulate release at two parallel fiber synapses." Neuron **36**(3): 475-482.
Deng, L., P. S. Kaeser, W. Xu and T. C. Sudhof (2011). "RIM proteins activate vesicle priming by reversing autoinhibitory homodimerization of Munc13." Neuron **69**(2): 317-331.
Denk, W., J. H. Strickler and W. W. Webb (1990). "Two-photon laser scanning fluorescence microscopy." Science **248**(4951): 73-76.
Ding, J. B., K. T. Takasaki and B. L. Sabatini (2009). "Supraresolution imaging in brain slices using stimulated-emission depletion two-photon laser scanning microscopy." Neuron **63**(4): 429-437.
Do, C. B. and S. Batzoglou (2008). "What is the expectation maximization algorithm?" Nature Biotechnology **26**(8): 897-899.
Donohue, D. E. and G. A. Ascoli (2011). "Automated reconstruction of neuronal morphology: an overview." Brain Research Reviews **67**(1-2): 94-102.

Douglas, R. J., H. Markram and K. A. Martin (2004). Neocortex. The Synaptic Organization of the Brain. G. M. Shepherd. New York, Oxford University Press**:** 499-559.
Douglas, R. J. and K. A. Martin (2004). "Neuronal circuits of the neocortex." Annual Review of Neuroscience **27**: 419-451.
Duguid, I. and P. J. Sjostrom (2006). "Novel presynaptic mechanisms for coincidence detection in synaptic plasticity." Current Opinion in Neurobiology **16**(3): 312-322.
Duguid, I. C. (2013). "Presynaptic NMDA receptors: are they dendritic receptors in disguise?" Brain Research Bulletin **93**: 4-9.
Duguid, I. C. and T. G. Smart (2004). "Retrograde activation of presynaptic NMDA receptors enhances GABA release at cerebellar interneuron-Purkinje cell synapses." Nature Neuroscience **7**(5): 525-533.
Duguid, I. C. and T. G. Smart (2009). Presynaptic NMDA Receptors. Biology of the NMDA Receptor. A. M. Van Dongen. Boca Raton (FL).
Dumitriu, D., A. Rodriguez and J. H. Morrison (2011). "High-throughput, detailed, cell-specific neuroanatomy of dendritic spines using microinjection and confocal microscopy." Nature Protocols **6**(9): 1391-1411.
Eccles, J. C. (1964). The physiology of synpases. Berlin, Springer.
Egger, V., D. Feldmeyer and B. Sakmann (1999). "Coincidence detection and changes of synaptic efficacy in spiny stellate neurons in rat barrel cortex." Nature Neuroscience **2**(12): 1098-1105.
Egger, V., T. Nevian and R. M. Bruno (2008). "Subcolumnar dendritic and axonal organization of spiny stellate and star pyramid neurons within a barrel in rat somatosensory cortex." Cerebral Cortex **18**(4): 876-889.
Engelman, H. S. and A. B. MacDermott (2004). "Presynaptic ionotropic receptors and control of transmitter release." Nature Reviews Neuroscience **5**(2): 135-145.
Faber, D. S. and H. Korn (1991). "Applicability of the coefficient of variation method for analyzing synaptic plasticity." Biophysical Journal **60**(5): 1288-1294.
Famm, K., B. Litt, K. J. Tracey, E. S. Boyden and M. Slaoui (2013). "Drug discovery: a jump-start for electroceuticals." Nature **496**(7444): 159-161.

Fatt, P. and B. Katz (1952). "Spontaneous subthreshold activity at motor nerve endings." The Journal of Physiology **117**(1): 109-128.
Feldman, D. E. (2009). "Synaptic mechanisms for plasticity in neocortex." Annual Review of Neuroscience **32**: 33-55.
Feldman, D. E. (2012). "The spike-timing dependence of plasticity." Neuron **75**(4): 556-571.
Fernandez-Chacon, R., A. Konigstorfer, S. H. Gerber, J. Garcia, M. F. Matos, C. F. Stevens, N. Brose, J. Rizo, C. Rosenmund and T. C. Sudhof (2001). "Synaptotagmin I functions as a calcium regulator of release probability." Nature **410**(6824): 41-49.
Ferreira, T. A., A. V. Blackman, J. Oyrer, S. Jayabal, A. J. Chung, A. J. Watt, P. J. Sjostrom and D. J. van Meyel (2014). "Neuronal morphometry directly from bitmap images." Nature Methods **11**(10): 982-984.
Fink, K., H. Bonisch and M. Gothert (1990). "Presynaptic NMDA receptors stimulate noradrenaline release in the cerebral cortex." European Journal of Pharmacology **185**(1): 115-117.
Fino, E. and R. Yuste (2011). "Dense inhibitory connectivity in neocortex." Neuron **69**(6): 1188-1203.
Fitzpatrick, D., K. Itoh and I. T. Diamond (1983). "The laminar organization of the lateral geniculate body and the striate cortex in the squirrel monkey (Saimiri sciureus)." The Journal of Neuroscience **3**(4): 673-702.
Flames, N., R. Pla, D. M. Gelman, J. L. Rubenstein, L. Puelles and O. Marin (2007). "Delineation of multiple subpallial progenitor domains by the combinatorial expression of transcriptional codes." The Journal of Neuroscience **27**(36): 9682-9695.
Galarreta, M. and S. Hestrin (1998). "Frequency-dependent synaptic depression and the balance of excitation and inhibition in the neocortex." Nature Neuroscience **1**(7): 587-594.
Garcia-Segura, L. M. and J. Perez-Marquez (2014). "A new mathematical function to evaluate neuronal morphology using the Sholl analysis." Journal of Neuroscience Methods **226**: 103-109.
Gelman, D., A. Griveau, N. Dehorter, A. Teissier, C. Varela, R. Pla, A. Pierani and O. Marin (2011). "A wide diversity of cortical GABAergic

interneurons derives from the embryonic preoptic area." The Journal of Neuroscience **31**(46): 16570-16580.
Gelman, D. M., F. J. Martini, S. Nobrega-Pereira, A. Pierani, N. Kessaris and O. Marin (2009). "The embryonic preoptic area is a novel source of cortical GABAergic interneurons." The Journal of Neuroscience **29**(29): 9380-9389.
Gibson, J. R., M. Beierlein and B. W. Connors (1999). "Two networks of electrically coupled inhibitory neurons in neocortex." Nature **402**(6757): 75-79.
Gidon, A. and I. Segev (2012). "Principles governing the operation of synaptic inhibition in dendrites." Neuron **75**(2): 330-341.
Gil-Sanz, C., S. J. Franco, I. Martinez-Garay, A. Espinosa, S. Harkins-Perry and U. Muller (2013). "Cajal-Retzius cells instruct neuronal migration by coincidence signaling between secreted and contact-dependent guidance cues." Neuron **79**(3): 461-477.
Gilbert, C. D. (1983). "Microcircuitry of the visual cortex." Annual Review of Neuroscience **6**: 217-247.
Gill, I., S. Droubi, S. Giovedi, K. Fedder, L. A. Bury, F. Bosco, M. P. Sceniak, F. Benfenati and S. L. Sabo (2014). "Presynaptic NMDA receptors: dynamics and distribution in developing axons in vitro and in vivo." Journal of Cell Science.
Glickfeld, L. L. and M. Scanziani (2006). "Distinct timing in the activity of cannabinoid-sensitive and cannabinoid-insensitive basket cells." Nature Neuroscience **9**(6): 807-815.
Glitsch, M. and A. Marty (1999). "Presynaptic effects of NMDA in cerebellar Purkinje cells and interneurons." The Journal of Neuroscience **19**(2): 511-519.
Gonchar, Y. and A. Burkhalter (1997). "Three distinct families of GABAergic neurons in rat visual cortex." Cerebral Cortex **7**(4): 347-358.
Gray, E. G. (1959). "Axo-somatic and axo-dendritic synapses of the cerebral cortex: an electron microscope study." Journal of Anatomy **93**: 420-433.
Groh, A., H. S. Meyer, E. F. Schmidt, N. Heintz, B. Sakmann and P. Krieger (2010). "Cell-type specific properties of pyramidal neurons in neocortex underlying a layout that is modifiable depending on the cortical area." Cerebral Cortex **20**(4): 826-836.

Gupta, A., Y. Wang and H. Markram (2000). "Organizing principles for a diversity of GABAergic interneurons and synapses in the neocortex." Science **287**(5451): 273-278.
Haider, B., M. Hausser and M. Carandini (2013). "Inhibition dominates sensory responses in the awake cortex." Nature **493**(7430): 97-100.
Halavi, M., K. A. Hamilton, R. Parekh and G. A. Ascoli (2012). "Digital reconstructions of neuronal morphology: three decades of research trends." Frontiers in Neuroscience **6**: 49.
Han, Y., P. S. Kaeser, T. C. Sudhof and R. Schneggenburger (2011). "RIM determines Ca(2)+ channel density and vesicle docking at the presynaptic active zone." Neuron **69**(2): 304-316.
Harris, K. D. and T. D. Mrsic-Flogel (2013). "Cortical connectivity and sensory coding." Nature **503**(7474): 51-58.
Hebb, D. O. (1949). The organization of behaviour : a neuropsychological theory. New York, Wiley.
Hell, S. W. (2007). "Far-field optical nanoscopy." Science **316**(5828): 1153-1158.
Helmstaedter, M. (2013). "Cellular-resolution connectomics: challenges of dense neural circuit reconstruction." Nature Methods **10**(6): 501-507.
Herron, C. E., R. A. Lester, E. J. Coan and G. L. Collingridge (1986). "Frequency-dependent involvement of NMDA receptors in the hippocampus: a novel synaptic mechanism." Nature **322**(6076): 265-268.
Hestrin, S. and W. E. Armstrong (1996). "Morphology and physiology of cortical neurons in layer I." The Journal of Neuroscience **16**(17): 5290-5300.
Hofer, S. B., H. Ko, B. Pichler, J. Vogelstein, H. Ros, H. Zeng, E. Lein, N. A. Lesica and T. D. Mrsic-Flogel (2011). "Differential connectivity and response dynamics of excitatory and inhibitory neurons in visual cortex." Nature Neuroscience **14**(8): 1045-1052.
Holmes, W. R. (1989). "The role of dendritic diameters in maximizing the effectiveness of synaptic inputs." Brain Research **478**(1): 127-137.
Hubel, D. H. and T. N. Wiesel (1959). "Receptive fields of single neurones in the cat's striate cortex." The Journal of Physiology **148**: 574-591.

Hubel, D. H. and T. N. Wiesel (1962). "Receptive fields, binocular interaction and functional architecture in the cat's visual cortex." The Journal of Physiology **160**: 106-154.
Hubel, D. H. and T. N. Wiesel (1972). "Laminar and columnar distribution of geniculo-cortical fibers in the macaque monkey." The Journal of Comparative Neurology **146**(4): 421-450.
Hubel, D. H. and T. N. Wiesel (1977). "Ferrier lecture. Functional architecture of macaque monkey visual cortex." Proceeding of the Royal Society of London. Series B, Containing Papers of a Biological Character. **198**(1130): 1-59.
Humeau, Y., H. Shaban, S. Bissiere and A. Luthi (2003). "Presynaptic induction of heterosynaptic associative plasticity in the mammalian brain." Nature **426**(6968): 841-845.
Inan, M., L. Blazquez-Llorca, A. Merchan-Perez, S. A. Anderson, J. DeFelipe and R. Yuste (2013). "Dense and overlapping innervation of pyramidal neurons by chandelier cells." The Journal of Neuroscience **33**(5): 1907-1914.
Inan, M., J. Welagen and S. A. Anderson (2012). "Spatial and temporal bias in the mitotic origins of somatostatin- and parvalbumin-expressing interneuron subgroups and the chandelier subtype in the medial ganglionic eminence." Cerebral Cortex **22**(4): 820-827.
Ishikawa, T., M. Kaneko, H. S. Shin and T. Takahashi (2005). "Presynaptic N-type and P/Q-type Ca2+ channels mediating synaptic transmission at the calyx of Held of mice." The Journal of Physiology **568**(Pt 1): 199-209.
Iwasaki, S., A. Momiyama, O. D. Uchitel and T. Takahashi (2000). "Developmental changes in calcium channel types mediating central synaptic transmission." The Journal of Neuroscience **20**(1): 59-65.
Iwasaki, S. and T. Takahashi (1998). "Developmental changes in calcium channel types mediating synaptic transmission in rat auditory brainstem." The Journal of Physiology **509 (Pt 2)**: 419-423.
Iwasaki, S. and T. Takahashi (2001). "Developmental regulation of transmitter release at the calyx of Held in rat auditory brainstem." The Journal of Physiology **534**(Pt 3): 861-871.
Jack, J. J. B., D. Noble and R. W. Tsien (1975). Electric current flow in excitable cells, Clarendon Press.

Jakovcevski, I., N. Mayer and N. Zecevic (2011). "Multiple origins of human neocortical interneurons are supported by distinct expression of transcription factors." Cerebral Cortex **21**(8): 1771-1782.
Jarvis, R. A. (1973). "On the identification of the convex hull of a finite set of points in the plane." Information Processing Letters **2**(1): 18-21.
Kalisman, N., G. Silberberg and H. Markram (2005). "The neocortical microcircuit as a tabula rasa." Proceedings of the National Academy of Sciences of the United States of America **102**(3): 880-885.
Katz, B. and R. Miledi (1968). "The role of calcium in neuromuscular facilitation." The Journal of Physiology **195**(2): 481-492.
Katzel, D., B. V. Zemelman, C. Buetfering, M. Wolfel and G. Miesenbock (2011). "The columnar and laminar organization of inhibitory connections to neocortical excitatory cells." Nature Neuroscience **14**(1): 100-107.
Kawaguchi, Y., F. Karube and Y. Kubota (2006). "Dendritic branch typing and spine expression patterns in cortical nonpyramidal cells." Cerebral Cortex **16**(5): 696-711.
Kepecs, A. and G. Fishell (2014). "Interneuron cell types are fit to function." Nature **505**(7483): 318-326.
Kisvarday, Z. F., K. A. Martin, M. J. Friedlander and P. Somogyi (1987). "Evidence for interlaminar inhibitory circuits in the striate cortex of the cat." The Journal of Comparative Neurology **260**(1): 1-19.
Kleinfeld, D., A. Bharioke, P. Blinder, D. D. Bock, K. L. Briggman, D. B. Chklovskii, W. Denk, M. Helmstaedter, J. P. Kaufhold, W. C. Lee, H. S. Meyer, K. D. Micheva, M. Oberlaender, S. Prohaska, R. C. Reid, S. J. Smith, S. Takemura, P. S. Tsai and B. Sakmann (2011). "Large-scale automated histology in the pursuit of connectomes." The Journal of Neuroscience **31**(45): 16125-16138.
Ko, H., L. Cossell, C. Baragli, J. Antolik, C. Clopath, S. B. Hofer and T. D. Mrsic-Flogel (2013). "The emergence of functional microcircuits in visual cortex." Nature **496**(7443): 96-100.
Ko, H., S. B. Hofer, B. Pichler, K. A. Buchanan, P. J. Sjostrom and T. D. Mrsic-Flogel (2011). "Functional specificity of local synaptic connections in neocortical networks." Nature **473**(7345): 87-91.

Koch, C., T. Poggio and V. Torre (1983). "Nonlinear interactions in a dendritic tree: localization, timing, and role in information processing." Proceedings of the National Academy of Sciences of the United States of America **80**(9): 2799-2802.
Koester, H. J. and D. Johnston (2005). "Target cell-dependent normalization of transmitter release at neocortical synapses." Science **308**(5723): 863-866.
Korn, H. and D. S. Faber (1991). "Quantal analysis and synaptic efficacy in the CNS." Trends in Neurosciences **14**(10): 439-445.
Kuhlman, S. J., N. D. Olivas, E. Tring, T. Ikrar, X. Xu and J. T. Trachtenberg (2013). "A disinhibitory microcircuit initiates critical-period plasticity in the visual cortex." Nature **501**(7468): 543-546.
Kunz, P. A., A. C. Roberts and B. D. Philpot (2013). "Presynaptic NMDA receptor mechanisms for enhancing spontaneous neurotransmitter release." The Journal of Neuroscience **33**(18): 7762-7769.
Lachica, E. A. and V. A. Casagrande (1992). "Direct W-like geniculate projections to the cytochrome oxidase (CO) blobs in primate visual cortex: axon morphology." The Journal of Comparative Neurology **319**(1): 141-158.
Larkman, A., T. Hannay, K. Stratford and J. Jack (1992). "Presynaptic release probability influences the locus of long-term potentiation." Nature **360**(6399): 70-73.
Larkman, A. and A. Mason (1990). "Correlations between morphology and electrophysiology of pyramidal neurons in slices of rat visual cortex. I. Establishment of cell classes." The Journal of Neuroscience **10**(5): 1407-1414.
Larkum, M. E., T. Nevian, M. Sandler, A. Polsky and J. Schiller (2009). "Synaptic integration in tuft dendrites of layer 5 pyramidal neurons: a new unifying principle." Science **325**(5941): 756-760.
Larkum, M. E., J. J. Zhu and B. Sakmann (1999). "A new cellular mechanism for coupling inputs arriving at different cortical layers." Nature **398**(6725): 338-341.
Larsen, R. S., R. J. Corlew, M. A. Henson, A. C. Roberts, M. Mishina, M. Watanabe, S. A. Lipton, N. Nakanishi, I. Perez-Otano, R. J. Weinberg and B. D. Philpot (2011). "NR3A-containing NMDARs promote neurotransmitter

release and spike timing-dependent plasticity." Nature Neuroscience **14**(3): 338-344.
Larsen, R. S., I. T. Smith, J. Miriyala, J. E. Han, R. J. Corlew, S. L. Smith and B. D. Philpot (2014). "Synapse-Specific Control of Experience-Dependent Plasticity by Presynaptic NMDA Receptors." Neuron **83**(4): 879-893.
Lavdas, A. A., M. Grigoriou, V. Pachnis and J. G. Parnavelas (1999). "The medial ganglionic eminence gives rise to a population of early neurons in the developing cerebral cortex." The Journal of Neuroscience **19**(18): 7881-7888.
Lee, C.-H., W. Lu, J. C. Michel, A. Goehring, J. Du, X. Song and E. Gouaux (2014). "NMDA receptor structures reveal subunit arrangement and pore architecture." Nature **advance online publication**.
Lee, W. C. and R. C. Reid (2011). "Specificity and randomness: structure-function relationships in neural circuits." Current Opinion in Neurobiology **21**(5): 801-807.
LeVay, S. and C. D. Gilbert (1976). "Laminar patterns of geniculocortical projection in the cat." Brain Research **113**(1): 1-19.
Lewis, D. A. (2014). "Inhibitory neurons in human cortical circuits: substrate for cognitive dysfunction in schizophrenia." Current Opinion in Neurobiology **26**: 22-26.
Lewis, D. A., T. Hashimoto and D. W. Volk (2005). "Cortical inhibitory neurons and schizophrenia." Nature Reviews Neuroscience **6**(4): 312-324.
Lichtman, J. W. and W. Denk (2011). "The big and the small: challenges of imaging the brain's circuits." Science **334**(6056): 618-623.
Linden, D. J. and J. A. Connor (1995). "Long-term synaptic depression." Annual Review of Neuroscience **18**: 319-357.
Lisman, J. E., J. T. Coyle, R. W. Green, D. C. Javitt, F. M. Benes, S. Heckers and A. A. Grace (2008). "Circuit-based framework for understanding neurotransmitter and risk gene interactions in schizophrenia." Trends in Neurosciences **31**(5): 234-242.
Liu, H., H. Wang, M. Sheng, L. Y. Jan, Y. N. Jan and A. I. Basbaum (1994). "Evidence for presynaptic N-methyl-D-aspartate autoreceptors in the spinal cord dorsal horn." Proceedings of the National Academy of Sciences of the United States of America **91**(18): 8383-8387.

Liu, Y. (2011). "The DIADEM and beyond." Neuroinformatics **9**(2-3): 99-102.
Livet, J., T. A. Weissman, H. Kang, R. W. Draft, J. Lu, R. A. Bennis, J. R. Sanes and J. W. Lichtman (2007). "Transgenic strategies for combinatorial expression of fluorescent proteins in the nervous system." Nature **450**(7166): 56-62.
Lodato, S., G. S. Tomassy, E. De Leonibus, Y. G. Uzcategui, G. Andolfi, M. Armentano, A. Touzot, J. M. Gaztelu, P. Arlotta, L. Menendez de la Prida and M. Studer (2011). "Loss of COUP-TFI alters the balance between caudal ganglionic eminence- and medial ganglionic eminence-derived cortical interneurons and results in resistance to epilepsy." The Journal of Neuroscience **31**(12): 4650-4662.
Lomo, T. (2003). "The discovery of long-term potentiation." Philosophical Transactions of the Royal Society of London. Series B, Biological Sciences **358**(1432): 617-620.
London, M. and M. Hausser (2005). "Dendritic computation." Annual Review of Neuroscience **28**: 503-532.
Longair, M. H., D. A. Baker and J. D. Armstrong (2011). "Simple Neurite Tracer: open source software for reconstruction, visualization and analysis of neuronal processes." Bioinformatics **27**(17): 2453-2454.
Losavio, B. E., Y. Liang, A. Santamaria-Pang, I. A. Kakadiaris, C. M. Colbert and P. Saggau (2008). "Live neuron morphology automatically reconstructed from multiphoton and confocal imaging data." Journal of Neurophysiology **100**(4): 2422-2429.
Lovett-Barron, M., G. F. Turi, P. Kaifosh, P. H. Lee, F. Bolze, X. H. Sun, J. F. Nicoud, B. V. Zemelman, S. M. Sternson and A. Losonczy (2012). "Regulation of neuronal input transformations by tunable dendritic inhibition." Nature Neuroscience **15**(3): 423-430, S421-423.
Lund, J. S. (1973). "Organization of neurons in the visual cortex, area 17, of the monkey (Macaca mulatta)." The Journal of Comparative Neurology **147**(4): 455-496.
Lund, J. S. (1988). "Anatomical organization of macaque monkey striate visual cortex." Annual Review of Neuroscience **11**: 253-288.
Ma, T., Q. Zhang, Y. Cai, Y. You, J. L. Rubenstein and Z. Yang (2012). "A subpopulation of dorsal lateral/caudal ganglionic eminence-derived

neocortical interneurons expresses the transcription factor Sp8." Cerebral Cortex **22**(9): 2120-2130.
MacDermott, A. B., M. L. Mayer, G. L. Westbrook, S. J. Smith and J. L. Barker (1986). "NMDA-receptor activation increases cytoplasmic calcium concentration in cultured spinal cord neurones." Nature **321**(6069): 519-522.
Malenka, R. C. and R. A. Nicoll (1999). "Long-term potentiation--a decade of progress?" Science **285**(5435): 1870-1874.
Malinow, R. and R. W. Tsien (1990). "Presynaptic enhancement shown by whole-cell recordings of long-term potentiation in hippocampal slices." Nature **346**(6280): 177-180.
Mameli, M., M. Carta, L. D. Partridge and C. F. Valenzuela (2005). "Neurosteroid-induced plasticity of immature synapses via retrograde modulation of presynaptic NMDA receptors." The Journal of Neuroscience **25**(9): 2285-2294.
Margolin, A. A., K. Wang, W. K. Lim, M. Kustagi, I. Nemenman and A. Califano (2006). "Reverse engineering cellular networks." Nature Protocols **1**(2): 662-671.
Markram, H. (2013). "Seven challenges for neuroscience." Functional Neurology **28**(3): 145-151.
Markram, H., W. Gerstner and P. J. Sjostrom (2011). "A history of spike-timing-dependent plasticity." Frontiers in Synaptic Neuroscience **3**: 4.
Markram, H., J. Lubke, M. Frotscher, A. Roth and B. Sakmann (1997). "Physiology and anatomy of synaptic connections between thick tufted pyramidal neurones in the developing rat neocortex." The Journal of Physiology **500 (Pt 2)**: 409-440.
Markram, H., M. Toledo-Rodriguez, Y. Wang, A. Gupta, G. Silberberg and C. Wu (2004). "Interneurons of the neocortical inhibitory system." Nature Reviews Neuroscience **5**(10): 793-807.
Markram, H. and M. Tsodyks (1996). "Redistribution of synaptic efficacy between neocortical pyramidal neurons." Nature **382**(6594): 807-810.
Markram, H., Y. Wang and M. Tsodyks (1998). "Differential signaling via the same axon of neocortical pyramidal neurons." Proceedings of the National Academy of Sciences of the United States of America **95**(9): 5323-5328.

Martinotti, C. (1889). "Contributo allo studio della corteccia cerebrale, ed all'origine central dei nervi." Ann Freniatr Sci Affini **1**: 14-381.
Marx, M., R. H. Gunter, W. Hucko, G. Radnikow and D. Feldmeyer (2012). "Improved biocytin labeling and neuronal 3D reconstruction." Nature Protocols **7**(2): 394-407.
Matveev, V. and X. J. Wang (2000). "Differential short-term synaptic plasticity and transmission of complex spike trains: to depress or to facilitate?" Cerebral Cortex **10**(11): 1143-1153.
McCormick, D. A. (2004). Membrane properties and neurotransmitter actions. The Synaptic Organization of the Brain. G. M. Shepherd. New York, Oxford University Press**:** 39-79.
McCormick, D. A., B. W. Connors, J. W. Lighthall and D. A. Prince (1985). "Comparative electrophysiology of pyramidal and sparsely spiny stellate neurons of the neocortex." Journal of Neurophysiology **54**(4): 782-806.
McGarry, L. M., A. M. Packer, E. Fino, V. Nikolenko, T. Sippy and R. Yuste (2010). "Quantitative classification of somatostatin-positive neocortical interneurons identifies three interneuron subtypes." Frontiers in Neural Circuits **4**: 12.
McLachlan, E. M. (1978). "The statistics of transmitter release at chemical synapses." International Review of Physiology **17**: 49-117.
Meijering, E. (2010). "Neuron tracing in perspective." Cytometry A **77**(7): 693-704.
Miller, E. K. and J. D. Cohen (2001). "An integrative theory of prefrontal cortex function." Annual Review of Neuroscience **24**: 167-202.
Min, R. and T. Nevian (2012). "Astrocyte signaling controls spike timing-dependent depression at neocortical synapses." Nature Neuroscience **15**(5): 746-753.
Miyoshi, G., J. Hjerling-Leffler, T. Karayannis, V. H. Sousa, S. J. Butt, J. Battiste, J. E. Johnson, R. P. Machold and G. Fishell (2010). "Genetic fate mapping reveals that the caudal ganglionic eminence produces a large and diverse population of superficial cortical interneurons." The Journal of Neuroscience **30**(5): 1582-1594.

Mortazavi, A., B. A. Williams, K. McCue, L. Schaeffer and B. Wold (2008). "Mapping and quantifying mammalian transcriptomes by RNA-Seq." Nature Methods **5**(7): 621-628.
Myatt, D. R., T. Hadlington, G. A. Ascoli and S. J. Nasuto (2012). "Neuromantic - from semi-manual to semi-automatic reconstruction of neuron morphology." Frontiers in Neuroinformatics **6**: 4.
Nabavi, S., R. Fox, C. D. Proulx, J. Y. Lin, R. Y. Tsien and R. Malinow (2014). "Engineering a memory with LTD and LTP." Nature **511**(7509): 348-352.
Nakazawa, K., V. Zsiros, Z. Jiang, K. Nakao, S. Kolata, S. Zhang and J. E. Belforte (2012). "GABAergic interneuron origin of schizophrenia pathophysiology." Neuropharmacology **62**(3): 1574-1583.
Nery, S., J. G. Corbin and G. Fishell (2003). "Dlx2 progenitor migration in wild type and Nkx2.1 mutant telencephalon." Cerebral Cortex **13**(9): 895-903.
Nery, S., G. Fishell and J. G. Corbin (2002). "The caudal ganglionic eminence is a source of distinct cortical and subcortical cell populations." Nature Neuroscience **5**(12): 1279-1287.
Nicoll, R. A. and R. C. Malenka (1995). "Contrasting properties of two forms of long-term potentiation in the hippocampus." Nature **377**(6545): 115-118.
Nissen, W., A. Szabo, J. Somogyi, P. Somogyi and K. P. Lamsa (2010). "Cell type-specific long-term plasticity at glutamatergic synapses onto hippocampal interneurons expressing either parvalbumin or CB1 cannabinoid receptor." The Journal of Neuroscience **30**(4): 1337-1347.
Nowak, L., P. Bregestovski, P. Ascher, A. Herbet and A. Prochiantz (1984). "Magnesium gates glutamate-activated channels in mouse central neurones." Nature **307**(5950): 462-465.
O'Rourke, N., L. Hatcher and E. J. Stepanski (2005). Measures of Bivariate Association. A Step-by-Step Approach to Using SAS for Univariate & Multivariate Statistics, Wiley-Interscience.
Oliva, A. A., Jr., M. Jiang, T. Lam, K. L. Smith and J. W. Swann (2000). "Novel hippocampal interneuronal subtypes identified using transgenic mice that express green fluorescent protein in GABAergic interneurons." The Journal of Neuroscience **20**(9): 3354-3368.

Osten, P. and T. W. Margrie (2013). "Mapping brain circuitry with a light microscope." Nature Methods **10**(6): 515-523.
Oswald, A. M. and A. D. Reyes (2008). "Maturation of intrinsic and synaptic properties of layer 2/3 pyramidal neurons in mouse auditory cortex." Journal of Neurophysiology **99**(6): 2998-3008.
Packer, A. M., D. J. McConnell, E. Fino and R. Yuste (2013). "Axo-dendritic overlap and laminar projection can explain interneuron connectivity to pyramidal cells." Cerebral Cortex **23**(12): 2790-2802.
Packer, A. M. and R. Yuste (2011). "Dense, unspecific connectivity of neocortical parvalbumin-positive interneurons: a canonical microcircuit for inhibition?" The Journal of Neuroscience **31**(37): 13260-13271.
Pan, Q., Y. Chanthery, W. C. Liang, S. Stawicki, J. Mak, N. Rathore, R. K. Tong, J. Kowalski, S. F. Yee, G. Pacheco, S. Ross, Z. Cheng, J. Le Couter, G. Plowman, F. Peale, A. W. Koch, Y. Wu, A. Bagri, M. Tessier-Lavigne and R. J. Watts (2007). "Blocking neuropilin-1 function has an additive effect with anti-VEGF to inhibit tumor growth." Cancer Cell **11**(1): 53-67.
Park, H., A. Popescu and M. Poo (2014). "Essential Role of Presynaptic NMDA Receptors in Activity-Dependent BDNF Secretion and Corticostriatal LTP." Neuron **Advance online publication**.
Peters, A. (1979). "Thalamic input to the cerebral cortex." Trends in Neurosciences **2**: 183-185.
Pi, H. J., B. Hangya, D. Kvitsiani, J. I. Sanders, Z. J. Huang and A. Kepecs (2013). "Cortical interneurons that specialize in disinhibitory control." Nature **503**(7477): 521-524.
Pologruto, T. A., B. L. Sabatini and K. Svoboda (2003). "ScanImage: flexible software for operating laser scanning microscopes." BioMedical Engineering OnLine **2**: 13.
Pouille, F. and M. Scanziani (2004). "Routing of spike series by dynamic circuits in the hippocampus." Nature **429**(6993): 717-723.
Pouille, F., O. Watkinson, M. Scanziani and A. J. Trevelyan (2013). "The contribution of synaptic location to inhibitory gain control in pyramidal cells." Physiological Reports **1**(5): e00067.

Pressler, R. T. and B. W. Strowbridge (2006). "Blanes cells mediate persistent feedforward inhibition onto granule cells in the olfactory bulb." Neuron **49**(6): 889-904.
Pugh, J. R. and C. E. Jahr (2011). "NMDA receptor agonists fail to alter release from cerebellar basket cells." The Journal of Neuroscience **31**(46): 16550-16555.
Ragan, T., L. R. Kadiri, K. U. Venkataraju, K. Bahlmann, J. Sutin, J. Taranda, I. Arganda-Carreras, Y. Kim, H. S. Seung and P. Osten (2012). "Serial two-photon tomography for automated ex vivo mouse brain imaging." Nature Methods **9**(3): 255-258.
Rall, W. (1957). "Membrane time constant of motoneurons." Science **126**(3271): 454.
Rall, W. (1959). "Branching dendritic trees and motoneuron membrane resistivity." Experimental Neurology **1**: 491-527.
Rall, W. (1964). Theoretical significance of dendritic trees for neuronal input-output relations.
Rall, W., I. Segev, J. Rinzel and G. M. Shepherd (1995). The theoretical foundation of dendritic function : selected papers of Wilfrid Rall with commentaries. Cambridge, Mass. ; London, MIT Press.
Ramón y Cajal, S. (1911). Histologie du système nerveux de l'homme & des vertébrés: Cervelet, cerveau moyen, rétine, couche optique, corps strié, écorce cérébrale générale & régionale, grand sympathique, A. Maloine.
Regehr, W. G. (2012). "Short-term presynaptic plasticity." Cold Spring Harbor Perspectives in Biology **4**(7): a005702.
Reyes, A., R. Lujan, A. Rozov, N. Burnashev, P. Somogyi and B. Sakmann (1998). "Target-cell-specific facilitation and depression in neocortical circuits." Nature Neuroscience **1**(4): 279-285.
Reyes, A. and B. Sakmann (1999). "Developmental switch in the short-term modification of unitary EPSPs evoked in layer 2/3 and layer 5 pyramidal neurons of rat neocortex." The Journal of Neuroscience **19**(10): 3827-3835.
Rodriguez-Moreno, A., M. M. Kohl, J. E. Reeve, T. R. Eaton, H. A. Collins, H. L. Anderson and O. Paulsen (2011). "Presynaptic induction and expression of timing-dependent long-term depression demonstrated by compartment-

specific photorelease of a use-dependent NMDA receptor antagonist." The Journal of Neuroscience **31**(23): 8564-8569.
Rodriguez-Moreno, A. and O. Paulsen (2008). "Spike timing-dependent long-term depression requires presynaptic NMDA receptors." Nature Neuroscience **11**(7): 744-745.
Rosenmund, C., A. Sigler, I. Augustin, K. Reim, N. Brose and J. S. Rhee (2002). "Differential control of vesicle priming and short-term plasticity by Munc13 isoforms." Neuron **33**(3): 411-424.
Rossi, B., G. Maton and T. Collin (2008). "Calcium-permeable presynaptic AMPA receptors in cerebellar molecular layer interneurones." The Journal of Physiology **586**(Pt 21): 5129-5145.
Rothman, J. S., L. Cathala, V. Steuber and R. A. Silver (2009). "Synaptic depression enables neuronal gain control." Nature **457**(7232): 1015-1018.
Rozov, A., N. Burnashev, B. Sakmann and E. Neher (2001). "Transmitter release modulation by intracellular Ca2+ buffers in facilitating and depressing nerve terminals of pyramidal cells in layer 2/3 of the rat neocortex indicates a target cell-specific difference in presynaptic calcium dynamics." The Journal of Physiology **531**(Pt 3): 807-826.
Rubin, A. N. and N. Kessaris (2013). "PROX1: a lineage tracer for cortical interneurons originating in the lateral/caudal ganglionic eminence and preoptic area." PLoS One **8**(10): e77339.
Rymar, V. V. and A. F. Sadikot (2007). "Laminar fate of cortical GABAergic interneurons is dependent on both birthdate and phenotype." The Journal of Comparative Neurology **501**(3): 369-380.
Sahara, S., Y. Yanagawa, D. D. O'Leary and C. F. Stevens (2012). "The fraction of cortical GABAergic neurons is constant from near the start of cortical neurogenesis to adulthood." The Journal of Neuroscience **32**(14): 4755-4761.
Salt, T. E. (1986). "Mediation of thalamic sensory input by both NMDA receptors and non-NMDA receptors." Nature **322**(6076): 263-265.
Sarid, L., D. Feldmeyer, A. Gidon, B. Sakmann and I. Segev (2013). "Contribution of Intracolumnar Layer 2/3-to-Layer 2/3 Excitatory Connections in Shaping the Response to Whisker Deflection in Rat Barrel Cortex." Cerebral Cortex.

Schaefer, A. T., M. E. Larkum, B. Sakmann and A. Roth (2003). "Coincidence detection in pyramidal neurons is tuned by their dendritic branching pattern." Journal of Neurophysiology **89**(6): 3143-3154.
Schiller, J., G. Major, H. J. Koester and Y. Schiller (2000). "NMDA spikes in basal dendrites of cortical pyramidal neurons." Nature **404**(6775): 285-289.
Schindelin, J., I. Arganda-Carreras, E. Frise, V. Kaynig, M. Longair, T. Pietzsch, S. Preibisch, C. Rueden, S. Saalfeld, B. Schmid, J. Y. Tinevez, D. J. White, V. Hartenstein, K. Eliceiri, P. Tomancak and A. Cardona (2012). "Fiji: an open-source platform for biological-image analysis." Nature Methods **9**(7): 676-682.
Scorcioni, R., S. Polavaram and G. A. Ascoli (2008). "L-Measure: a web-accessible tool for the analysis, comparison and search of digital reconstructions of neuronal morphologies." Nature Protocols **3**(5): 866-876.
Segev, I. (1998). Cable and Compartmental Models of Dendritic Trees. The Book of GENESIS, Springer New York**:** 51-77.
Senft, S. L. (2011). "A brief history of neuronal reconstruction." Neuroinformatics **9**(2-3): 119-128.
Shabel, S. J., C. D. Proulx, J. Piriz and R. Malinow (2014). "GABA/glutamate co-release controls habenula output and is modified by antidepressant treatment." Science **345**(6203): 1494-1498.
Shin, J. H. and D. J. Linden (2005). "An NMDA receptor/nitric oxide cascade is involved in cerebellar LTD but is not localized to the parallel fiber terminal." Journal of Neurophysiology **94**(6): 4281-4289.
Shipp, S. and S. Zeki (1989). "The Organization of Connections between Areas V5 and V1 in Macaque Monkey Visual Cortex." The European Journal of Neuroscience **1**(4): 309-332.
Sholl, D. A. (1953). "Dendritic organization in the neurons of the visual and motor cortices of the cat." Journal of Anatomy **87**(4): 387-406.
Silberberg, G. and H. Markram (2007). "Disynaptic inhibition between neocortical pyramidal cells mediated by Martinotti cells." Neuron **53**(5): 735-746.
Sjostrom, P. J. and M. Hausser (2006). "A cooperative switch determines the sign of synaptic plasticity in distal dendrites of neocortical pyramidal neurons." Neuron **51**(2): 227-238.

Sjostrom, P. J., E. A. Rancz, A. Roth and M. Hausser (2008). "Dendritic excitability and synaptic plasticity." Physiological Reviews **88**(2): 769-840.
Sjostrom, P. J., G. G. Turrigiano and S. B. Nelson (2001). "Rate, timing, and cooperativity jointly determine cortical synaptic plasticity." Neuron **32**(6): 1149-1164.
Sjostrom, P. J., G. G. Turrigiano and S. B. Nelson (2003). "Neocortical LTD via coincident activation of presynaptic NMDA and cannabinoid receptors." Neuron **39**(4): 641-654.
Sjostrom, P. J., G. G. Turrigiano and S. B. Nelson (2007). "Multiple forms of long-term plasticity at unitary neocortical layer 5 synapses." Neuropharmacology **52**(1): 176-184.
Sloper, J. J., R. W. Hiorns and T. P. Powell (1979). "A qualitative and quantitative electron microscopic study of the neurons in the primate motor and somatic sensory cortices." Philosophical Transactions of the Royal Society of London. Series B, Biological Sciences **285**(1006): 141-171.
Somogyi, P. (1977). "A specific 'axo-axonal' interneuron in the visual cortex of the rat." Brain Research **136**(2): 345-350.
Song, S., P. J. Sjostrom, M. Reigl, S. Nelson and D. B. Chklovskii (2005). "Highly nonrandom features of synaptic connectivity in local cortical circuits." PLoS Biology **3**(3): e68.
Strasser, G. A., J. S. Kaminker and M. Tessier-Lavigne (2010). "Microarray analysis of retinal endothelial tip cells identifies CXCR4 as a mediator of tip cell morphology and branching." Blood **115**(24): 5102-5110.
Stuart, G. and N. Spruston (1998). "Determinants of voltage attenuation in neocortical pyramidal neuron dendrites." The Journal of Neuroscience **18**(10): 3501-3510.
Stuart, G. J. and M. Hausser (2001). "Dendritic coincidence detection of EPSPs and action potentials." Nature Neuroscience **4**(1): 63-71.
Sumbul, U., S. Song, K. McCulloch, M. Becker, B. Lin, J. R. Sanes, R. H. Masland and H. S. Seung (2014). "A genetic and computational approach to structurally classify neuronal types." Nature Communications **5**: 3512.
Sun, H. Y. and L. E. Dobrunz (2006). "Presynaptic kainate receptor activation is a novel mechanism for target cell-specific short-term facilitation

at Schaffer collateral synapses." The Journal of Neuroscience **26**(42): 10796-10807.
Sussel, L., O. Marin, S. Kimura and J. L. Rubenstein (1999). "Loss of Nkx2.1 homeobox gene function results in a ventral to dorsal molecular respecification within the basal telencephalon: evidence for a transformation of the pallidum into the striatum." Development **126**(15): 3359-3370.
Svoboda, K. (2011). "The past, present, and future of single neuron reconstruction." Neuroinformatics **9**(2-3): 97-98.
Sylwestrak, E. L. and A. Ghosh (2012). "Elfn1 regulates target-specific release probability at CA1-interneuron synapses." Science **338**(6106): 536-540.
Takesian, A. E., V. C. Kotak, N. Sharma and D. H. Sanes (2013). "Hearing loss differentially affects thalamic drive to two cortical interneuron subtypes." Journal of Neurophysiology **110**(4): 999-1008.
Thomson, A. M. (1997). "Activity-dependent properties of synaptic transmission at two classes of connections made by rat neocortical pyramidal axons in vitro." The Journal of Physiology **502 (Pt 1)**: 131-147.
Thomson, A. M. (2003). "Presynaptic frequency- and pattern-dependent filtering." Journal of Computational Neuroscience **15**(2): 159-202.
Thomson, A. M. and W. E. Armstrong (2011). "Biocytin-labelling and its impact on late 20th century studies of cortical circuitry." Brain Research Reviews **66**(1-2): 43-53.
Thomson, A. M. and A. P. Bannister (1999). "Release-independent depression at pyramidal inputs onto specific cell targets: dual recordings in slices of rat cortex." The Journal of Physiology **519 Pt 1**: 57-70.
Thomson, W. (1854). "On the Theory of the Electric Telegraph." Proceedings of the Royal Society of London **7**: 382-399.
Toledo-Rodriguez, M., P. Goodman, M. Illic, C. Wu and H. Markram (2005). "Neuropeptide and calcium-binding protein gene expression profiles predict neuronal anatomical type in the juvenile rat." The Journal of Physiology **567**(Pt 2): 401-413.
Tomassy, G. S., D. R. Berger, H. H. Chen, N. Kasthuri, K. J. Hayworth, A. Vercelli, H. S. Seung, J. W. Lichtman and P. Arlotta (2014). "Distinct profiles

of myelin distribution along single axons of pyramidal neurons in the neocortex." Science **344**(6181): 319-324.
Toth, K. and C. J. McBain (2000). "Target-specific expression of pre- and postsynaptic mechanisms." The Journal of Physiology **525 Pt 1**: 41-51.
Tsay, D. and R. Yuste (2002). "Role of dendritic spines in action potential backpropagation: a numerical simulation study." Journal of Neurophysiology **88**(5): 2834-2845.
Tsiola, A., F. Hamzei-Sichani, Z. Peterlin and R. Yuste (2003). "Quantitative morphologic classification of layer 5 neurons from mouse primary visual cortex." Journal of Comparative Neurology **461**(4): 415-428.
Ungerleider, L. G. and R. Desimone (1986). "Cortical connections of visual area MT in the macaque." The Journal of Comparative Neurology **248**(2): 190-222.
Urban-Ciecko, J., J. A. Wen, P. K. Parekh and A. L. Barth (2014). "Experience-dependent regulation of presynaptic NMDARs enhances neurotransmitter release at neocortical synapses." Learning & Memory **22**(1): 47-55.
Usoskin, D., A. Furlan, S. Islam, H. Abdo, P. Lonnerberg, D. Lou, J. Hjerling-Leffler, J. Haeggstrom, O. Kharchenko, P. V. Kharchenko, S. Linnarsson and P. Ernfors (2014). "Unbiased classification of sensory neuron types by large-scale single-cell RNA sequencing." Nature Neuroscience.
Vetter, P., A. Roth and M. Hausser (2001). "Propagation of action potentials in dendrites depends on dendritic morphology." Journal of Neurophysiology **85**(2): 926-937.
Vu, E. T. and F. B. Krasne (1992). "Evidence for a computational distinction between proximal and distal neuronal inhibition." Science **255**(5052): 1710-1712.
Wang, B., J. E. Long, P. Flandin, R. Pla, R. R. Waclaw, K. Campbell and J. L. Rubenstein (2013). "Loss of Gsx1 and Gsx2 function rescues distinct phenotypes in Dlx1/2 mutants." The Journal of Comparative Neurology **521**(7): 1561-1584.
Wang, Y., C. A. Dye, V. Sohal, J. E. Long, R. C. Estrada, T. Roztocil, T. Lufkin, K. Deisseroth, S. C. Baraban and J. L. Rubenstein (2010). "Dlx5 and

Dlx6 regulate the development of parvalbumin-expressing cortical interneurons." The Journal of Neuroscience **30**(15): 5334-5345.
Wang, Y., A. Gupta, M. Toledo-Rodriguez, C. Z. Wu and H. Markram (2002). "Anatomical, physiological, molecular and circuit properties of nest basket cells in the developing somatosensory cortex." Cerebral Cortex **12**(4): 395-410.
Wang, Y., M. Toledo-Rodriguez, A. Gupta, C. Wu, G. Silberberg, J. Luo and H. Markram (2004). "Anatomical, physiological and molecular properties of Martinotti cells in the somatosensory cortex of the juvenile rat." The Journal of Physiology **561**(Pt 1): 65-90.
Wasling, P., E. Hanse and B. Gustafsson (2004). "Developmental changes in release properties of the CA3-CA1 glutamate synapse in rat hippocampus." Journal of Neurophysiology **92**(5): 2714-2724.
Wichterle, H., J. M. Garcia-Verdugo, D. G. Herrera and A. Alvarez-Buylla (1999). "Young neurons from medial ganglionic eminence disperse in adult and embryonic brain." Nature Neuroscience **2**(5): 461-466.
Williams, P. A., P. Larimer, Y. Gao and B. W. Strowbridge (2007). "Semilunar granule cells: glutamatergic neurons in the rat dentate gyrus with axon collaterals in the inner molecular layer." The Journal of Neuroscience **27**(50): 13756-13761.
Wilson, N. R., C. A. Runyan, F. L. Wang and M. Sur (2012). "Division and subtraction by distinct cortical inhibitory networks in vivo." Nature **488**(7411): 343-348.
Wonders, C. P., L. Taylor, J. Welagen, I. C. Mbata, J. Z. Xiang and S. A. Anderson (2008). "A spatial bias for the origins of interneuron subgroups within the medial ganglionic eminence." Developmental Biology **314**(1): 127-136.
Woodhall, G., D. I. Evans, M. O. Cunningham and R. S. Jones (2001). "NR2B-containing NMDA autoreceptors at synapses on entorhinal cortical neurons." Journal of Neurophysiology **86**(4): 1644-1651.
Woodruff, A., Q. Xu, S. A. Anderson and R. Yuste (2009). "Depolarizing effect of neocortical chandelier neurons." Frontiers in Neural Circuits **3**: 15.

Xu, Q., I. Cobos, E. De La Cruz, J. L. Rubenstein and S. A. Anderson (2004). "Origins of cortical interneuron subtypes." The Journal of Neuroscience **24**(11): 2612-2622.
Xu, Q., L. Guo, H. Moore, R. R. Waclaw, K. Campbell and S. A. Anderson (2010). "Sonic hedgehog signaling confers ventral telencephalic progenitors with distinct cortical interneuron fates." Neuron **65**(3): 328-340.
Yang, J., G. L. Woodhall and R. S. Jones (2006). "Tonic facilitation of glutamate release by presynaptic NR2B-containing NMDA receptors is increased in the entorhinal cortex of chronically epileptic rats." The Journal of Neuroscience **26**(2): 406-410.
Yu, X. and N. Zecevic (2011). "Dorsal radial glial cells have the potential to generate cortical interneurons in human but not in mouse brain." The Journal of Neuroscience **31**(7): 2413-2420.
Zhang, Z. W. (2004). "Maturation of layer V pyramidal neurons in the rat prefrontal cortex: intrinsic properties and synaptic function." Journal of Neurophysiology **91**(3): 1171-1182.
Zhu, Y., R. L. Stornetta and J. J. Zhu (2004). "Chandelier cells control excessive cortical excitation: characteristics of whisker-evoked synaptic responses of layer 2/3 nonpyramidal and pyramidal neurons." The Journal of Neuroscience **24**(22): 5101-5108.
Zucker, R. S. and W. G. Regehr (2002). "Short-term synaptic plasticity." Annual Review of Physiology **64**: 355-405.